SOME ASPECTS OF THE ROLL COMPACTION OF STRIP FROM IRON POWDER BY THE BISRA PROCESS

by

MARTIN DONNELLY, B.Eng., A.I.M.

A Doctoral Thesis

Submitted in partial fulfilment of the requirements for the award of

Doctor of Philosophy of the Loughborough University of Technology

June 1975

Supervisor: R.Haynes, B.Met.,Ph.D.,M.Inst.P.,F.I.M.
Department of Materials Technology

ACKNOWLEDGEMENTS

This thesis would not have been written without the sponsorship of the British Steel Corporation and the provision of facilities by Loughborough University of Technology. Particular thanks are due to the following:

J.Bellis, B.S.C. who operated the plant during rolling trials at Shotwick;
D.S.Coleman, L.U.T. for discussion, advice and Fig. 17;
P.Costelloe, B.S.C. for continued support of the work after the project moved to Shotwick;
I.Davies, B.S.C. for discussion, advice and provision of strip samples;
A.G.Harris, B.S.C. for discussion, advice and assistance with experiments particularly E3.6;
R.Haynes, L.U.T. for supervising this work;
W.G.Jaffrey, B.S.C. for arranging the sponorship of this work;
P.J.James , L.U.T. for discussions on powder compaction;
N.Leah, B.S.C. for assistance in sintering and rolling at Sketty Hall;
R.F.Mallender, L.U.T. for operation of the instrumented press and discussions on the effects of trapped air; and for Fig.17;
I.A. Menzies,L.U.T. for use of Departmental facilities;
B.Scarlett , L.U.T. for advice on the integration of roll load equations;
K.Selby, L.U.T. for Fig. 44;
D.Tomkins, L.U.T. for ion etching and for Fig.15;
E.Williams, B.S.C. for discussion and advice;

and to the many other members of L.U.T. and B.S.C. staff who have helped in various ways, especially in the Departments of Chemical Engineering and Polymer Technology

ABSTRACT

Steel strip has been made from iron powder by the BISRA process. A water atomised powder and a reduced powder have been characterised. The water atomised powder has been sieved, elutriated and re-blended to form a series of approximately log-linear size distributions, and these have also been characterised. Particular attention has been paid to particle size distribution, apparent density, tap density, compressibility and weight specific surface.

Mechanical and physical properties of the strip have been measured at various stages in its production. The properties have been found to depend on the processing conditions and on the powder characteristics. The processing conditions used did not produce satisfactory strip when very fine water atomised powder was used; an explanation for this has been proposed.

A relationship between powder compressibility, roll loading and green strip density has been observed. By assuming a simple geometrical shape for the rolls when they are deformed by the rolling pressure, an equation has been developed relating green strip density to powder compressibility and the parameters of the rolling process. This equation fits the experimentally observed relationship well, except at very high roll loads. A mechanism has been proposed whereby the probability of the formation of defects by the expansion of trapped air is increased by high roll load; this would lead to lower green strip densities than those calculated by the proposed equation.

A new method for measuring the porosity of small specimens of low porosity has been devised. This has been found to be satisfactory for finished strip.

TABLE OF CONTENTS

Experimental Work:

Experimental Work cont'd.

Results: Page 62

Results:

Discussion Page 71

Discussion

TABLE OF CONTENTS continued

ILLUSTRATIONS: Page 114

TABLE OF CONTENTS continued.

ILLUSTRATIONS continued.

TABLES: Page 163

APPENDICES: Page 183

INTRODUCTION:

The subject of this thesis is the production of thin steel strip from iron powder by the BISRA process [1]. The process is shown schematically in Fig. 1. The process may be summarised as follows: iron powder, water, and a suitable binder are mixed to form a slurry. This is deposited as a film on a temporary substrate and dried. It is removed from the substrate, rolled and subsequently sintered in a reducing atmosphere. This sintered strip is re-rolled, sintered for a second time and then given a final planish or temper roll.

The preparation of the slurry is at present carried out on a discontinuous basis. Iron powder is mixed with water and binder in a container equipped with a mechanical stirrer (Fig.2); also added are an inhibitor and an anti-frothing agent. The viscosity is carefully controlled, normally by adjusting the ratio of water to iron. A typical formulation that has given consistant results is 70% by weight of iron powder, 29.4% water , 0.6% binder [2].

The slurry is transferred to a tank in which is the first roll of a roller-coater (Fig.3) With coarse powder, some of the powder may tend to settle out of the slurry, and so constant stirring of the slurry may be necessary. Each of the rolls of the roller coater is independently driven and so a range of film thicknesses may be deposited. One of the rolls is positioned above the pick-up roll and serves to limit the film thickness on that roll and so prevent the formation of patches or ribs of uneven thickness in the deposited film. Satisfactory coatings can be produced in the thickness range 0.4 - 1.0 mm.

The film is deposited on an endless stainless steel belt, which has been coated with a release agent dissolved in a voltaile solvent.

The belt is tensioned between two large pulleys to keep it flat. This is important because at the viscosities used at present it is possible for some flow of the slurry to take place if the belt is not flat, and this would lead to variations in thickness and density of the finished strip.

The belt, with the film on it, passes through an oven in which the film is dried (Fig. 4). The film reaches a temperature of about 420 K (150°C) and most of the water is driven off. The binder used has the advantage that it 'sets' as the slurry is heated up, rather than becoming thinner; this minimises the variation in film thickness caused by flow of the slurry before it is dried. The film shrinks slightly on drying, and this facilitates its subsequent removal from the belt. The film is trimmed by two rotating discs, to 0.2 m wide, after emerging, dry, from the oven (Fig. 5). At this stage the film is flexible, and has a tensile strength of about 0.5 N/mm^2. Strip in this condition is called 'flexistrip'.

The flexistrip is lifted from the belt and is fed directly into the rolling mill (Fig. 6). This is a two-high mill having rolls of 300 mm diameter. The rolling force is about 5 kN per millimetre of strip width. The strip enters the mill at a density of about 3.0 Mg/m^3 and emerges at about 6.5 Mg/m^3. At this stage the strip is known as 'green' strip and is brittle, but has higher strength than flexistrip, typically about 5 N/mm^2.

The green strip passes on to an endless mesh belt and into a hump-backed muffle furnace (Fig. 7). The entry zone is water-cooled and has a nitrogen atmosphere, which prevents air from getting into the hot zone. The hot zone has a hydrogen atmosphere and operates at

1420-1475 K (1147-1202°C); the muffle in this zone is constructed of a Nimonic alloy. The exit zone is, like the entry zone, water-cooled with a nitrogen atmosphere. The binder is burned off and the strip reaches furnace temperature in about ten seconds; the sintering time may be as little as thirty seconds. Little change in density takes place at this stage but there is an appreciable increase in strength to about 150 N/mm^2. Ductility is negligible at this stage: typical values for elongation are ½-1½%. In this thesis strip in this state will be referred to as 'first-sintered' strip (Fig. 8).

Although ideally the process would be a continuous process, having separate furnaces for each sintering operation and separate rolling mills for each rolling operation, at present the first sintered strip is coiled and transferred to a separate rolling mill for the next operation. This is a two-high mill with 350 mm dia. rolls, 650 mm wide, cambered 0.2 mm. The rolling force is about 8 kN per millimetre of strip width. The strip is rolled in tension but the tensile load is not metered at present; it is known to be considerable as strip breakages have occurred. The strip emerges from the rolls with a density of about 7.4Mg $/m^3$. Strip in this state will be referred to in this thesis as 'second-compacted' strip. Second-compacted strip has also been produced using a four-high mill having 130 mm diameter work rolls (Fig. 9). The four-high mill produced a slightly higher density, about 7.55 Mg/m^3 for the same roll force.

After the second compaction the strip is coiled and returned to the sintering furnace. The second sintering operation is the same as the first. After the second sinter (Fig. 10) the strip has a density in the range 7.5-7.8 Mg $/m^3$ and strength and ductility comparable to

those of conventional strip, tensile strength being up to 400 N/mm^2 and elongation up to 35%. Strip in this condition will be referred to as 'second-sintered' strip.

Finally, the strip is rolled a third time to planish it and give it a good surface finish; and if required, to roll it to the required hardness.

The conventional method of making thin steel strip is more capital intensive. In particular, more sets of rolls are needed. The process is shown schematically in Figure 11.

Molten steel is poured into a mould and allowed to cool until the outside of the ingot is solidified. The mould is then removed from the ingot and the ingot is transferred to a 'soaking pit'. This is a large furnace in which the ingot is kept until its temperature is uniform and correct for the first stage of rolling, 1500 K to 1600 K (1225°C to 1325°C) depending on composition[3].

The soaked ingot is delivered to the primary mill, usually a two-high reversing mill, and here it is reduced in a number of passes, during which the coarse crystalline structure of the ingot is broken up into a more refined structure and blowholes and other solidification voids are closed up. As the surface area of the slab increases, the rate of loss of heat increases, and the slab cools despite the work being done on it. The slab is then transferred to a shear and the front and back ends are cropped, removing those portions of the slab which are likely to be defective. The principal defect involved here is piping, a void at the top of the cast ingot being produced by shrinkage of the metal on solidification. The length of pipe is

uncertain, and it may be necessary to check the cropped slabs for defects, usually by ultrasonics. The cropped discards are returned to the steelmaking departments and recharged into the furnaces as scrap.

The slab is reheated in furnaces and enters the hot strip mill. It passes through a set of roughing, scalebreaking rolls, and immediately is sprayed with high-pressure water jets to remove the scale. If the finished strip is to be wider than the slab is at this stage, it is rotated 90° on a turntable and rolled in a broadside mill to the required width. It is then rotated back on a second turntable and the edges squared up by a slab squeezer. It passes through a number of further roughing mills, and may at this stage be again trimmed in a shear and passed through a further scalebreaking and scale removal process. It then passes through a series of about six four-high rolls, and is cooled by a water-spray and coiled. During the hot rolling processes the strip is kept at working temperature by the heat of working. At this stage the strip is typically about 2 mm thick.

After the coil from the hot mill has cooled to room temperature, the oxide from the hot mill must be removed before cold rolling. The strip is zig-zagged through a number of small diameter rolls, and the reversed bending resulting from this cracks the surface scale, making the subsequent picking easier by allowing the picking solution to penetrate beneath the oxide. The strip is then passed through a number of pickling tanks, containing a hot solution of mineral acid, inhibitor, and wetting agent. After pickling, the strip is rinsed by a cold water spray and immersed in a hot water tank. When the strip emerges from the hot water it is dried by evaporation in hot air and passes between a set of oiling rolls, following which it is recoiled, or if

the cold mill is in line with the pickling line, passes directly to the cold mill.

The cold strip mill normally consists of about four stands of four-high rolls. The speed of successive rolls determines the tension, and the coiler also supplies a constant tension. After cold rolling the oil is removed from the strip by an alkaline detergent rinse, which may be followed by an electrolytic cleaning process. The strip is then cold rinsed, hot rinsed, and dried as it was after pickling. The subsequent annealing process may be carried out by placing the strip in a furnace in coils, or it may be continuous. In continuous annealing the time at temperature is very short. A controlled atmosphere is used and the strip is zig-zagged between rollers through a heating zone, a holding zone and a cooling zone. The strip then passes through a set of rolls which roll it to the desired temper, and is finally coiled.

The conventional process for the production of thin steel strip involves a considerable amount of plant, occupying a considerable amount of land. A considerable fraction of the cost of converting molten steel to strip is incurred in servicing the capital involved. Hence, a less capital-intensive process with comparable marginal costs would offer a worthwhile saving.

A conventional strip mill has a limited production capacity. If more strip is required than can be produced on existing equipment, that equipment cannot easily be modified to increase capacity, and it is necessary to construct another strip mill. Although it is possible to make thin strip using only a few roughing rolls and a few finishing rolls, with many passes through each stand, the economies of size are

significant. As a result of this, any increase of production capacity is usually a large increase, which leads to overcapacity - a state which may last for years, particularly in periods of slow economic growth.

Technological progress is such that a new rolling mill is likely to be more efficient than an old one. Hence, overcapacity does not necessarily result in the underutilisation of new plant, but rather in the decline in utilisation of older plant. Unless new strip mills are sited near established plant, so that workers from one may be employed at the other, redundancies are a likely result from the construction of a new rolling mill. A process for the production of thin steel strip which will make it possible to increase production capacity in smaller increments than are feasible with the conventional process is, therefore, desirable on economic and social grounds.

What is required is a process for making a specific shape - thin strip - cheaply, preferably having a smaller production capacity than the typical conventional process. There are many different ways of producing specific shapes from steel, such as casting, machining, deformation, electrodeposition, chemical deposition, vapour deposition, and sintering. For complex shapes, a combination of processes, for example, casting followed by machining, is common. The conventional strip-making process is such a combination: casting followed by deformation. Some machining is involved, in cropping at the primary mill and in edge trimming. A variant of the conventional process, whereby the cast product is in strip form, rather than ingot form, is clearly attractive. Such a technique is already in use in the aluminium industry; in some cases the cast strip is hot-rolled and subsequently cold-rolled while in others the hot-rolling is ommitted[4,5,6].

At the Keihin works of Nippon Kokan, steel sheet of 0.9 mm thickness has been produced from continuously cast slab which is subsequently hot-rolled and cold-rolled[7].

The various deposition processes are capable of producing thin steel strip, but would be generally unsuitable for large scale production; it is unlikely that they could be made less expensive than the conventional process for strip production. Vapour deposition, for example, is more suited to laboratory scale production of thin films[8].

The powder metallurgy route for the production of thin strip has an advantage over the continuous casting route, in that it is possible to produce strip which is near to the desired thickness at the green stage, whereas it is not at present possible to continuously cast thin strip in mild steel - rather it is necessary to cast thick strip and roll it down. Thus, in principle, the powder metallurgy route requires less rolling equipment, and the principal cost is the cost of the powder. Iron powder is not at present used in quantities which are comparable with those that would be required if one or more powder rolling lines were in full scale production. The present price of iron powder is too high to make powder rolling an attractive proposition for mild steel (although for other materials it is already profitable) but the price should fall if powder production increases.

SCHEMATIC OUTLINE OF THE INVESTIGATION

The objective of the work on which this thesis is based was to investigate the technical factors affecting the roll compaction of steel strip from iron powder by the BISRA process. In particular, the intention was to relate the properties of the strip, at various stages in the process, to the processing conditions and to its properties at the preceding stage.

The system used in the investigation was, therefore, to measure the properties of the raw materials, process them through the first stage under varying processing conditions, and measure the properties of the product. Where possible the measured properties of the product were related systematically to the processing conditions and the properties of the strip at the preceding stage (i.e. in the case of the first stage, the raw materials). The strip was then taken through the next stage of the process, again under varying conditions, and its properties again measured and related to its previous history. This procedure was repeated as far through the process as was practicable in the time available.

The number of factors affecting the properties of the strip is large. It is not certain that they have all been identified. Among the more obvious are the powder characteristics: twelve different characteristics are considered here, and some of these may be further subdivided - for example, particle density may be considered to be determined by the theoretical density of the solid material, the amount of open porosity and the amount of closed porosity. The slurry has six constituents and one of these - water - certainly contains impurities. Similarly, there are many variables in each of the other stages of the process. It follows that a full factorial investigation

of the process would take a considerable amount of time. This is an exceptionally complex problem and an approximate solution has been sought.

The problem may be simplified by considering first those factors which have only weak interactions with the other variables. Here it is assumed that the optimum value is substantially independent of the other operating conditions and may be determined separately. Variables which have little evident effect on the properties of the strip may be held constant. Further simplification results from holding constant those parameters whose preferred values are strongly influenced by considerations other than their influence on the properties of the strip: for example, considerations of cost lead to a choice of preferred sintering temperature. To similify the problem in the ways described above, it is necessary to have a qualitative understanding of the various processes; the investigation is still in the stage where this understanding is being extended through the process, and relatively simple experiments are being used to determine which factors may be varied without affecting others, and which might be expected to have strong interactions.

The British Steel Corporation has, of course, carried out its own investigations of the process, formerly at the BISRA Laboratories in Swansea, and more recently at the Strip Mills Division Product Development Centre in Shotwick, North Wales. The present author was preceded at Loughborough University of Technology by S. H. Williams who worked on the same project. In planning the investigation consideration was given to the work of Williams and of the British Steel Corporation to minimise duplication. It was decided jointly with the Corporation that the work was to be concentrated on two specific types

of iron powder. Responsibility for formulation of the slurry and investigation of its properties was undertaken by the Corporation. Sintering temperature was chosen to suit the available furnaces. Sintering time was selected with consideration to the results obtained by Williams. The present investigation was, therefore, reduced to making strip from two different types of powder under various rolling conditions, and measuring its properties at various stages in the process. The measured properties were used firstly to assess the effects of the previous operation, and secondly to carry out subsequent operations on specimens covering a range of initial properties. Properties which influence the effects of subsequent operations are particularly important because of their potential use for predicting the behaviour of the strip during the production process. Density and compressibility are the most important such properties in rolling operations.

Because the other characteristics of the bulk powder are affected by the size distribution, one of the powders was sieved and re-blended to give a range of different size distributions, and hence, of other characteristics. In characterising the powder, consideration was given to the time available and the possible usefulness of the results. Particle shape was not quantified because the work involved was thought to be relatively great in relation to the use likely to be made of the result. Conductivity was not measured because Williams had shown that it was not easy to interpret the results. The characteristics were determined in the simplest way that gave reproducible results. In the case of the surface area determination, for example, an air permeability method was used. This could be done easily and quickly but the accuracy of the results is affected by the particle shape and size distribution.

Whenever possible, strip was made in bulk on the B.S.C. pilot plant because this produced more uniform strip than could be made in laboratory-scale samples. However, in some cases there was not sufficient powder to use the pilot plant.

Chronological Note

The work on which this thesis is based was begun in January, 1971. Much of 1971 was spent in a study of the literature and of the problems likely to be involved in the work, in particular in density determination and mechanical testing. In the autumn of 1971, a batch of B.S.A. water atomised powder was delivered to the Sketty Hall Laboratories of BISRA, and part of that batch was taken to Loughborough. This material was used for all the experimental work done from then until the end of 1972, when at the request of The British Steel Corporation a parallel investigation using Hoganas sponge iron powder was started.

Considerably more work was done using the water atomised powder than using the sponge powder, mainly because it was available earlier. No work was done on variation of size distributions of sponge powder, nor on finished strip made from sponge powder.

The experimental work was concluded in January, 1974.

LITERATURE SURVEY

L1.0 Historical Background

The earliest recorded case of production of strip from particles was in 1843, when Bessemer[9] accidentally produced brass strip by rolling fine brass turnings. The accidental nature of Bessemer's discovery was undoubtedly responsible for the lack of interest in the process at the time: Bessemer's objective was the production of flat brass particles, and he 'corrected' the defects in the process which had led to the production of continuous strip.

Intentional production of strip from powder first took place in Germany more than half a century later: in 1902 Siemens and Halske[10] patented a process in which two rolls were mounted with their axis in a common horizontal plane, and powder was passed between them from above, emerging below as compacted strip. This process was the basis of one of the main lines of subsequent research - the cold rolling of dry powder followed by a sintering process. At the time it was considered that the process would be useful mainly where strip could not be produced by the conventional process of casting and rolling; the patented process was described as a process for the production of homogeneous bodies of refractory powders. The process was not developed further until the Second World War, when a pilot plant for rolling steel strip was set up in Germany in 1942. Publication of this work by Naeser and Zirm[11] was delayed until 1950; parallel research was carried out by Hardy[12,13] in America. Both these groups of investigators used vertical rolling mills, supporting the powder in a horizontal plane with a temporary substrate as it was fed into the rolls[14]. By this time it was clear that the system of feeding the powder to the rolls was important, and the subject was investigated in some detail by Evans and Smith[15].

By the late nineteen fifties, there were two main approaches to the problem: hot rolling and cold rolling. In each case the feed to the rolling mill may consist of either separate particles or a pre-bonded strip. The strip may be bonded either by sintering or with a binder; or by enclosing the particles in a container.

L1.1 Hot Rolling of Powder

Hot rolling is a process which permits the use of coarser powder than cold rolling, because the deformation of the particles during rolling is greater. Indeed Evans[16] pointed out that when hot rolling powder, it is important to prevent the powder from sintering before it reaches the rolls. In 1961 Schloemann A.G. patented a process for either hot rolling or hot pressing metal particles in an atmosphere of nascent hydrogen[17]. The Reynolds Metal Corporation developed a process for rolling hot 'cigar shaped' granules of aluminium in air. Dangherty[18] has speculated that air trapped in the spaces between the granules as they are rolled reacts with the aluminium to form aluminium nitride and aluminium, giving increased strength. The International Lead Zinc Research Organisation Inc. has patented a process for making strip from zinc alloy powders by hot rolling at high roll load intensities, giving up to 80% reduction and producing a fully dense strip in one pass[19]. The General Electric Co. has developed a process for making heating elements by incorporating an insulated specially shaped resistance wire in aluminium strip. The wire is fed into the rolls simultaneously with coarse pre-heated aluminium powder, and fully dense strip is produced in one pass[20]. This process is not, however, operating as a production process[21]. Theoretical aspects of the rolling of pre-heated granules of aluminium alloys have been investigated by Ramakrishnan[22].

L1.12 Hot Rolling of Pre-Bonded Strip

In 1957 Kalling, Eketorp and Backstrom reported their work on sintering a mixture of granulated pig iron and iron oxide in a tray to form a slab, which is subsequently rolled[23]. Schloemann A.G. developed a system of enclosing powder in a can, and evacuating the can before rolling[24]. The Amplex Division of Chrysler Corp. has a process for making strip from powders of low compressibility: a slip-cast strip is dried, sintered and hot-rolled[21]. Weaver, Butters and Lund have produced slabs from iron powder by loose sintering, and rolled these to densities approaching 99% of the density of fully dense material[25].

The spray rolling process developed by Singer[26] may be considered here. A stream of molten metal is gas-atomised vertically above one roll of a horizontal rolling mill. The still-molten droplets fall onto the roll, where they flatten on impact to form a thin layer. The rolls rotate continuously, and the layer of hot metal is fed through the roll gap to emerge as coherent strip. It is interesting to note that there is no backward slip between strip and rolls; if there was it would be necessary to remove the strip from the roll on which it is cast to feed it to a separate rolling mill.

A further process related to hot rolling is the resistance sintering process of Sakai[27]. This is a development of the method used by Lenel[28] for resistance sintering of powder compacts in insulated dies. Loose powder is fed into the roll gap of a horizontal rolling mill, and an electric current is passed from one roll to the other through the strip, which heats the strip as it is rolled. This produces strip of density up to 7.5 Mg/m^3 at a roll load intensity of 3 MN/m [29].

L1.3 Cold Rolling of Dry Powder

One of the principal drawbacks of the direct rolling process is that the expulsion of trapped air limits the rolling speed. In 1959 Worn and Perks showed that higher rolling speeds could be reached if the rolling was done in an atmosphere of hydrogen, because the viscosity of hydrogen is lower than that of air[30]. In 1960 a paper by Hunt and Eborall[31] described progress made by the British Non-Ferrous Metals Research Association in the rolling of copper strip. By 1966 Sherritt Gordon Mines Ltd. were producing nickel strip for coinage by first cold rolling dry nickel powder, and subsequently hot rolling the green strip[32]. In 1967 Metal Innovations Inc. patented a process for making strip for transformers from atomised iron alloy powder[33]; in 1968 Alloys Unlimited Inc. patented a process for making foil from nickel-cobalt-iron alloys by powder rolling, sintering, re-rolling and re-sintering[34].

In Great Britain the Manganese Bronze Co. Ltd. produced porous nickel sheet for electric cells by powder rolling. The porosity was controlled by the use of fine Celacol powder, mixed dry with the nickel powder before rolling. It is interesting to note that this is one of relatively few powder rolling processes to use small diameter work rolls: a four-high rolling mill was used, and the work rolls were only 25 mm diameter[35].

The most common development in the last few years has been the application of the powder rolling process to a variety of materials. At Gorki Polytechnic Institute the process has been applied to iron, stainless steel, nickel, copper, aluminium, cobalt and titanium; an interesting development is the rolling of mixtures of bronze powder and diamond to form an abrasive medium suitable for the grinding of

glass[36]. Coast Metals Inc. have a patent on the production of ductile cobalt strip from a mechanical mixture of cobalt powder and 2-4% of iron powder, the alloy resulting being cold-formable[37]. Maltsev, Khromov and Malyshkina have produced titanium strip of nearly theoretical density by four rolling operations with vacuum sintering between each rolling stage[38]. British Steel Corporation have a pilot plant for producing stainless strip of high density using two cold rolling operations and two sintering operations[39].

A process involving both cold rolling and hot rolling is that of the Republic Steel Corporation[40]. Iron powder is cold rolled to about 75% of theoretical density. It then enters a furnace, where it is heated to rolling temperature under a protective atmosphere. Outside the furnace, but still in a protective atmosphere, the strip receives three rolling passes while still hot. This strip is claimed to have properties near to, but not equal to, those of conventional strip at the hot rolled stage; normally it would also be subsequently cold rolled. The potential savings are not, therefore, as great as are claimed for the British Steel Corporation process[39,41].

L1.4 Cold Rolling of Pre-Bonded Strip

In 1966, Texas Instruments Inc. patented a process for making sintered foil as thin as 0.025 mm by coating a stainless steel carrier with a slurry of the powder and a solution of a binder, which could be dried and compacted to bond the particles, giving sufficient strength to remove the strip from the carrier. The strip was then sintered, rolled, and re-sintered[42]. The Clevite Corporation patented a similar process in 1967[43]. Their patent covered the use of titanium or nickel powder, and specified a cellulose binder with a plasticiser such as polyglycol. In this patent the possibility of depositing a second

layer, possibly of a different material, on top of the first layer, was mentioned. Union Carbide Corporation patented a process for making porous strip which was substantially the same as the two processes described above except that the second rolling and sintering operation were omitted[44]. The BISRA process described in the introduction is similar to these, but the strip is removed from the backing sheet before rolling[45]. This is made easier by the use of a release agent consisting of a fatty acid dissolved in trichlorethylene or ethanol[1].

The use of a binder limits the density which can be attained in the first rolling operation because the binder occupies space which could otherwise be filled by powder. An experimental Russian technique[46] avoids this by containing the powder in a paper jacket during the rolling operation. Tungsten carbide particles are either coated with nickel or mixed with iron powder. The strip is sintered in cracked ammonia, re-rolled and re-sintered in hydrogen.

L1.5 Summary of Literature on Powder Rolling Processes

The continuous roll compacting of metal powders into sheet or strip is now accepted as a viable process, particularly in the case of metals which work harder rapidly, and so need many annealing operations during the production of strip by the conventional process. Alloys which have a large freezing range are prone to severe segregation on casting, and this segregation can be avoided by the powder route to strip. Very expensive alloys may be powder rolled profitably because of the potential 100% utilisation of material by avoiding cropping and trimming. The process is of course ideal for ceramics and ceramic-metal mixtures. There are good prospects for powder rolling of base metals because of the low capital costs, and the process is well-established for aluminium[18].

It should be kept in mind, however, that powder rolling is not the only alternative to the conventional process, and Siemens A.G. have developed a process[47] for making green strip by feeding powder on a conveyor belt under a reciprocating punch.

Despite the lack of progress between discovery of the process and the second world war, interest in the process is now growing rapidly, as shown in reviews of the process by Evans[48] (who has himself patented a process for compacting dry powder in a vertical rolling mill[49]), Williams[50] and Nayar[21].

L2.0 Theoretical Background

It is not proposed to deal with theoretical aspects of the various experimental techniques used in this investigation in this section. Such matters will be considered in the discussion section of this thesis as an essential part of the evaluation of the results.

There can be little doubt that the processing conditions and powder characteristics affect the properties of the finished strip. Qualitative relationships of this type have been established for other powder metallurgical processes. Pearson and Hirschorn[51] investigated the effect of particle size and shape on powder density, and on the density of compacts made from that powder; Zborovskii endeavoured to show that powders of high apparent density had low compressibility[52]; Krishnamoorthy showed that the type of powder used influenced the properties of sintered iron to an extent which varied with the density of the compact[53]; Koczak and Cawley measured the effect of particle size on the mechanical properties of sintered compacts[54]; Bhattacharyya and Parikh used a computer analysis to find the processing conditions necessary to optimise the

properties of sintered compacts made from iron and stainless steel[55]. There are other examples far too numerous to mention; in the case of powder rolling processes Costelloe et al. have shown that the deformation characteristics of aluminium particles can be related to their behaviour when rolled on the surface of steel strip[56], although in contrast, Hayden et al. found that powder characteristics have little effect on the compaction angle in the direct rolling process[57].

L2.1 Compression of Powder

The majority of the investigations of the compression of powders have been concerned with die compaction. However, where a moving punch compresses powder in a die, friction between the powder and the die wells contributes to the force opposing the punch. As a result of this, the density is not uniform throughout the compact. The situation is improved by lubrication or by isostatic compaction. A considerable number of pressure-density relationships has been proposed; many of these apply only to specific powders or only over a limited range of pressures. Some of the latter are based on hypothetical descriptions of the densification process. As the densification process is believed to consist of a number of overlapping stages[58] it is not to be expected that the equation based on a hypothetical description of one of these stages would apply equally well to the others.

However, the various stages can generally be regarded as aspects of either particle rearrangement or particle deformation, and the latter at least is possible at all pressure values, since the weight of a particle will cause some deformation of its areas of support, either elastic or plastic. It has been shown by Strömgren et al. that some particle rearrangement takes place at pressures up to 500 N/mm^2

during isostatic pressing of spherical aluminium powder[59]. It is, therefore, more reasonable to regard rearrangement and deformation as two continuous processes which take place simultaneously. Nevertheless, Bockstiegel has suggested that no interparticle movement takes place below a pressure of 25 N/mm^2 for electrolytic iron powder[60]. Particle fragmentation is an aspect of powder compaction which will not be considered here because the iron powders used were relatively ductile and no evidence of fragmentation was found.

When density and compacting pressure for a given powder are plotted against each other using simple linear axes, a smooth curve results. This indicates that it is possible to describe the compaction process in a single equation. Kawakita and Tsutsumi[61, 62], and Kawakita and Ludde[63] have considered the range over which various proposed equations of powder compaction may be valid. In particular they have found the predicted values of porosity at infinite pressure and at zero pressure, and shown that some of these equations cannot fit both extremes of the pressure range. The equations of Ballhausen[63a], Murray[63b], Konopicky[63c], Athy[63d], Tanimoto[63e] and Kawakita[61, 62, 63] were found to be mathematically capable of describing the complete range of pressures. For the purpose of this comparison Athy's equations, which describes the porosity of clays in terms of depth below the surface of the ground, was treated as a pressure-density relationship. Heckel[64] tested the equations of Balshin[64a], Smith[64b], Murray[63b], Ballhausen[63a] and Konopicky[63c] on experimental data, and found that Konopicky's equation gave the best fit. Chare and Sheppard[65] tested the theories of Kawakita[61], Balshin[64a] and Athy[63d] on aluminium alloy powder, and concluded that the best fit to the data was obtained using the equation of Kawakita. Brackpool[66] also considered a number of equations, using

both die compaction and isostatic compaction and seven different types of powder. He also found that Kawakita's equation fitted the data best, but found that the equation could be modified so that the constants in the equation could be related to the tap density, particle hardness and Meyer work-hardening index of the powder.

Kawakita's equation is:-

$$(V_o - V)/V_o = abP/(1 + bP) \quad .....(1)$$

where V_o is the initial volume, V the volume at pressure P, and a and b are constants characteristic of the powder.

Kawakita et al.[67] have found that both Athy's and Kawakita's equations may apply to the compression of hand materials; Kawakita and Tsutsumi[61] have demonstrated that Athy's equation is substantially the same as Konopicky's but expressed differently. Hersy and Rees[68] have also found experimental evidence to support Konopicky's equation.

Konopicky's equation is:-

$$\ln \left[1/(1 - D)\right] = kP + \ln \left[1/(1 - D_o)\right] \quad .....(2)$$

where D is the fractional density at pressure P, D_o the fractional density at zero pressure, and k a constant characteristic of the material.

It is possible to manipulate Kawakita's equation to a form comparable with Konopicky's:-

$$1/(1 - D) = cP + 1/(1 - D_o) \quad .....(3)$$

where c is another constant (Appendix VI) and D, D_o and P are as for Konopicky's equation. However, James has found that for electrolytic

copper and Shemitt Gordon nickel[69], equation (1) fits the data better than equation (3)[70].

It should be noted, however, that these equations have been established only for relatively large volumes of powder. Lohan[71] has found that for compacts thinner than 1 mm the density produced by a given pressure is lower than for thicker compacts. The presence of a binder will also affect the density of a compact by occupying space which might otherwise be occupied by powder[50, 72].

L2.2 Compression of Strip

In principle, it should be possible to relate the force used to compress powder by rolling to the force used to compress powder by die compaction. This depends on the assumption that the density produced by a given pressure in rolling is the same as the density produced by the same pressure (after allowing for die-wall friction) in die compaction. Thus, if the maximum specific pressure in rolling is known, and the pressure-density relationship of the powder is known, then the density of the strip can be calculated. Generally, however, the maximum specific pressure is unknown. Vinogradov and Katashinskii[73], and Maltsev[74] have however, measured the specific pressure in particular cases. Lee and Schwartz[75] have developed a mathematical model of the distribution of roll pressure in powder rolling, based on a relationship between shear stress and compressive stress. The model gives a more sharply peaked pressure distribution than that found in practice by Katashinskii[73, 76]. Ioffe suggests that the stress varies throughout the thickness of the strip during compaction[77].

Radchenko[78] has considered the contact stresses from a different viewpoint, using classical elasticity theory based on the work of Hertz[79], and has calculated contact arc lengths[80].

Sorokin[81] has compared maximum calculated specific pressures with relative densities of strip made from powder, and has found that the results fit Balshin's equation[61] for powder compaction, but do not fit Konopicky's equation.

Aksenov has used an equation[82] which can be rearranged to give Kawakita's equation for powder compaction (Appendix VI). Assuming a circular arc of contact with an undeformed roll, he has integrated the pressure over the area of contact to give an equation for total roll force F:

$$F = \frac{2ABRh}{Z_o}\left[\frac{Z}{Z_o}\sqrt{\frac{Z_o}{2h(Z_o - Z)}} \quad \text{arctg}\sqrt{\frac{Z_o}{2h(Z_o - Z)}} - \frac{\alpha}{Z_o - 1}\right] \qquad \ldots\ldots\ldots(4)$$

where A is a constant characteristic of the powder, B the width of the strip, R the roll radius, h the ratio of rolled strip thickness to roll diameter, α the compacting angle, Z the ratio of strip density to powder apparent density, and Z_o the ratio of solid metal density to powder apparent density. This equation was tested in an actual powder rolling experiment and found to give a value 14% below the true roll force[83]. This is clearly because it does not take into account either elastic deformation of the rolls or elastic recovery of the strip.

The direct rolling process does not permit high-speed rolling. There is generally an upper critical speed[84] above which the escape of trapped gases (usually air) and poor flow of powder[85] produce defects in the strip, normally because of increased and non-uniform porosity[86]. Musikhin and Vinogradov[87], using a forced powder feed to the rolls involving a rotating screw, found that an increase in rolling speed from 20 mm/s to 170 mm/s produced a small but measurable increase in roll loading, with constant roll gap. This is in contrast to the situation in the cold rolling of conventional strip, where the reduction in gauge produced by a given roll force is greater at higher speeds[88]. Ford has found that this effect is greater with thin strip, and has reported a 30% reduction in roll force with a speed increase from 40 mm/s to 1250 mm/s[89]. It has been suggested that these changes may be attributed to changes in the coefficient of friction between strip and rolls, and Bowden and Tabor have shown that the coefficient is reduced with increased speed[90], while Golten has found that it increases with specific roll pressure[91].

That change in coefficient of friction with speed may also be found with powders has been demonstrated by El Wakil and Davies[92], who investigated the high speed pressing of iron powders, and this is confirmed by Mallender et al[72] at lower speeds. If interparticle friction contributes significantly to the pressure-density relationship of the powder, or if there is any slipping of the strip relative to the rolls in rolling, then changes in the coefficient of friction will affect the density of strip produced under constant roll loading at varying speeds. Satoh et al.[93] varied the compacting speed from 5 mm/s to 150 mm/s and found that density increased with compacting speed at constant compacting pressure, but the effect was smaller with increased pressure.

At higher velocities of compaction Dorofeev and Prutsakov[94] have found that the density produced by a given amount of energy applied at various speeds is greater at higher speeds; a 7% increase in density resulted from a speed increase from 20 m/s to 50 m/s. Mathematical work by Carrol and Holt[95, 96] based on the work of Herrmann[97], and Mackenzie's model of a hollow sphere under external pressure[98], suggests that at speeds of about 300 m/s for aluminium, the pressure required to produce a given density may decrease with speed. Such speeds are, however, far above the speeds required for rolling strip.

In the BISRA process, the powder particles are held together by a binder during the initial stages of the rolling operation. There is, therefore, no difficulty with the flow of powder[85] and the escape of trapped air does not interfere with the forward movement of the powder as in direct rolling[84]. Nevertheless, the air may cause problems if the rolling speed is greater than the speed at which most of the air can escape. Mallender has reported that compacts ejected from dies in less than one second after compaction may fracture if the lubricant content is high, but will not fracture if held in the die for more than five seconds; he attributes this to the slow escape of trapped air[99]. Williams[100] has measured the pressure of trapped air in compacts after removing them from the die. The expansion of the compact after removal from the die will cause some loss of pressure. Long and Alderton[101] measured the gas pressure without removal from the die, and found that with fine powder most of the gas present in the loose powder as it filled the die was retained in the compact, the gas pressure being inversely proportional to the porosity.

Clearly if the gas pressure is greater than the compact can stand, the compact will be damaged. The pressure at which this occurs will depend on the green strength of the compact. Klar and Shafer[102, 103] have found that the green strength of powder compacts is attributable to interparticle metallic contacts made during the compaction process. Easterling and Tholen[104] have derived a theoretical relationship between green strength and the radius of curvature of the interparticle contact faces. Strömgren et al.[59] obtained a green strength of 11 N/mm^2 from aluminium pressed to near solid density, and found that the contact area was near to the cross-sectional area of the specimen. They concluded that the contacts between particles were weaker than the solid metal.

L2.3 Sintering

When an aggregate of particles is heated, normally there will be three major effects: change in pore shape, change in pore size, and change in grain size. The processes cause the aggregate of particles to become a single porous body. Prolonged sintering may result in a change in overall density. These changes tend to minimise the total free energy of the system, and in particular, the surface free energy and the grain boundary free energy. The sintering process has been reviewed by Thummler and Thomma[105] and by Coble and Burke[106].

Coble[107] considers the sintering process to consist of three phases:

(a) a neck is formed at the point of contact between adjacent particles.

(b) grain growth and neck growth take place, but the pores

remain continuous and are intersected by grain boundaries.

(c) Some of the pores are closed and some of the closed porosity is isolated within grains, out of contact with the grain boundaries.

The surface area of the powder is considered to be one of the more important parameters affecting the sintering process. Tikkanen and Lahtinen[108] and Kisly and Kuzenkova[109] have studied the effect of surface area by varying particle size; they found that the densification during sintering was greater for finer powders.

Heavily deformed particles having a high density of lattice defects have been studied by Naeser[110] and by Pines et al.[111] who found that the sintering was faster than for annealed powders. Easterling and Tholen, however, found that for particles smaller than 200 nm dislocation movement was relatively unimportant unless an external load was applied[112].

During the intermediate stage of the sintering process, a correlation between grain size and density has been noted[113, 114]. The volume changes of pores interacting with grain boundaries have been studied by Stevanic[115] and Moon[116]; the latter found that the rate of pore size reduction is dependent on the grain size.

During the final stages of sintering, when pores become isolated, only those pores in contact with grain boundaries shrink appreciably. This is because the rate of diffusion within the grain is significantly slower than the rate of diffusion along grain boundaries. Because grain growth reduces the total area of grain boundary,

and also the number of pores in contact with grain boundaries, it can also reduce the shrinkage rate[117]. When most of the pores are isolated from each other and from grain boundaries, the sintering process becomes very slow[118].

Where gases are trapped in the pores, densification will stop when the pressure of the gas is sufficient to balance the surface tension of the inner surface of the pore[119]. Amato [120] has shown that this does not prevent sintering to 98% of theoretical density. The use of a hydrogen atmosphere for sintering minimises this problem[118].

In the present investigation only short sintering times were used. Williams[50] found that mechanical properties develop most rapidly during the first minute of sintering. Katrus and Aleshina[121] sintered rolled sheet made from stainless steel powder in hydrogen at 1650 K (1377°C) and found that there was no change in electrical conductivity after two minutes. Sturgeon et al.[39] used sintering times of five minutes on stainless steel strip at temperatures up to 1673 K (1400°C) and obtained sufficient strength to cold roll the strip to a reduction of 80%.

L2.4 Rolling of Sintered Strip

There is not much published work which deals with the rolling of sintered strip, as distinct from the rolling of powder. Radchenko[78, 80] considers the effect on the rolls in terms of roll deformation and strip deformation; he has found that the elastic recovery of the strip is not sufficient to affect the length of the arc of contact, although the elastic deformation of the rolls is important, and can produce an arc of contact up to twice the length of the arc which would be produced by undeformed rolls, resulting in a lower

maximum pressure for a given roll load. However, the fact that the strip is strong enough to apply strip tension during rolling has the opposite effect, in so far as a lower roll load intensity is required for a given reduction in gauge in the biaxial stress system produced by the strip tension. The effect of strip tension on the pressure distribution over the arc of contact has been analysed by Nadai[122].

Sturgeon et al.[39] have studied the effect of the degree of reduction in the second compaction operation on the properties of the strip after a subsequent sinter. They found that tensile strength increased with increasing reduction up to a certain value, and then remained constant despite increasing reduction. Elongation, however, increased to a maximum and then declined. A higher temperature in the first sintering operation lowered the reduction necessary to give maximum elongation, if the density of the strip before rolling was the same in each case. The optimum cold reduction varied from 50% to 75%, corresponding to sintering temperatures of 1673 K (1400°C) and 1473 K (1200°C) respectively.

L2.5 Properties of Strip Made from Powder

It is now well established that strip made from powder can have properties comparable to those of conventional materials, particularly if the porosity is less than 2%[21, 40, 123]. For example, Sturgeon et al.[39] have produced stainless steel strip with 55% elongation and ultimate strength of 650 N/mm^2.

The properties can, however, vary, particularly if there is a measurable amount of residual porosity. In the case of the stainless steel strip quoted above, for example, the elongation could be as low

as 10% with less cold reduction of the strip after the first sintering operation. It is generally agreed that the amount of porosity is the principal factor affecting the properties of a sintered material[124,125,126]. Haynes[125] has shown that the ratio R, of tensile strength of porous material to that of solid material is given by:

$$R = (1 - e)/(1 + be)$$

where e is the fractional porosity and b a constant. Similar relationships have been found for Young's modulus and work hardening exponent[127]. These relationships are substantially linear over a small range of low porosity such as might be encountered in strip made from powder. Unfortunately, much of the published work deals with die-compacted material having typically more than 5% porosity; Eudier, for example, gives the strengths of steel components made from MH 100 powder for porosities greater than 7%.

Despite this preponderant influence of the amount of porosity on material properties, other factors may be involved. Evans and Smith[128] suggested that pore size could be significant; Gessinger et al.[129] support this. Buch and Goldschmidt[130] found that some sintered materials do not behave as though the pores were uniform spherical holes; Kaufman[131] showed that mechanical properties may depend on pore shape. Kuroki and Tokunaga[132] found that not only the pore shape but also the pore location relative to grain boundaries influenced the mechanical properties of sintered iron. Bache[133] has proposed a relationship between strength and particle size; McClintock[134] has related ductility to the ratio of pore diameter to spacing between pores. Rostoker and Liu[135] have confirmed the validity of McClintock's relationship.

Fischmeister et al.[127] find that the implications of McClintock's relationship, which they support, are different for sponge iron and atomised iron. The former may have a homogeneous pore structure because of the high porosity within the particles; the latter may tend to have porosity concentrated on the inter-particle boundaries, which tend to become grain boundaries on sintering. Thus, fracture paths may follow the grain boundaries and sintered materials made from atomised powder may have less ductility than materials of the same density made from sponge iron powder.

Williams and Haynes[136] found that pore shape can affect the fatigue life of sintered materials. They found that porosity can deviate from the idealised spheriodal shape to the extent of being film-like in sintered Sherritt-Gordon nickel. In specimens containing both film-like and rounded porosity, the fatigue behaviour was determined primarily by the film-like porosity.

Kajman and Mocarski[137] investigated the properties of high-density powder metal forgings. They found that the influence of the porosity was greatly reduced if the amount of the porosity was less than 0.5% Although the properties were affected by pore shape they seemed to be independent of the powder particle size.

L3.0 The Investigation of the BISRA Process by Williams

Williams worked at Loughborough University of Technology, sponsored by BISRA, from 1968 to 1970. He characterised eight different iron powders, made by four different manufacturers.

These were:

(1)	Sintrex electrolytic powder	-300 mesh
(2)	Woodall Duckham	-100 mesh
(3)	B.S.A. water atomised	-100 mesh
(4)	B.S.A. water atomised	-300 mesh
(5)	Makin JJM 300	-300 mesh
(6)	Makin JJM 300 severely milled	
(7)	Makin JJM 300 air-elutriated	finer than 0.03 mm
(8)	Makin JJM 300 air-elutriated	coarser than 0.03 mm.

The characteristics which he investigated were:

(1) Size distribution

(2) Particle shape

(3) Surface area

(4) Particle hardness

(5) Particle density.

Green strip was prepared at a range of roll loads and the variations in green strength, density and resistivity were measured. The strip was sintered for a range of times and the variation in tensile strength was measured. For B.S.A. powder the change in resistivity was also measured.

L3.1 Results of Williams' Investigation

Williams found that chemically reduced powders of fine particle size and large surface area could be rolled to make green strip of higher strength but lower density than powders of coarse particle size. The green strength and density were reduced at high roll loads.

Significant strength was developed within a few seconds during sintering. Strength increased further with long sintering times but no change in density occurred after sintering for five minutes.

L3.2 Williams' Conclusions

Williams concluded that:

(1) Of the factors investigated, particle size distribution has the greatest effect on green strength. To obtain maximum strength a large percentage of fine material must be present in the powder.

(2) The presence of a binder causes a reduction in green strength and density at high roll loads.

(3) Finer powders give better sintering characteristics, although grain growth may occur if high roll loads are used.

(4) Mechanical properties develop most rapidly in the first minute of sintering.

EXPERIMENTAL WORK

E1.0 Materials

Two different types of iron powder were used. These were received in 50 kg (1 cwt) bags. They were a -100 mesh water atomised powder made by B.S.A. Metal Powders Ltd. and a -300 mesh sponge iron powder made by Hoganas (MH 300.25).

E1.1 Sampling of As-Received Powders

A Pascal six-chamber sample divider (Fig. 12) was used to sample the Hoganas MH 300.25 powder. The apparatus consists of a hopper with a controlled outlet aperture which is vertically above the apex of a cone. The cone is centred on the axis of a rotating turntable on which stand six containers, open at top, each occupying 60° of the periphery of the turntable.

The powder was placed in the hopper in approximately 5 kg loads. Similar quantities of the powder were delivered to each of the six containers. The contents of two diametrically opposite containers were transferred to one bin, and the contents of the other four, to another. The process was repeated until all the powder had been sampled in this fashion. The smaller of the two samples so produced was re-divided in the same way, and this process was repeated until the smaller sample size was approximately 60 g.

The 60 g sample was further subdivided using a 48-compartment spinning riffler (Fig. 13). The sample dividing head was rotated at 75 revolutions per minute. All the 60 g of powder was poured through a fine funnel positioned vertically above the compartmented section of the dividing head. Powder from four compartments at 90° intervals was

retained and re-riffled. This produced a sample of about 0.35 g, which was used for compressibility and weight specific surface determinations. A further 0.35 g sample was produced to mount in thermosetting resin for metallographic examination, and this was riffled again to obtain a small quantity for examination by optical and scanning electron microscopy.

The B.S.A. water-atomised powder was sampled on a different basis. The powder was removed from the bag in a scoop which held approximately a kilogramme. Every sixth scoopful was retained, and these were mixed together. Random samples were taken from the mixture and these samples were re-mixed and re-sampled until a sample weight of about 20 g was reached. This was then subdivided on the 48-compartment spinning riffler in the same way as the Hoganas powder.

E1.2 Production of Controlled Size Distributions from B.S.A. Powder

The B.S.A. powder was sieved on an Endecotts sieve shaker in 250 g loads[138] with a nest of eight sieves at fourth-root-of-two size intervals for one hour. The sieve sizes used were from 150 μm to 45 μm. The powder which passed through the finest sieve was further subdivided using five cut speeds on an Alpine centrifugal zig-zag air classifier (Fig. 14) In this apparatus, the powder was fed to a rotor in which air was sucked from outside to centre along zig-zag channels. The powder was accelerated to the peripheral speed of the rotor by radial blades. The centrifugal force drove the oversize particles to the outer circumference of the classifying chamber, where they were collected in a wide-necked bottle. Undersized particles passed into the centre of the rotor with the air flow and were carried into a cyclone from which they were deposited in another bottle.

The air flow rates were determined from the equation[139]

$$V = 55 - n \times 10^{-3}$$

where V is the volumetric air flow in cubic metres per hour and n is the number of revolutions of the rotor per minute. The five speeds chosen were 2080, 3000, 4000, 6000 and 8000 revolutions per minute. The particle sizes assigned to the different cut speeds were based on the manufacturers' classification curve for limestone, using the relationship

$$D = d \sqrt{p/R}$$

where D is the cut diameter of the iron powder and d the cut diameter of the limestone; p the particle density of the limestone and R the particle density of the iron. The value of p used was 2.65 Mg/m^3. The cut diameter was defined as being that diameter at which the probability of classification as undersize was equal to the probability of classification as oversize.

The different size fractions of the B.S.A. powder produced by sieving and air classification were identified by letters of the alphabet as shown in Table 1.

The powder was then reblended by using weighed amounts of different fractions as required, to give a series of different particle size ranges for each of three different mean sizes. These blends were also identified by letters of the alphabet; the compositions of the blends are shown in Table 2.

E2.0 Characterisation of the Powders

The following powder characteristics were determined:

(a)	Material properties:	1. Chemical composition
		2. Microstructure
		3. Microhardness
(b)	Particle properties:	4. Particle density
		5. Particle shape
(c)	Bulk properties:	6. Particle size distribution
		7. Segregation
		8. Apparent density
		9. Tap density
		10. Compressibility
		11. Compactibility
		12. Weight specific surface

E2.1 Chemical Composition of the Powders

Chemical analysis of both types of powder has been carried out by British Steel Corporation, Strip Mills Division. The sample of Hoganas MH 300.25 was taken from the Pascal sample divider. The sampling method used for the B.S.A. water atomised powder is not known.

Hydrogen loss was determined in a separate experiment. A silica boat was weighed on a fourth-place Stanton single-pan balance, and placed in the cold zone of a tube furnace. The furnace was flushed with a mixture of 3% hydrogen in nitrogen, and then with a mixture of 75% hydrogen, 25% nitrogen. A steady slow flow of this mixture was maintained for two hours. After thirty minutes the boat was pushed to the

hot zone of the furnace, which was at 1300 K (1027°C); after a further hour the boat was pushed through to the cold zone. At the end of the two hour period, the gas flow was stopped, and the boat was removed and reweighed. This procedure was repeated until the loss in weight of the boat was less than 0.005 g.

10 g of powder was dried in an air-oven at 400 K (123°C) for six hours. The boat was weighed, the powder was placed in the boat, and the full boat was reweighed to find the exact weight of powder. The boat was then placed in the furnace and the procedure described for the empty boat was followed. The combined weight of boat and powder was found. The powder (which had sintered to a solid mass) was removed, and the empty boat reweighed. The total loss in weight was found, and the loss in weight of the boat subtracted. The loss in weight of the powder was calculated as a percentage of the original weight to the recrest 0.1%.

E2.2 Microstructure of the Powders

The B.S.A. powder was mounted in clear thermoplastic resin and polished, using wet silicon carbide paper on four grades to 600 BS mesh size and finishing on diamond paste to ¼ μm. It was etched in 2% nital for 15 seconds. The Hoganas powder was mounted in conducting thermosetting resin and polished similarly. It was etched cathodically by a beam of argon ions under the following conditions:

Potential difference	4,500 V
Current density	10 A/m^2
Argon pressure	2 N/m^2
Time	3,600 s

The apparatus is shown in Fig. 15.

Some of the B.S.A. powder particles were found to be fine grained. The volume fraction of fine grained powder was estimated visually. The grain size of the fine grained powder was measured by a mean linear intercept method. Photomicrographs of the powder were taken on a Vickers projection microscope at a magnification of x400. Straight lines were drawn across six of the particles. The number of grains intercepted by the lines was counted, and the length of the lines measured with a ruler. The mean linear intercept was calculated by dividing the length of the lines by 400 x (the number of grains).

E2.3 Microhardness of the Powders

The polished specimens prepared for microstructural examination were used for microhardness testing using a Vickers microhardness tester. Twenty indentations were made in the B.S.A. powder, using a 20 g load. Ten indentations were made in the Hoganas powder, using a 10 g load.

E2.4 Particle Density

Particle density was determined using a Rees-Hugill flask[140]. This is a calibrated displacement flask (B.S. 2701). The flask was filled with xylene to just below its lowest mark. It was allowed to stand, with the stopper in place, for five minutes, to allow liquid in the neck to drain. A few drops of xylene were added to bring the level exactly up to the mark. 300 g of iron powder were added to the flask, a few grammes at a time. Powder in the neck of the flask was washed down by tilting the flask and rotating it. The stopper was replaced and the flask allowed to stand for five minutes. The level of the xylene was then read off the calibrated neck of the flask, and

the reading multiplied by 3 because the flask was designed for 100 g samples in the density range 2.0 - 2.7 g/cm^3, which gave the density of the powder in Mg/m^3. One determination was done on each powder, in the as-received state, using riffled samples. The riffled samples were slightly over 300 g. The excess was removed with a spatula from the top of the heap of powder while it was on the balance pan.

E2.5 Particle Shape

Particle shape was not determined quantitatively. A photographic record of particle shape has been made. Photomicrographs of polished cross-sections of particles were taken, using the samples prepared for microstructural examination as described in section E2.2.

Scanning electron micrographs of powder particles were taken; some of these were at high magnifications (up to x 100,000) to show the surface texture.

E2.6 Particle Size Distribution

A 100 g sample of each of the as-received powders was sieved on an Endecotts sieve-shaker, using eight sieves (150, 125, 104, 90, 75, 63, 53 and 45 micrometres aperture, respectively) for the B.S.A. powder, and six sieves (152, 106, 75, 64, 53 and 45 micrometres aperture) for the Hoganas powder *. The powder retained in the top sieve was emptied onto a sheet of paper; the sieve was inverted over the paper and rapped sharply several times. The powder was poured from the paper onto the pan of a Stanton 2nd-place top-pan balance and

* The original sieves were damaged and replaced in 1972.

weighed. The powder from the second sieve was added to that from the first, and the cumulative weight noted; and this was repeated up to and including the receiving pan at the bottom of the nest of sieves.

Size distributions were also determined microscopically using an Imanco Quantimet B image analysing computer. The size distributions of the made-up mixtures were determined, in addition to those of the as-received powders. Samples for this purpose were not riffled except for the Hoganas powder* ; random samples were mixed together and further random samples were taken from the mixture to give a sample weight of approximately 1 - 2 mg. This was added to a mixture of glycerol and xylene in a test-tube. The proportions of glycerol and xylene were adjusted to suit the particle size: the water-atomised fraction coarser than 150 micrometres was mixed with glycerol alone, while for the finest powder a ratio of approximately 3 parts xylene to 1 part glycerol was used. The volume of liquid was about 10 ml. The test-tube was partly immersed in the water tank of a Dawe Soniclean type 1141 B ultrasonic cleaner for five minutes to break up agglomerates. The mixture was stirred with a glass rod, and a drop of the mixture was transferred on the end of the rod to a microscope slide. The slide was placed in a vacuum jar and the pressure reduced to approximately 500 N/m^2 to remove air bubbles. After 30 minutes the slide was removed from the vacuum jar and a thin cover-glass placed on it. The slide was then placed on the stage of the microscope.

A x10 objective was used for those samples which were mainly finer than 300 mesh size, and a x3 objective for the others.

* Work on the B.S.A. powder started before the riffler had been constructed.

The instrument was set to scan 100 fields in a 10 x 10 square pattern, counting the number of particles having a chord in the scanning direction greater than each of six different preset values, and also the total number of particles. The preset values were 10, 20, 30, 40, 50 and 60 μm. Where more than ten particles having chords greater than 60 μm were detected, the same 100 fields were scanned again, with the minimum chord presets at 70, 80, 90, 100, 110 and 120 μm. Where more than ten particles greater than 120 μm were detected, the process was repeated with the size range extended to 180 μm; and if necessary, to 240 μm.

The total number of particles greater than each of the various chord sizes was then found by addition. These were converted to a percentage of the total number of particles detected in the sample concerned, to give a cumulative number percentage oversize size distribution.

The number size distribution of the Hoganas powder was converted to a mass size distribution by finding the number of particles in each size interval (by subtracting successive oversize totals) and multiplying it by the mass of a spherical particle having a diameter midway between the class limits. This was then converted back to a cum ulative oversize mass, and again represented as a percentage of the total mass.

For the synthetic size distributions of the B.S.A. powder, mean particle size by weight and standard deviation of particle size by weight were calculated, using the nominal mean size of each fraction from which the distributions were made up. The calculation was done on an Olivetti Programma 101 programmable calculator. The programme is shown in Appendix I.

E2.7 Segregation

The B.S.A. powders were kept in glass jars with screw tops. Each jar was shaken by hand for one minute. Segregation was visible as striations of different shades as seen through the jar wall. The jars were arranged in order of apparent degree of segregation, and the order was noted. No quantitative measurements were made.

E2.8 Apparent Density

Because the quantity of powder available was small for the synthetic size distributions of the water-atomised powder, non-standard apparatus was used. Powder was poured down a funnel into a flat-bottomed glass phial 49 mm tall, of 5200 mm^3 capacity. When the phial overflowed the powder was scraped off level with the top and the phial and powder weighed on a Mettler top-pan 2nd place balance, tared to the weight of the phial. The apparent density was obtained by dividing the weight of the powder by the capacity of the phial.

E2.9 Tap Density

The same phial full of powder at apparent density was tapped on the bench and further powder added; this was repeated until no further powder could be added. The powder was scraped off level with the top of the phial and the tap density found in a similar manner to apparent density.

E2.10 Compressibility

An empty Griffin and George 5 mm pellet press was placed in a compression loading attachment on a Hounsfield Tensometer fitted with

a 1 ton (Imperial) beam and a 10 kN scale. The press was loaded manually to 8 kN and unloaded, and the load-strain curve was plotted using a chart strain magnification of 16:1.

A weighed powder sample (0.269-0.279 g) was poured into the die of the pellet press. To minimise the effect of segregation during pouring, the press was vibrated for about 15 seconds by standing it on a metallurgical vibratory polishing machine. This also had the effect of compacting the powder to approximately tap density. The punch was then pushed into the press by hand. The press was replaced in the Tensometer and reloaded to 8 kN; the loading and unloading curves were plotted on the same chart as the previous (no powder) curves (Fig. 16). The distance between the two loading curves, at 1 kN load intervals, was measured and converted to the length of powder fill. The best straight line fit to the equation

$$\frac{1}{1 - M/LA\rho} = BP + \frac{1}{1 - D_o} \qquad \text{(from Kawakita}^{61}\text{)}$$

was calculated by the method of least squares, using an Olivetti Programma 101 programmable calculator. The programme used is shown in Appendix II.

In the equation

- B = a constant
- P = applied load ÷ punch cross-sectional area
- M = weight of powder
- L = length of powder compact at pressure P
- A = cross-sectional area of pellet
- ρ = particle density
- D_o = fractional density of compact at the intercept of the fitted line with the axis $\frac{1}{1 - M/A\rho L}$

Compressibility measurements were also made with larger quantities of both as-received powders using a production powder metallurgy press which had been modified and instrumented to give a record of the stress in the top and bottom punches, the strain on the die wall, and the top punch movement (Fig. 17). [72,141,142] The press is a single compression mechanically driven camshaft press with a floating die of 25.2 mm diameter. The powder was poured into the die from a hand-held scoop and excess powder was scraped off the top. The compacts were weighed after ejection. The change of density with pressure was calculated from graphs of top punch load against punch travel, made on an x - y recorder. A straight line was fitted to Kawakita's equation as was done for the measurements made on the pellet press.

E2.11 Compactibility

The pellets made in the Griffin and George pellet press for compressibility determination were ejected from the press by removing the bottom punch and forcing the top punch through the die, applying the necessary force on the Hounsfield Tensometer. The condition of the pellets on ejection was noted.

E2.12 Weight Specific Surface

The pellets made in the Griffin and George pellet press for compressibility determination were used for specific surface measurement before they were ejected from the die. Both punches were removed from the press. The combined weight of the die and the pellet was measured on an Oertling4th place single pan automatic balance; the known weight of the die was subtracted to find the weight of the pellet. The length of the pellet was calculated from the distance between the unloading curves on the Tensometer chart (Fig. 16) at a load of 0.2 kN.

The die and pellet were then used as a permeametry cell.

A simple atmospheric pressure air permeameter was constructed (Fig. 18). A 100 cm^3 burette was inverted over a beaker of deionised water. The level of the water was adjusted to the zero mark on the burette. A pipette filler was used to suck the water up to the top of the burette, and the tap was closed. The cell was then connected to the top of the burette by a rubber tube. The tap was opened, and air drawn through the cell into the burette by the f lling water. The time was noted as the water level fell past the 100 cm^3 mark, and at subsequent 10 cm^3 intervals. A graph of time against $\log_{10}$ volume was plotted (Fig. 19). The weight specific surface was calculated from the equation:-

$$Sw^2 = \frac{\left[1 - \frac{4M}{\pi\rho D^2 L}\right]^3 (T_2 - T_1) \quad \frac{\rho_w g \pi D^2}{4} \quad H}{K\eta\rho^2 L \left[\frac{4M}{\rho\pi D^2 L}\right]^2 \quad 2.303(\log_{10} V_1 - \log_{10} V_2)\ V}$$

where Sw = weight specific surface

M = weight of powder

ρ = particle density

D = diameter of cell

L = length of powder column

$\frac{T_2 - T_1}{\log_{10} V_1 - \log_{10} V_2}$ = slope of graph of time v. volume

ρ_w = density of water

g = gravitational constant

V/H = ratio of head of water to volume of water in the burette

K = a constant (the value used was 5)

η = viscosity of air

The derivation of this equation is given in Appendix III. The measurements were carried out at temperatures ranging from 294 K-299K (21°C - 26°C). In calculating the weight specific surface, the viscosity of air was taken to be 18.2 μN s/m^2 and the density of water 997.5 kg/m^2.

E3.0 Production of Strip

Strip was made from Hoganas powder on the B.S.C. pilot line at Shotwick. The procedure is described in the Introduction.

Strip was made from B.S.A. powder in quantities too small for the pilot plant roller-coating apparatus.

A solution was made of the following composition:

20 g Celacol DSM 450

5 ml glycerol

1 g Geigy inhibitor

0.5 ml Supronic

dissolved in tap water and made up to a volume of 1 litre. 165 g of iron powder were mixed with 65 ml of solution; the same proportions were used where different quantities were prepared. The mixture was stirred mechanically for 15 minutes. The viscosity was not measured.

Two different sizes of template were used to prepare flexistrip. The smaller, made of stainless steel, was 62 mm x 200 mm x 1 mm; the larger was 200 mm x 300 mm x 1 mm, made of glass with mild steel edging strips. Before use the steel template was wiped with a release agent which consisted of a 5% solution of oleic acid in methylated spirits; a 1% solution of Armid O* in isopropanol was used on the glass template.

* Armour Hess Chemicals Ltd., Westgate, Leeds 1.

The mixture of iron powder and binder solution, which was a slurry, was poured onto the template from a breaker, and scraped off above the level of the edging strips with a steel straight-edge. The template was then placed in an oven at 423 K (150°C) until the flexistrip appeared dry, as shown by a change of colour from dark grey to light grey. This took about 15 minutes. A scalpel was used to separate the strip from the edges of the stainless template; strip made on the glass template was removed without difficulty.

A two-high 300 mm diameter mill was used to compact the strip. A roll load intensity of 4.7 MN/m was used, except when the effect of roll loading was being investigated. The rolling speed was approximately 25 mm/s for the synthetic size distributions and for the as-received water-atomised strip processed at the same time. Subsequent samples were rolled at about 50 mm/s; the samples were too short for an accurate determination of the rolling speed.

For sintering, the green strip samples were supported by a nichrome frame. They were inserted into a cold zone of the furnace, in a hydrogen atmosphere, and held for one minute, then transferred to the hot zone, where they were held at 1453 K (1180°C) for 30 seconds. They were then returned to the cold zone of the furnace and held for one minute before removal from the furnace.

The rolling mill used for the first compaction was also used for the second compaction. The roll load intensity was 7.8 MN/m. The second sintering operation was the same as the first. The strip was not temper rolled.

E3.1 Annular Bend Testing of Flexistrip

A 40 mm square piece of flexistrip made from Hoganas powder was lightly clamped between two flat plates, 10 mm thick, in each of which was a circular hole 100 mm in circumference. The clamping bolts located the plates so that the holes were coaxial within 0.025 mm. A punch weighing 0.35 kg was carefully placed in one of the holes, so that it was supported by the flexistrip. The punch was 1 mm smaller in diameter than the hole for 3 mm of its length. The shaft of the punch was 0.1 mm smaller in diameter than the hole. This assembly was located on top of a 500 N compression load cell in an Instron mechanical testing machine. The crosshead was lowered at 0.0083 mm/s, forcing the punch through the flexistrip. The thickness of the disc of flexistrip was measured with a micrometer.

The test was repeated with, successively, 2, 3, 4 and 6 layers of flexistrip clamped together.

A section through the tool and strip is shown in Fig. 20.

E3.2 Tensile Testing of Flexistrip

A 10 mm square piece of flexistrip made from Hoganas powder was placed on the end of a piece of "Sellotape" so that 4 mm of the flexistrip overlapped the tape and adhered to it. A similar piece of tape was then placed on top of the first piece of tape so that the flexistrip was sandwiched between the tapes. Two further pieces of tape were stuck to the other end of the flexistrip. The tape was lightly pressed onto the strip to ensure good adhesion. One end of the tape was joined by a further length of tape to the crosshead of an Instron mechanical testing machine; the other end was joined to a 1 kg weight

resting on a 500 N compression load cell. The crosshead was raised at 0.0083 mm/s. The reduction of the load from an initial value of 9.8 N was recorded on the chart.

Four further pieces of strip were tested. The thickness of the flexistrip was measured by micrometer.

E3.3 Compressibility of Flexistrip

The compressibility of flexistrip was measured on the instrumented press used to measure the compressibility of powder. A sheet of flexistrip made from Hoganas powder was placed over the die and discs were blanked out by the punch and allowed to fall into the die, but not compressed. This was repeated until the die was full. The punch was then manually backed up to its standby position and the press was operated. A line was fitted to Kawakita's equation as was done for the powder.

E3.4 Compressibility of Celacol

6 g of Celacol powder were weighed out and poured directly into the die of the instrumented press. It was necessary to lightly precompact some of the powder to get all the powder into the die. The precompaction stress level was recorded, and in fitting a line to Kawakita's equation only that part of the graph which was at stresses above the precompaction stress level was used.

E3.5 The Effects of Roll Loading in the First Compaction Operation

Six pieces of flexistrip made from B.S.A. powder were cut to a tapered shape so that a constant roll force would give a varying roll

load per unit width of strip as the strip was rolled. These and six rectangular pieces were rolled on the pilot line rolls at roll loads ranging from 80 kN to 1010 kN, giving a range of roll load intensity from 0.66 kN/mm to 16.8 kN/mm. The strip samples were measured before and after rolling, using a ruler, to determine elongation and change in width.

Twenty tests were carried out on the compacted strip, using samples representing the full range of roll loading, with the annular bend test tool described in section E3.1. A single layer of compacted strip was used in each test. The disc and conical annulus of strip punched out during the test were weighed. The thickness of the disc was measured by micrometer at four points near the circumference, and at the centre; the mean thickness was calculated, and from it the density and strength. In the case of test pieces taken from tapered samples the roll load intensity was calculated for the centre of the test piece.

E3.6 Measurement of Strip Speed During Rolling

The circumference of each of the rolls on the two-high rolling mill was measured with a steel tape. These rolls were cylindrical, not cambered. A mark was made on the top roll and the time for one revolution was measured by stopwatch. Six revolutions were timed, and the mean peripheral speed was calculated.

A distance of 400 mm was measured out and marked on the run-out table and on the feed-in table. Strip 205 mm wide, made from sponge iron powder, was rolled continuously, under a total roll load of 660 kN. The time for a given point on the strip to pass through the marked out 400 mm was measured five times on the entry side and six

times on the exit side. The mean speed of the strip on entry and exit was calculated.

E3.7 The Effect of High Compaction Rate

Flexistrip samples made from Hoganas powder have been compacted under the impact of a falling weight. The tensile test jig shown in Fig. 21 was modified by removing the chain and the grips. The base of the machine was clamped to a massive block of steel. A piece of flexistrip was placed on the bottom plate. The trolly was raised to 119 mm above the specimen and allowed to fall on the specimen under its own weight. The energy of the trolly was calculated from its weight and the distance through which it fell. The specimen was weighed, and measured by micrometer, to find its density. The experiment was repeated with a range of sample weights from 0.05 g to 0.35 g, giving a range of energy/mass from 3 J/g to 30 J/g.

The work done in low speed compaction was calculated by graphical integration from the pressure v. punch displacement graph obtained during the measurement of flexistrip compressibility, described in section E3.3.

E3.8 Properties of Green Strip

Tensile tests were carried out on strip made from Hoganas sponge iron powder on the pilot line. The test pieces were cut out with a scalpel, and were rectangular, 60 mm long (in the direction in which the tensile stress was applied) and 100 mm wide. The tensile testing jig shown in Fig. 21 was used. This was designed so that test pieces could be fixed in the grips without damage. The test pieces were clamped in the moving grip, 5 mm being allowed for grip length.

The moving grip was then lowered until 5 mm of the test piece was within the open lower grip, and this was then clamped onto the specimen, giving a gauge length of 50 mm. Both sets of grips were lined with neoprene to grip the test pieces without damage. The slight compression of the rubber between the grip and the strip caused it to exert an initial compressive force on the strip. The tests were carried out on an Instron mechanical testing machine at a strain rate of 0.0083 mm/s. After fracture the thickness of the specimen was measured with a micrometer at four positions across the width near the fracture, and the mean thickness was calculated. Ten longitudinal samples and ten transverse samples were tested.

Two pieces of mild steel bar 9.4 mm in diameter were machined so that each had one end shaped to fit the grips of a Hounsfield Tensometer and the other end flat at right-angles to the axis of the bar (Fig. 22). The flat ends were smeered with Araldite X83/521*. An oversized piece of green strip was placed between the ends, which were pressed together and rotated to spread the resin evenly over the strip. A spring clamp was placed over the ends of the bars to press them lightly together, and the assembly was placed in a supporting jig which held the bars coaxial. This was then placed in an oven, set at 433 K (160°C) for 40 minutes. The specimen was then allowed to cool freely in air. The clamp was removed and the excess strip and resin were rubbed off with 240 grade silicon carbide paper. The strip was then tested by applying tension at right-angles to the plane of the strip, i.e. along the axis of the bars, using a Hounsfield Tensometer.

* CIBA (A.R.L.) Ltd., Duxford, Cambridge.

The load was applied manually. After testing the flat ends the bars were re-machined for the next test. Ten tests were done on sponge iron strip. Two tests were carried out without any green strip to find the strength of the resin or the resin-steel bond. Ten scanning electron micrographs were taken of the fracture surfaces at a magnification of X1100. These were examined for signs of broken interparticle bonds.

Ten single-layer annular bend tests were carried out on the strip using the procedure described in section E3.1.

One annular bend test was also carried out on each of the synthetic size distributions of the B.S.A. water-atomised powder. For these tests the tool used for the other annular bend tests was used, but a bottom punch was incorporated (Fig. 23). The tool was mounted in a vertical Hounsfield Tensometer fitted with a 30 kgf beam. The zero was offset to allow for the weight of the bottom punch, which was clamped to the strip by means of bolts joining it to the top punch. The load was applied manually. The strip thickness was measured by micrometer. The sheared-out discs were weighed and the density was calculated.

Macrohardness was measured in six positions on each of the discs produced from the water-atomised powder, using a Vickers hardness testing machine with a load of 5 kg.

Transverse and longitudinal sections of green strip made from each of the synthetic size distributions of water-atomised powder were mounted together in Araldite epoxy resin, and held under vacuum for 15 minutes to allow the resin to penetrate the pores. They were polished finishing with 1 μm diamond paste, and examined unetched on

the Quantinet "B" image analysing computer. A X10 objective was used with a blank frame height of 100 lines and area 1000 area units. This gave a line length of 8.7 mm for each frame. 50 frames were examined on each transverse section, and the projection P and detected area A were measured. The mean linear intercept I in micrometers was calculated for each frame as $\frac{87}{10P/A - 1}$. The derivation of this expression is given in Appendix IV.

Using an Olivetti Programma 101, the mean $\bar{I}$ and the standard deviation σ of the mean linear intercept were calculated for each strip sample. The parameter $\sigma N/\bar{I}^2$ was then calculated, N being the total number of intercepts counted for the particular strip sample concerned, and this parameter was taken to be a measure of the degree of segregation. The derivation of this expression is also given in Appendix IV.

The discs produced by the annular bend test on strips B, I, P, Q, W and Y were used to measure the permeability of green strip, using the apparatus described in section E2.12, with the exception of the permeametry cell. This was formed by clamping the discs tightly between the top and bottom punch of the annular bend test tool; the circumference of the disc was sealed with adhesive tape (Fig. 24). The punches have concentric 17.5 mm diameter holes through them, and thus a 17.5 mm diameter permeametry cell was formed. The total weight specific surface of the green strip, including that of the binder, was calculated, using the assumptions that the binder was present in the form of discontinuous pieces of film, and did not close off any of the pores, and that the theoretical density of the iron powder/binder mixture at zero porosity was 7.37 Mg/m^3.

E3.9 Properties of Sintered Strip

Areas of relatively uniform thickness were selected on the strip samples prepared from B.S.A. powder. The selected areas were all about 10 mm from the edge of the samples. The thickness was measured by micrometer. A disc of 6.5 mm diameter was punched from each selected area, and weighed; the density was then calculated from the weight and volume.

The hardness of the strip was tested at four positions near the edge and at four positions near the centre using a Vickers hardness testing machine with a load of 1 kg. Values for the edge, the centre and overall were calculated.

The permeability of sintered strip P was measured by the technique used for green strip. The theoretical density was assumed to be 7.84 Mg/m^3.

E3.10 Compressibility of Sintered Strip

Compressibility was measured on strip made from sponge iron powder and from water-atomised powder 'as received'. A disc of 14.75 mm diameter was punched out from a piece of strip in the as-sintered condition. This was compressed between two punches of that diameter in a cylindrical die at a load of 9.1 kN. It was then removed and its thickness measured by micrometer. It was replaced in the die and repressed, the load increasing by 9.1 kN (20000 lb) each time, up to a maximum load of 100 kN. The die was weighed and its density calculated.

A 12.7 mm diameter tool of stronger construction was used to attain higher pressures. In this experiment a new disc of B.S.A. strip was used at each pressing load. The highest load was 300 kN. The discs were weighed and measured, and the densities calculated.

E3.11 The Effect of Roll Loading on Sintered Strip

A length of 200 mm wide sintered strip was made on the pilot line from sponge iron powder. This was cut into 300 mm lengths and these were rolled at a series of roll loading intensities up to 5 MN/m, using the two-high 300 mm diameter rolling mill. A similar experiment was also done on the 350 mm diameter rolling mill at roll loading intensities up to 8.1 MN/m. A 100 mm wide piece of the same strip was rolled on the 350 mm diameter mill at 10.3 MN/m calculated roll loading intensity, but despite the roll camber the rolls were observed to touch each other at both sides. After rolling the strip samples were weighed. Length and breadth were measured with a ruler. The thickness was measured by micrometer, at four places across the strip width, and the mean thickness was calculated. Density was calculated from the dimensions.

E3.12 Properties of Strip that has been Sintered and Re-Rolled

The hardness of strip made from B.S.A. water-atomised powder was tested as described in section E3.9 for sintered strip.

The mean linear intercept between grain boundaries was determined on strips I, P, Q, R, S, T, U, V and X, using transverse sections. These were mounted in Araldite epoxy resin as described in section E3.8 for green strip, polished to ¼ micrometre diamond and etched with 2% nital for 20 seconds. The number of intercepts on a 0.2 mm straight

line was counted in five positions in the plane of the strip and five positions normal to the plane of the strip; the mean distance between intercepts was then calculated.

Densities were determined as described in section E3.9 for sintered strip.

E3.13 Properties of Strip that has been Sintered Twice

Strip made from B.S.A. powder was hardness tested as described in section E3.9.

Tensile tests were carried out on parallel strip samples 10 mm wide, the gauge length being 25 mm. The test pieces were necked slightly towards the centre. The edges of the samples were smoothed with 600 grade silicon carbide paper. Tests were done on longitudinal samples from both edge and centre, and on transverse samples. An Instron mechanical testing machine was used. The strain rate was 0.083 mm/s.

Density determinations were done on both edge and centre samples from the strips. Samples approximately 12 mm x 25 mm were cut from the strip with scissors. A 6.5 mm diameter hole was punched out of each specimen. The specimens were weighed, cut and reweighed until the weight of the specimen was between 0.50 g and 0.51 g. They were washed in acetone and dried, and reweighed on an Oertling single pan automatic fourth place balance.

A glass tube 1 m long, 40 mm diameter, was clamped in a vertical position and the lower end sealed (Fig. 25). The tube was filled with deionised water which had been distilled once. A coiled glass tube

was placed round the top of the vertical tube, and warm water was circulated through it. The water was stirred occasionally with a glass rod, and the temperature gradient in the water column was checked with a thermometer. When a temperature gradient of between 10 K/m and 20 K/m was achieved, not necessarily uniformly, the heating coil was removed.

A calibrated glass float was hooked onto a coated strip sample. The calibration of the float is described in Appendix V. The float and sample were lowered into the water in the temperature gradient column, and released below the surface. They were visually inspected to see if any air bubbles adhered to either float or specimen. If so, the air bubbles were dislodged with a glass rod, or the float and specimen were withdrawn from the water and re-immersed. The float was allowed to sink in the water until it reached a position where the density of the water was equal to the effective density of the specimen-float composite, where it remained stationary. An E-Mil Gold Line thermometer covering the range 268 K to 323 K (-5°C to 50°C) graduated in 0.1 K intervals, was lowered into the water until the bulb of the thermometer was level with a mark on the float. The temperature was read to 0.05 K.

After determination of the approximate flotation temperature using the temperature gradient column, a more accurate determination was done in a conical flask. The water in the flask was heated to 333 K (60°) and allowed to cool. This minimised the formation of air bubbles on the specimens. When the water reached a temperature 3 K higher than predetermined flotation temperature, the thermometer was used to test the uniformity of the temperature. If the temperature

range was more than 0.2 K, or if there was a temperature inversion (the water at the top being colder than the water at the bottom), the water was stirred. The specimen and float were then lowered into the water and released below the surface; they sank to the bottom. When the water had cooled further, the float and specimen rose from the bottom. The temperature of the water, level with the mark on the float, was noted, and the uniformity of the water temperature tested as before. In the event of excessive water temperature variation, the water was heated about 3 K and the test was repeated. The porosity was then calculated as described in Appendix V.

Longitudinal and transverse sections taken half-way from edge to centre of each strip made from B.S.A. powder were mounted in thermo-setting resin. They were polished finishing on 1 micrometre diamond and etched in 2% nital for 15 seconds. The number of grain boundary intercepts on each of 6 lines was counted. Each line was 158 micrometres long. Two of the lines were in the plane of the strip, two normal to the plane of the strip, and two were at 45^{o} to the plane of the strip. The mean linear intercept was found by dividing the total length of line examined (0.948 mm) by the number of intercepts.

RESULTS

R1.1 Chemical Composition of the Powders

The chemical compositions of both as-received powders are shown in Table 3. The Hoganas powder is of higher purity than the B.S.A. powder, having a lower content of each of the elements detected.

R1.2 Microstructure of the Powders

The microstructures of the powders are shown in Fig. 26. The B.S.A. powder consists of two different types of particle, one light etching with grains of the same size as the particles (some of these have fine grains on the particle surface) and one dark-etching with fine grains. The grain size of the fine-grained particles is about 2.5 μm (Table 4). Few internal pores are visible, and there are few inclusions. The grain size of the Hoganas powder is the same as the particle size. There is considerable porosity and the volume fraction of inclusions is greater than in the B.S.A. powder.

R1.3 Microhardness of the Powders

The fine-grained B.S.A. powder was found to be harder than the coarse-grained powder, but both varied widely. The highest value was 484 and the lowest 222. The Hoganas powder was softer, ranging from 116 to 257. The mean values are shown in Table 4.

R1.4 Particle Density

The density of the Hoganas powder is higher than that of the B.S.A. powder (Table 4).

R1.5 Particle Shape

Photomicrographs of sections through both types of powder are shown in Fig. 26. The Hoganas powder is more irregular and contains considerable porosity. In some cases this porosity is coarse, while in other cases it is very fine, with pore diameters of about 1 μm. Scanning electron micrographs of both types of powder are shown in Fig. 27. The Hoganas powder again appears more irregular, and in some cases intricately convoluted. Both powders have a smooth surface with a rounded appearance.

R1.6 Particle Size Distribution

Particle size distributions by weight are shown in Table 5 and Table 7; these are represented graphically in Fig. 28. The B.S.A. powder is coarser than the Hoganas powder, which is mainly finer than 350 mesh B.S. sieve size. The size distribution of the Hoganas powder is skewed, with a large proportion of the mass nearer to the upper size limit than the lower. Size distribution by number is shown in Table 6.

A statistical analysis of the synthetic size distributions of B.S.A. powder is shown in Table 8. In the group F, P, Q, R, S the mean diameter of S is significantly smaller than the mean diameter of the others in the group. In the group M, W, X, the mean diameter of X is significantly larger than that of M and W. The size distribution by number does not show this; on the contrary, it indicates that X is significantly finer than M and W.

R1.7 Segregation

The ranking order of increasingly obvious segregation is shown in Table 9. No visible segregation was seen in the Hoganas powder. The segregation was particularly severe in F, R, A, T, Q, and S.

1.8 Apparent Density

Apparent densities are shown in Table 10. They range from 2.5 Mg/m^3 for B to 3.5 Mg/m^3 for S. In the group F, P, Q, R, S, the apparent density initially falls with increasing range of size distribution, and then rises again. In the group I, T, U, V, the apparent density increases with increasing range; M, W and X have all the same apparent density. The single cut sizes B, F, I and M show an increase in apparent density with decreasing mean particle size.

R1.9 Tap Density

Tap densities are shown in Table 10. They range from 2.8 Mg/m^3 (B) to 4.7 Mg/m^3 (V). In the group F, P, Q, R, S, having a mean particle size of about 80 μm, the tap density shows a slight decrease and then a large increase with increasing range of size distribution. The groups having means of 50 and 20 μm both show continuously increasing density with increasing spread of size distribution. The single cut sizes show increasing tap density with decreasing size.

R1.10 Compressibility

The slope of the line fitted to Kawakita's equation, and the density at the intercept of the line with the porosity axis, are shown in Table 10. The intercept densities are similar to the tap densities, although generally somewhat lower. Both the larger groups (80 and 50 μm

mean diameter) show an initial decrease of intercept density with increasing spread of size distribution, and an increase in intercept density with further increase of range of size distribution. The group having a mean diameter of about 20 micrometres shows an increase of intercept density with increase of range. The slopes follow a similar pattern to the densities. Some typical graphs are shown in Fig. 29.

R1.11 Compactibility

Compactibilities are shown in Table 9. M and X were in two pieces on ejection, the plane of fracture being at right-angles to the axis of the cylinder. Q and Y were powdery on the bottom face. S, T, U and W were powdery round the bottom edge. Only the Hoganas compact was not visibly defective in some way, all the others having surface regions of loose powder.

R1.12 Weight Specific Surface

The graphs from which the specific surfaces were calculated are shown in Fig. 19. The calculated values are shown in Table 9. These show an increasing surface area with decreasing particle size. The MH300.25 powder has a similar specific surface to V.

R2.1 Annular Bend Testing of Flexistrip

Where more than one layer of strip was tested, the fracture surface was slightly conical. No allowance was made for this in calculation. The sheared out discs were slightly convex on the side away from the punch. The calculated maximum stress values are shown in Table 11. They appear to have a minimum value with three layers, the single-layer value being greater than that for six layers.

The equations used and the approximations involved are given in the discussion (section D3.1).

R2.2 Tensile Testing of Flexistrip

In all five cases the flexistrip failed by tearing from one side to the other. The results were all similar, and the mean value was 0.27 N/mm^2 (Table 11).

R2.3 Compressibility of Flexistrip

The graph is shown in Fig. 29; the slope and intercept density are listed in Table 12.

R2.4 Compressibility of Celacol

The graph is shown in Fig. 29; the slope and intercept density are listed in Table 12. That part of the graph which was omitted because of the necessity for precompaction would have shown a steeper initial slope than the graph has as plotted. No allowance was made for this in fitting the line.

R2.5 The Effects of Roll Loading in the First Compaction Operation

The annular bend strength, density and elongation resulting from various roll loading intensities are shown in Table 13. The bend strength increases with loading up to 4 MN/m, and fluctuates between 31 N/mm^2 and 16 N/mm^2 at higher loadings as shown in Fig. 30. The density follows a similar pattern, the maximum value being 7.3 Mg/m^3, as shown in Fig. 31. A graph of annular bend strength against density (Fig. 32) produces a smooth curve of increasing slope.

Elongation increases to a maximum of 19% at 4.4 MN/m, and is less at higher loadings.

R2.6 Measurement of Strip Speed During Rolling

The strip speed was greater leaving the rolls than entering the rolls, but both speeds were slower than the peripheral speed of the rolls (Table 15). The increase of strip speed at the exit side of the rolls corresponds to an elongation of 2%.

R2.7 The Effect of High Compaction Rate

The energy used in compacting to four different densities is shown in Table 16. This is compared with the work done in die compaction in Fig. 33. Very much less work is done in die compaction for any density below 5.9 Mg/m^3.

R2.8 Properties of Green Strip

The mechanical properties of green strip made from Hoganas powder are listed in Table 17. The tensile strength is lowest in the transverse direction and highest in the normal direction; the strength in annular bending is higher than any of these. Both the annular bend test and the tensile test normal to the plane of the strip give good reproducibility; the other two tensile tests give greater standard deviations in proportion to the mean strengths.

The standard deviation of the mass per unit area is 4% of the mean value, but that of the density is only 2% . Above-average density was associated with above-average mass per unit area.

The fracture surfaces shown in Fig. 34 do not include any visible ductile fractures of interparticle bonds. Fig. 35 shows a transverse fracture surface in green strip made from water-atomised powder A. The particles do not appear to have been deformed, and are not packed together as closely as in the case of the sponge iron strip shown in Fig. 34.

The strips made from water-atomised powder varied considerably in thickness (Table 18) but were of comparatively uniform density. B, P, R, S and V had good annular bend strength (above 15 N/mm^2) but the others were weak. Macrohardness varied from 132 to 76 (HV/5) and seemed not to correlate with either bend strength or density. The segregation index varied from 0.55 (Q) to 1.68 (V). The pattern of variation of segregation index with size distribution is similar to that observed for density and compressibility in Table 10.

The weight specific surface of the green strip is much higher than that of the powder, ranging from 0.11 m^2/g (B) to 0.46 m^2/g (Y). There is an increase in weight specific surface with a decrease in particle size.

R2.9 Properties of Sintered Strip

Table 19 shows the properties of the sintered strip made from B.S.A. powder. Densities vary more widely than for green strip and on average are lower by 80 kg/m^3. Hardness does not seem to be a function of density. The calculated weight specific surface of P is higher than that of the powder by a factor of 3.

R2.10 The Compressibility of Sintered Strip

Both types of strip increase in density with increasing pressure up to 580 N/mm^2. The increase in density in the Hoganas strip was slightly greater than that in the B.S.A. strip. At this pressure there is 6.4% porosity in the Hoganas strip and 9% porosity in the B.S.A. strip (Table 20).

The punch used to achieve the high pressures was found to be slightly bent after pressing at 1970 N/mm^2 and badly bent after pressing at 2360 N/mm^2. The highest density attained was 7.35 Mg/m^3 at 1580 N/mm^2. This corresponds to 6.25% porosity.

R2.11 The Effect of Roll Loading on Sintered Strip

Table 21 shows a considerable variation in the effect of loading on density. The general trend is to increase in density up to a certain load intensity - 3.1 MN/m for the 300 mm diameter rolls, 5.2 MN/m for the 350 mm diameter rolls - and not to increase in density with further increases in loading. The highest density achieved with the 300 mm diameter rolls was 7.42 Mg/m^3 (5.4% porosity), and with the 350 mm diameter rolls, 7.52 Mg/m^3 (4.1% porosity).

The elongation resulting from the rolling operation also varies considerably, but shows a general trend to increase with increased roll loading.

R2.12 Properties of Strip that has been Sintered and Re-Rolled

Table 22 shows the grain-size, hardness and density of second-compacted strip made from B.S.A. powder. The grain size is relatively uniform. The edge hardness is higher than the centre hardness in 9 out of 15 tests; the lowest mean hardness is 188 and the highest 233 HV/1.

The highest mean density is 7.6 Mg/m^3, and the lowest, 7.2 Mg/m^3, corresponding to 3% porosity and 9% porosity, in M and Y respectively. Hardness and density do not seem to vary systematically with particle size distribution.

R2.13 Properties of Strip that has been Sintered Twice

Grain size, hardness and density of second-sintered strip are shown in Table 23. S, X, and Y have relatively large grains. In 10 out of 14 cases, the centre of the strip is harder than the edge. Mean hardness ranges from 136 (P) to 95 (Y). In 10 out of 14 cases, the edge of the strip is denser than the centre. A and P had the highest density, 7.81 Mg/m^3 (0.5% porosity) and Y had the lowest, 7.67 Mg/m^3 (2.3% porosity). The results of the tensile tests (Table 24) are of uncertain accuracy, because the test pieces varied in thickness along the gauge length. Six broke outside the gauge length; seven of the others broke so that significant part of the elongation was outside the gauge length. Four of the remainder failed by tearing in such a manner that the elongation could not be measured accurately; mean values of the relatively good tests are shown.

Table 24 shows that longitudinal yield stress values are generally higher than transverse, and edge values higher than centre values. The tensile strengths do not differ to the same extent. The highest mean ultimate stress was 405 N/mm^2 (V) and the lowest, 256 N/mm^2 (B).

Elongation varied from 3% (B) to 18% (X). The elongation of the transverse test piece of X was 27%. In general the properties of the strips made from coarser powder (B, F, P, Q, R and S) are slightly inferior to those of the other strips.

DISCUSSION

D1.1 Sampling

The use of a spinning riffler for powder sampling is believed to give the most representative sample[143]. The Pascal sample divider rotated more slowly than the 48-compartment riffler. Nevertheless, the total number of revolutions of the divider during the sampling process was large. Charlier and Goossens[144] have shown that the sample will be representative as long as the divider rotates sufficiently often during the sampling process so that the amount of powder delivered during one revolution is small compared with the volume of the segregated regions of the powder in the delivery hopper.

The sampling procedure used on the B.S.A. powder will not necessarily produce a sample representative of the rest of the powder. Sampling procedures which involve halving the sample at each stage (e.g. coning and quartering, or chute riffling) necessitate repeated transfer of the powder from one container to another. Where the same batch of powder is sampled repeatedly this is likely to lead to a loss of fines. The fines may be lost in crevices in the apparatus, blown away when filling from a funnel, or simply adhere to the surface of the apparatus when the remainder of the sample is removed. Hence a sampling procedure which gives the required sample size in the least number of operations is preferred.

It is feasible to arrange that a riffled sample shall be any desired weight but this was not done as it would have involved more handling of the powder.

D1.2 Production of Controlled Size Distributions

It is undesirable that two different mechanisms - sieving and air classification - should be used for size fractionation of the powder. Unfortunately, the Alpine air classifier cannot deal with iron powder particles heavier than about one microgramme, which for spherical particles corresponds to a diameter of about 0.06 mm (Fig. 36).

The exact size of an irregular particle depends on how the term 'size' is defined. The size measured by the air classifier is the diameter of a spherical particle which when falling through air has the same ratio of mass to air resistance. The size measured by sieving is the size of the aperture through which the particle just passes. This is, in effect, the largest dimension at right-angles to the longest axis of the particle. In practice, some particles which could pass through a sieve are not presented to a sieve aperture appropriately orientated during the sieving process, and so there are always some undersize particles in the oversize fraction. Oversize particles may be found in the undersize fraction if the sieve mesh is non-uniform; older sieves are likely to be worse in this respect. The sieves used were old.

The original intention was to produce a set of log-linear size distributions: that is to say, the size distributions were to be composed of equal weights of powder occupying equal intervals of the logarithm of size. This is easily done in terms of sieving, as the sieves are arranged at equal log size intervals. However, there was not enough fine material to do this, and so the fine material is graded in successive size ranges in which each cut size is about 1.8 times the next lower size; for the sieve sizes the ratio is only 1.189.

Because for both the fine material and the coarse material there is powder in each fraction which is either larger or smaller than the nominal cut sizes, none of the size distributions produced are exactly log-linear. The log-linear relationship is approximated best by those size distributions which are made up of sieved material only, and fairly well by those which are made up of air-classified material only. The original intention was that blends of large mean particle size should have a similar ratio of sizes to those of small mean particle size, and so be comparable except in absolute size. This was not achieved.

D2.1 Chemical Composition of the Powders

The B.S.A. powder might reasonably be described as mild steel powder, while the Hoganas powder is of higher purity than typical mild steel. Probably the most important difference between the two lies in the hydrogen loss, as the reduction of surfaces in contract may lead to more active sintering. However, other factors affecting the sintering activity are so many and varied between the two powders that any such effect would be difficult to detect.

D2.2 Microstructure of the Powders

That part of the B.S.A. powder which is coarse-grained has, in many cases, some fine grains on the surfaces of the particles. This also happens with some of the relatively solid Hoganas particles. In this respect the two powders are quite similar. There is, however, far less porosity in the B.S.A. powder. That part of the B.S.A. powder which is fine-grained has a structure which was not easily resolved. It is possible that the two types of particle in the B.S.A.

powder represent two different batches, one of which was annealed more thoroughly than the other.

D2.3 Microhardness of the Powders

The microhardness of the powders may be significant in so far as it may affect the compressibility. Although at low loads much of the densification results from particle re-arrangement, particle deformation becomes significant at high pressures, and Evans and Smith[145] have shown that there may be an increase in particle hardness if high loads are used in compaction, while Brackpool[66] has shown that work hardening affects the compressibility. Therefore it would be expected that the B.S.A. powder would be less compressible at high loads than the Hoganas powder.

D2.4 Particle Density

The higher density of the Hoganas powder indicates that the porosity shown in the photomicrographs (Fig. 26) is largely open porosity. It is possible that some of the fine open pores were not filled with xylene, and that the density of the particles is higher still. Methods relying on impregnation with a liquid are usually unreliable in this matter; the use of a gas pycnometer should in theory give more reliable results[146].

D2.5 Particle Shape

The more irregular shape of the Hoganas powder would seem likely to make it more compressible; however, it would also tend to produce a lower initial density. The possibility of producing a greater density by re-arranging the particles is clearly higher than for the

B.S.A. powder; however, such re-arrangement would be more difficult as the irregularities would impede relative movement of the particles. They would however, facilitate particle interlocking, and might, therefore produce a higher green strength than would be obtained from the B.S.A. powder at the same green density. The larger surface area of the Hoganas powder should lead to faster sintering.

D2.6 Particle Size Distribution

The sieve series used for determination of the size distribution of the B.S.A. powder was damaged subsequently and so a different series was used for the Hoganas powder. This has not affected the results because 99% by weight of the Hoganas powder is finer than 75 μm. The conversion from number size distribution to mass size distribution[147] gives an apparently coarser particle size. This is to be expected because the particles are not spherical and the measuring technique is different[148]. The Quantimet measures the longest chord of the projection of the particle in the direction of scanning[149]. The measured particles will normally have settled on the slide with the smallest dimension of the particle normal to the slide. Hence, the smaller dimension of a particle as viewed will be the one which determines the size of sieve aperture through which it will pass. Thus, the more irregular the particles, the greater the difference between the size distribution as measured by Quantimet and by sieving. The size distribution by number indicates that powder S is considerably finer than was intended. A possible source of this error is in the counting errors resulting from the more irregular particles, where surface irregularities may be counted as separate particles[150]. If this is indeed the explanation, then the size distribution may in fact be as intended.

D2.7 Segregation

There is no evidence that the segregation noted in the dry powder is carried over to the strip. In particular, there is no correlation with the microsegregation reported in the results in section R2.8 (Table 18).

D2.8 Apparent Density

Pearson and Hirschorn[51] reported that for single cut sizes the apparent density increased with increasing particle size. The present result is the opposite of this. The most probable explanation is that interparticle friction is greater for the coarser powder. The weight specific surface of the fine powder (Table 9) is nearer to that of spherical powder (Fig. 36) than is that of the coarse powder, and this supports the hypothesis that the coarse powder is more irregular.

Dexter and Tanner[151] found that for mixed spheres with log-normal size distributions apparent density increased linearly with increasing standard deviation. They did not, however, use a continuous range of sizes, but mixed various sizes of ball-bearings. The size distributions used in the present investigation have less central tendancy than log-normal and are skewed towards the coarse side of the logarithmic mean. The particles used are not spherical. It is, therefore, not surprising that the results differ from those of Dexter and Tanner.

The trend of initial decrease and subsequent increase of density with increasing standard deviation is easily explained. Particles of identical size may have a degree of short-range ordering with which particles of slightly greater or smaller size will interfere, and the

packing efficiency will decrease. Furthermore, a wide range of particle size will permit interstitial packing of the particles. Thus the use by Dexter and Tanner of discreet sizes of spheres rather than a continuous range of sizes may have precluded the decrease in apparent density because of segregation and short-range ordering in groups of large and small balls.

D2.9 Tap Density

Hausner[152] has described the ratio of tap density to apparent density as a friction index, reasoning that low apparent density results from friction between particles. As in the present investigation, the coarse particles are more irregular than the fine particles, it would be expected on this basis that the ratio of tap density to apparent density would be greater for coarser powders. This is not found to be the case here. Brackpool[66] found that the ratio was greater for powders of high specific surface, and this is found to be the case in the present investigation. It is possible that this depends on the size distribution rather than on the specific surface as such, the large range of sizes permitting a greater densification by particle re-arrangement.

D2.10 Compressibility

The surface finish of the die wall of the Griffin and George pellet press was not good. Consequently, there was considerable die-wall friction, not only with the powder but also with the punch.

The first attempts to use the instrumented production press to measure the pressure-density relationship of iron powders produced graphs of much the same shape regardless of the powder or lubricant used.

These graphs were characterised by an inflexion at about half the maximum pressure and in some cases appeared to indicate that the pressure decreased as the density increased. This was attributed to the cam profile, which was checked with a dial-gauge and found to have an arc through which the punch travel increased rapidly, followed by an arc of relatively little movement, and then a final arc of more rapid movement. The cam was built up with weld metal and hand ground to a better profile; it is still not perfect.

The load-strain characteristic of the press is not linear. To correct for this it is necessary to compare graphs produced by compaction of powder with a graph produced by directly impacting the top punch on the bottom punch. This correction is likely to produce an error of up to 2% because of the small scale of the graphs produced. The scale of the graphs is limited by the speed of the pens on the x-y recorder.

Nevertheless, the compressibility measurements made on the instrumented press are likely to be more accurate than those made with the pellet press. This is because the compacts have a lower length to diameter ratio; the surface finish of the tools is much better; the length of punch in contact with the die is proportionally much less; and a floating die is used. All these factors serve to reduce friction. It would be expected, therefore, that the slope of the compressibility graphs would be steeper, and this is found to be the case.

It is unfortunate that the pressures used were not high enough to produce compacts of the same density as was reached in rolled strip. This is because of the limited strength of the tooling. Brackpool[66]

has indicated that die wall friction is less significant at very high pressures, and so greater accuracy would have been attained. The applicability of Kawakita's equation to the materials used in the present investigation has not been established for pressures above 400 N/mm^2. However, correlation coefficients up to 0.999 have been obtained with powder A, and Brackpool has reported correlation coefficients of up to 0.999965 over a larger range of pressures. There is no doubt that Kawakita's equation fits the data well over the range investigated.

The trend of density to first decrease and then increase with increasing standard deviation at a constant mean particle size is brought out clearly in the compressibility data, and particularly by the density of the green pellets. This shows that particle packing plays an important part in the densification process.

D2.11 Compactibility

There is a degree of qualitative correlation between compactability and green strength (Table 18). This is to be expected because a compact which disintegrates on ejection from the die is clearly not very strong.

D2.12 Weight Specific Surface

Two methods are in general use for determination of the specific surface of powders. These are the B.E.T. method[153] and the permeability method [154]. The B.E.T. method, named after Brunauer, Emmett and Teller[155] who devised it, is based on the adsorption of gas onto clean surfaces at low temperatures, and relies on the measurement of the amount of gas required to form a monomolecular layer on the surface of

the powder. Although reproducibility is good for powders having surface areas of about 1 m^2/g, for powders of about 0.02 m^2/g, as in the present case, reproducibility is poor unless particularly sophisticated procedures are used. The adsorption of dyes or fatty acids from dilute solutions is also used[156].

The permeability method measures the resistance of a packed bed of particles to the flow of a fluid. It involves assumptions about the shape of the passages through which the fluid flows, and these assumptions may be invalid, particularly for irregular powders or powders of a wide particle size range. Simple methods give a value for specific surface which varies with the porosity of the bed[157]. The method usually measures only the "envelope" surface area, and does not take account of fine surface irregularities or blind pores. It can be made more accurate by using low-pressure gas as the permeating fluid[158].

If assumptions can be made about particle shape, it is possible to calculate the specific surface from the particle size distribution [153, 159].

In the present investigation it was intended that the surface area determination should be an indication of particle shape, and a measure of the surface energy available to promote sintering. For the latter purpose the "heat of wetting" method[160] is, in principle, ideal. This method measures the energy change when particles suspended in the saturated vapour of a liquid are lowered into the liquid. Unfortunately, the method is unsatisfactory for powders of low specific surface, because the energy change is small.

The permeability method adopted is not ideal but it has two major advantages: it is simple and it gives high reproducibility.

A variation of 3% has been found with powder R, and this is attributed to segregation of the powder within the bed.

The results show that the coarse powder is more irregular than the fine powder, and comparison of the MH 300.25 with powder T (which has a similar size distribution) indicates that the Hoganas powder is more irregular, as is confirmed by the micrographs (Figs. 26 and 27).

D3.1 Annular Bend Testing of Flexistrip

The tool with which this test was carried out was originally designed as a shear test tool. The intention was to produce a strength test for flexistrip and green strip which obviated the difficult edge preparation then believed to be necessary for tensile testing. Early tests using 0.05 mm radial clearance between punch and die indicated that the strength was proportional to particle size. The inference was made that where the particles were larger than the clearance, particles had to be deformed before a disc could be sheared out. It was deduced that to measure the strength of the strip by this method, the clearances would have to be so large that bridging between die and punch by arrays of large particles was insignificant. The radial clearance was therefore increased to 0.5 mm.

The effect of the increased clearance was that the strip was bent rather than sheared, a conical annulus being produced between punch and die. When the test was applied to the more brittle green strip, the fracture produced a separate ring of material in some cases, but with flexistrip a disc of irregular periphery was punched out. The fracture is analogous to four-point bending, and is in effect a circular mode of four-point bending with the outside surface clamped.

In effect the test measures the angle through which the strip can be bent while subjected to increasing tension, and the force required to break it in this manner.

For the single-layer test, the failure is attributed to the tensile stress in the top surface of the specimen, around the circumference of the upper strip clamping block. This stress is given by[161]

$$\text{radial stress} = 3P\,(R^2 - r^2)/2\pi t^2 R^2 \qquad ..(1)$$

where P = load on punch

R = radius of die and clamping block

r = radius of punch

t = strip thickness

Where more than one layer is used, the shear stress may not be fully transmitted from one layer to the next. As a result, the maximum stress is not necessarily the radial tensile stress at the surface. If it is assumed that the shear stress is distributed parabolically within each layer, the maximum shear stress is $3P/4\pi rt$. The radial tensile stress at a distance Y above the centre line is given by[161]:

$$\text{radial tensile stress} = 3Py\,(R^2 - r^2)/\pi t^3 R^2 \qquad ..(2)$$

If it is assumed that for a multilayer system the principal stress approximately coincides with the maximum shear stress in the top layer, and the failure is at the outer edge of the conical annulus (as is found experimentally to be the case), then the principal stress is given approximately by[162]

$$\text{principal stress} = \frac{3Py(R^2 - r^2)}{\pi\ 2\ t^3\ R^2} + \sqrt{\left(\frac{3Py(R^2 - r^2)}{\pi\ 2\ t^3 R^2}\right)^2 + \left(\frac{3P}{4\pi rt}\right)^2} \qquad ..(3)$$

The greater the number of layers involved, the more closely will the principal stress approach the position of maximum stress. For the case with two layers the principal stress will be significantly further from the centre-line than the maximum shear stress and this approximation will be less accurate, underestimating the true principal stress.

Another factor affecting the validity of equation (3) will be the ductility of the strip. If the deflection of the strip before failure approaches the strip thickness, the extension of the central plane of the strip will introduce a tensile stress additional to the tensile stress associated with the bending of the strip[163].

The relative consistency of the calculated stress values, allowing for underestimation in the multilayer situation, supports the theory that the mode of failure is approximately as described.

D3.2 Tensile Testing of Flexistrip

The strength as measured by tensile testing is lower than as measured by annular bending. In part this may be caused by the assymetrical failure in tensile testing, the fracture starting from the weakest point. The tensile failure may follow the weakest path through the material, but the locus of the failure in annular bending is determined by the tool, and so a higher strength in annular bending would be expected.

Part of the difference in the results may be attributed to the existence of a film of binder on the surface of the strip. This is illustrated in Fig. 37. Although the binder generally also exists in a film-like state within the body of the strip, as shown in Fig. 38,

the film on the surface is normally considerably thicker. It is unlikely that this film would contribute to the strength of the strip to the same degree both in annular bending and in tensile testing.

D3.3 Compressibility of Flexistrip

The results indicate that flexistrip may be slightly more compressible than powder (Fig. 29). The difference is small and may be within the margin of error of the experiment. Furthermore, the density range investigated does not extend beyond 5.5 Mg/m^3. It may be that below this density the lubricating effect of the Celacol is more important than the reduction in pore space caused by the Celacol occupying part of the pore volume. As the Celacol is relatively compressible, it would have to be considerably compressed before it would contribute significantly to the resistance to the punch movement, which is provided almost entirely by the iron powder. The Celacol in the flexistrip would almost certainly contain more moisture than the powder used in the compression test illustrated in Fig. 29, and would occupy a greater volume for a given mass of cellulose. When the flexistrip is compressed to such a density that the Celacol completely fills the pores, it cannot be compressed further except elastically. This effect is shown clearly in Fig. 31, where all the experimentally determined points fall below the calculated maximum density.

Fig. 29 shows that Celacol has a measurable resistance to compression, particularly when its density is greater than 50% of its theoretical maximum density. In the case of the Celacol in the flexistrip, it may be considered that the Celacol is free to occupy all the space that is not occupied by iron, and so the relative

density of the Celacol may be regarded as being the ratio of (the volume of the Celacol) to (the volume of Celacol plus air). This is based on the supposition that because Celacol is relatively soft it will be squeezed from between iron particles into the pore spaces, permitting metal-to-metal contact. Thus, when the relative density of the Celacol is greater than 0.5 it will contribute to the pressure required to densify the flexistrip. The magnitude of this effect may be estimated if it is supposed that in a plane cross-section the total pressure P_t is made up of the pressure required to compress the iron powder, P_i, plus the pressure required to compress the Celacol (P_c) multiplied by the fraction of the cross section over which that pressure acts, which is the same as the porosity e (defined as the fraction of the total volume which is not iron):

$$P_t = P_i + e\,P_c \qquad .. (1)$$

For a given density of flexistrip, P_i can be related to the density from the pressure-density relationship for iron powder; P_c can be approximately found from the pressure-density relationship for Celacol powder if the relative density D_c of the Celacol is found in terms of the porosity e.

$$D_c = V_c/(V_c + V_a) \qquad .. (2)$$

where V_c is the volume of Celacol and V_c the volume of air.

$$(V_c + V_a)/(V_c + V_a + V_i) = e \qquad .. (3)$$

where V_i is the volume of iron.

$$\therefore \quad D_c = V_c/(V_c + V_a + V_i)\, e \qquad .. (4)$$

$$1 - e = V_i/(V_c + V_a + V_i) \qquad .. (5)$$

$$\therefore \quad D_c = V_c(1 - e)/V_i\, e \qquad .. (6)$$

V_c/V_i is known from the composition of the flexistrip, and so D_c can be found in terms of e.

If Kawakita's relationship

$$P_i = \frac{1}{B_i}\left[\frac{1}{1 - D_i} - A_i\right] \qquad .. (7)$$

for iron, where A_i and B_i are constants and D_i is the relative density of iron, is equally valid for Celacol at high densities, then

$$P_c = \frac{1}{B_c}\left[\frac{1}{1 - D_c} - A_c\right] \qquad .. (8)$$

where the subscript c designates Celacol, then from equations (1), (6), (7) and (8),

$$P_t = \frac{1}{B_i}\left[\frac{1}{e} - A_i\right] + \frac{e}{B_c}\left[\frac{1}{1 - V_c(1 - e)/V_i e} - A_c\right] \qquad .. (9)$$

Fig. 39 shows the calculated graph for this equation for MH 300.25 powder with 0.9% Celacol by weight, using the compressibility constants in Tables 10 and 12. The theoretical maximum density is closely approached at a pressure of 2 GN/m^2; the relationship between this curve and the curve in Fig. 31 is striking. It should be noted that at densities below 7 Mg/m^3 the binder does not contribute to the total pressure, and because of its lubricating effect - for which no allowance was made in the equation - reduces the pressure required to attain a given density. The pressure-density relationship for flexistrip was determined entirely from its behaviour in the density range

below 7 Mg/m^2 (Fig. 29). Therefore, if the compressibility constants for flexistrip are substituted for those for sponge powder in equation 9, a pressure-density curve which allows for both the pore-filling and lubricating effects of the binder will be obtained. This curve is also shown in Fig. 39; it probably gives a better representation of the actual behaviour of the flexistrip.

The difference between the two curves is probably exaggerated by die wall friction. The effect of this will have been greater on the powder than on the flexistrip. Therefore, the compressibility of the powder was probably underestimated.

No allowance has been made here for the contribution of air to the pressure required to densify the flexistrip; it has been assumed that all the trapped air escapes. The validity of this assumption will depend on the rate of compaction and the permeability of the flexistrip. This will be discussed in section D3.7.

D3.4 Compressibility of Celacol

The need to compact the Celacol in two stages made this test inaccurate. Furthermore, Celacol is viscoelastic, and so the compressibility will be rate-dependent. Each of the two compressing operations took about 1 second; there was an interval of about 30 seconds between them. The Celacol in the flexistrip is physically different, being in the form of films, and relatively moist. The compressibility constants obtained in this investigation are, therefore, only a qualitative indication of the compressibility of the Celacol in flexistrip.

D3.5 The Effects of Roll Loading in the First Compaction Operation

The results indicate that the strength of green strip depends more on its density than on the load under which it was rolled. The density is determined mainly by the highest specific pressure during rolling, not by the total roll load. The specific pressure cannot easily be related to the total roll load because the rolls deform and the deformed shape depends on the strip thickness and the load, and is not known. However, an approximate relationship between powder compressibility, roll loading and strip density is proposed in Appendix VII. In that approximation a simple deformed roll shape is assumed. This consists of a circular arc on the input side and a flat contact zone on the output side. It can be shown theoretically that the pressure distribution on the roll is not such as to produce a circular arc of contact, and further that an arc of the proposed radius is not consistent with a flattened output contact zone of the proposed width. Nevertheless, the derived relationship corresponds well with the measured values. The scatter of the points in Fig. 31 may be partly explained by the variability of the mass per unit area of the strip. Those samples having above average mass per unit area may behave as high spots, and carry a disproportionate share of the roll load, so becoming more highly compressed; conversely less dense areas are less compressed.

The relationship derived in Appendix VII depends on the validity of Kawakita's equation. In section D3.3 it was shown that at high pressures the volume occupied by the binder limits the density of the strip. This effect is, however, negligible at strip densities below about 7.2 Mg/m^3 for strip containing 0.9% w/w Celacol.

In current practice, the amount of binder used has been reduced[164], and so the range of relative validity of the proposed relationship may be extended to cover roll load intensities above 10 MN/m; rolling is normally carried out at a load of about 5 MN/m. The equation has been tested by using it to determine the roll loads used for compacting six of the water-atomised green strip samples (Table 14). The actual roll loads used in each case were not recorded; the rolls were preset to a load which was expected to alter to 4.7 MN/m during rolling. The actual loads would have been lower than this for the thinner strip samples. It can be seen from the table that with the exception of B, the calculated roll loads do increase with thickness. B may be exceptional because the particle size is comparable to the strip thickness. Compressibility data obtained from the powder in bulk are likely to be invalid in this case. Hence, the data may be considered to support the theory.

The variation of elongation with roll loading is consistent with the hypothesis that it depends on the roll curvature. At low loads the elongation increases as the reduction in thickness of the strip is increased, because when the strip first meets the rolls the normal pressure at the roll surface has a component in the plane of the strip, and this component is increased if the rolls are smaller or if they "bite" more deeply into the strip. At high loads the rolls deform elastically to a flatter shape, and the pressure is more nearly normal to the plane of the strip, so that the elongation is reduced.

D3.6 Measurement of Strip Speed During Rolling

The fact that the strip emerges from the rolls at a speed lower than the peripheral speed of the rolls is not easily explained. If the rolls are slipping both at entry and exit, then they would probably be slipping all through the arc of contact; if the coefficient of friction did not increase with speed then the strip would not go through the rolls. In general, the coefficient of friction falls with increasing speed[90], and so it seems likely that at some point the strip is not slipping with respect to the rolls. One possible explanation is that the strip is elastically deformed between the rolls to give an elongation corresponding to the difference observed between the roll speed and the strip speed. The elongation necessary for this would be 2%. On emerging from the rolls the strip would contract 2% and its speed would therefore be 2% slower than that of the rolls. A 2% strain is exceptional and would not be expected from this material in uniaxial tension; the low strength of the material (about 4 N/mm^2) indicates that a modulus of about 200 N/mm^2 would be necessary to attain this strain. 200 N/mm^2 is about one thousandth of the modulus for fully dense material, and this seems improbable. The strip could of course be strengthened by the compressive support of the rolls. However, the force compressing the strip decreases to zero as the strip emerges from the rolls, and so fragmentation of the strip would be expected as the strength of the strip falls to a value below the applied stress.

It is feasible that the compression of the strip between the rolls should cause an expansion in the rolling direction of about one third of the amount by which it is compressed; the exact value of Poisson's ratio for this material has not been measured. From Fig. 39 the

maximum specific pressure can be estimated to be about 1 GN/m^2. Thus, for a compressive strain of about 6%, the elastic modulus would be $1/0.06 = 17$ GN/m^2. For a sintered material of the same porosity, the elastic modulus would be expected to be about 150 GN/m^2.

Pohl[165] has implied that the elastic modulus of a porous material may be represented by the equation:

$$E = E_o(1 - Ke)$$

where E = elastic modulus of porous material

E_o = elastic modulus of pore-free material

K = a stress-concentration factor

e = porosity.

If here $e = 0.15$ and $E_o = 200$ GN/m^2, then $K = 6$; reported values for sintered materials are from 2 to 4[165, 125].

Sintering would be expected to reduce the stress-concentration factor because of neck-growth. Therefore, the stress-concentration factor should be higher and the elastic modulus lower for the un-sintered material than for sintered material of the same density. This has been found to be the case by Mallendar[99]. Nevertheless, the value of the elastic modulus found by this calculation seems to be low, and the explanation is not wholly satisfactory. It may be that the elastic behaviour is modified by the presence of binder and trapped air.

D3.7 The Effect of High Compaction Rate

Some of the energy of the falling trolley was lost in the compaction of the most dense sample; the trolley was observed to rebound about 3 mm. It is likely that some energy was lost in all

the other impact tests. Therefore, the energies quoted in Table 16 are upper limits and not necessarily true values. It is not necessarily true that more energy is required at high compaction rates, although this is indicated to be the case in Fig. 33. From Newton's laws of motion[166], assuming linear deceleration, the compaction time was estimated to be less than 0.3 ms. The deceleration will in fact be non-linear, increasing as the density of the compact (and its resistance to further compression) increases: the compaction time will therefore, be less than calculated. With short compaction times the visco-elastic nature of the binder may increase the resistance to compression; the trapped air in the pores will certainly do so.

The permeability tests on green strip (Table 18) shows that the strip is permeable and some air will escape if it is compressed slowly. Hence, the proportion of the air initially in the pores that remains during the compaction will vary with the speed of rolling. For the air to escape, it would have to diffuse backwards through the strip at a speed equal to the forward speed of the strip. If the strip were rolled at 1 m/s, for example, the air would have to diffuse through the strip at 1 m/s to escape. A considerable pressure gradient would be necessary for this: in the permeability investigation air flowed through strip made from powder B at 0.64 mm/s under a pressure gradient of 0.023 N/mm^3. Because the shape and length of the compaction zone are unknown, it is not possible to determine exactly what pressures may be reached by the trapped air. However, an order-of-magnitude estimate can be made by assuming a compressive arc length of 10 mm, a uniform permeability and a uniform pressure gradient, and that the flow of the air is similar at the higher velocity. This indicates that a pressure gradient of about 30 N/mm^3 would be required

to permit backward escape of trapped air in strip rolled at 1 m/s; this implies a pressure at the roll centre-line of 300 N/mm^2. Such a pressure would not of course be reached unless the specific roll pressure was higher than this.

If all the air is trapped, the air pressure may be calculated from the change in volume of the pore space:

$$P = (T - F)\ G/(T - G)\ F \text{ atmospheres}$$

or: $$P \simeq 0.1\ (T - F)\ G/(T - G)\ F\ N/mm^2$$

where P = pressure of trapped air

F = density of flexistrip

G = density of green strip

T = theoretical density of pore-free strip (allowing for the volume of the binder)

Fig. 40 shows the relationship between green strip density and the pressure of trapped air for T = 7.4 Mg/m^3. This indicates that the pressure is not likely to be sufficient for the air to escape.

If each particle is almost completely surrounded by pore space, as the scanning electron micrographs in Figs. 34 and 35 seem to indicate, the air pressure will be fully effective across complete non-planar cross-sections. If the air pressure exceeds the green strength, some of the bonds between particles will be broken, and the pores will expand to reduce the air pressure. Comparison of Fig. 40 with Fig. 32 indicates that this is likely to happen when strip is rolled to densities greater than 7 Mg/m^3 (for water-atomised powder). This would, of course, lead to a fall in density corresponding to an increase in roll load. Such a fall in density has in fact been reported by Williams[50], and the data in Table 13 support this.

At very low rolling speeds, where some air may escape, this effect will depend on rolling speed. At speeds above about 100mm/s the effect will be independent of rolling speed.

D 3.8 Properties of Green Strip

The transverse and longitudinal tensile tests are easy to perform. Both tests measure the strength of the weakest cross section in the relevant orientation. Thus if a long test piece were broken and then the broken edge held in the grips and the same specimen were re-tested, the strength would be higher. Harris [167] has confirmed this experimentally. Thus the average strength may be much higher than the measured strength. The lower strength in the transverse direction may simply indicate that lines of weakness parallel to the rolling direction are more continuous than those at right angles. This is supported by the observation that in seven of the longitudinal tensile tests and only one of the transverse tests, two cracks were formed during the test, one starting from each edge of the strip. In the remaining cases one crack propagated across the full width of the specimen.

During 1973 transverse tensile tests at Shotwick have shown strength comparable to or greaterthan that given by longitudinal tests [164].

The strip is stronger normally to the plane of the strip than in either of the other two directions. This is to be expected as it is the direction in which the strip was compressed. The standard deviation of the strength is only 8% of the mean strength, compared with 10% for the longitudinal test; the results are more consistent, but not greatly so.

The annular bend test is slightly easier to perform than the tensile test because the specimen does not have to be cut to size. Where the disc was not clamped to the punch the stress was calculated from equation (1) of section D3.1. In the case where the punched out disc is clamped to the punch by a bottom punch, the radial tensile stress at the top surface of the specimen at the edge of the upper strip clamping block is given by [161]:

$$\text{radial stress} = 3P(2\ln R/r + r^2/R^2 - 1) \;/\; 2\,t^2\pi(1-r^2/R^2)$$

where the symbols are as in section D3.1

The unclamped test is probably preferable because it does not involve the risk of damaging the specimen while clamping the bottom punch.

In the present experiment the scale of the apparatus was smaller than would be desired for the best results. The breaking force depends on the raio of R to r and not on the actual size of the apparatus. It can be seen from figure 41 that the weight of the punch represents a significant part of the breaking load, and so the scale cannot be much increased without the punch becoming too heavy, although a lighter design could be used. In the present case, R = 15.9mm and r = 15.4mm; a bigger difference between R and r could be more accurately measured. A reduction in r would however reduce the force needed to break the specimen and increase the risk of damage in setting up. An increase of scale would permit more accurate measurement without making the test more difficult.

Furthermore it would reduce the shear forces involved and the width of the annulus would become large compared with the thickness of the strip, so that the test would approach more closely to the idealised conditions represented by the equations from which the stress is calculated. Suitable dimensions would be R = 50, r = 49mm.

The results show that the strength in annular bending is greater than in tension. This may be because the surface material is stronger than the material in the centre of the strip because surface particles are more heavily cold worked and are subjected to direct normal pressure from the rolls, rather than components of pressure in many directions from irregular particles. The film of binder on the surface may contribute to the strength. Much of the film structure of the binder within the strip may be broken up by rolling (Fig.35). A greater strength in annular bending than in tension would be expected because the strip is broken along a predetermined line, rather than the weakest line.

The effect of particle size distribution on green strength is complex. The high strength of strip made from powder B may be attributed to the effect of the large particle size so that interparticle bonds are mainly near the centre of the strip rather than at the surface. This would allow the strip to bend through a greater angle and increase the contribution of central plane tension to the load at failure. In that case the equation used would not really be appropriate. The strips made from fine powder are generally weaker than those made from powders mainly in the size range 0.05 to 0.1mm. The wider size ranges of R, S and V may have contributed to their higher strength, but the larger particles may have led to some bridging between punch and die. A larger tool would eliminate this possibility.

The segregation test used was qualitative rather than quantitive. The principal reason for this is that the correction for the ratios of particle size to frame size was empirical and not based on statistics. At the magnification used the resolution of the instrument is about 0.002mm. As the mean intercept is normally less than two thirds of the particle diameter, this would cause significant errors in blends containing the finest powder. Nevertheless the high values recorded for R,S, V,W and X indicate a higher degree of segregation for these strips than for others.

The observed relationship between density, compressibility and segregation index may be achieved by packing fine particles in the spaces between the coarse particles and where this happens there is a region of "segregated" fine powder. Hence in this sense it would be expected that a high degree of segregation would be associated with high density.

It is by no means certain that the method used to determine the permeability of green strip can be used to calculate the weight specific surface. The films of binder may close off some channels through which air would otherwise flow, giving a specific surface above the true value. However if the films are sufficiently broken up in rolling, the results may be meaningful. For the coarser particles sizes B, Q and I, the calculated surface is about $0.1m^2/g$ higher than for the powder alone. For a binder concentration of 0.9%w/w, this corresponds to a weight specific surface for the binder of about $10m^2/g$. This implies a mean film thickness of about 200nm. Figs. 34, 35,37 and 38 do not make it possible to estimate the mean film thickness but certainly a considerable amount of the film is very much thicker than this.

The higher surface calculated for the finer powders implies that the film is finer; this is reasonable as the film is formed in contact with the particle surfaces, and the finer powders have greater surface areas and therefore form a larger area of film from a similar amount of binder.

D3.9 Properties of Sintered Strip

A change in density on sintering is to be expected. Some weight loss from the binder would certainly take place, although a residue would be left. The binder film would contain an amount of moisture before sintering which might be up to 0.5% of the total weight; in the case of the water-atomised powder a hydrogen loss of 0.6% would also be expected. Thus if the volume was unchanged during sintering a fall in density of about 1% would be expected. The loss in density as measured is about 0.1%; the variability of the density is such that this is not significant. Therefore it would seem that the best estimate of shrinkage that can be made from the available data is that it is sufficient to maintain a roughly constant density and is 1% by volume or 0.3% by length.

The low hardness of the strip made from the fine powder may be associated with internal defects because the strips blistered on sintering. The blisters may be caused by the expansion of enlarged pores produced by the expansion of trapped air during rolling. Relatively more air would be trapped in the strips made from fine powder because those strips are less permeable, and so those strips would be more prone to blistering.

The general decrease in hardness compared with green strip may be attributed to annealing; the particles themselves were not well annealed as received, and some work hardening of asperities would have taken place during rolling.

The permeability of strip P was low, and so the measurement was relatively inaccurate as a much smaller volume of air was measured than in the test on powder. Some of the pores may have been closed during sintering; some may be blocked by residue from the binder.

In either case the calculated value does not represent the specific surface of the metal in the compact; this is indicated by the fact that the figure is greater than that for the unsintered powder.

D3.10 The Compressibility of Sintered Strip

The discs used for the tests were not of uniform thickness at the start of the experiment, although those made from sponge iron powder were more uniform that those made from water-atomised powder. Because of this the measurement of the thickness of the disc may have been in error by as much as 3%. An estimate of the thickness was made and the density calculated from that figure, but the error in the density may be as much as 200 kg/m^3 and the extent of the error is not necessarily the same in successive determinations so that only the trend of increasing density with pressure has been established.

D3.11 The Effect of Roll Loading on Sintered Strip

As in die compaction, the density determinations are inaccurate. However, it does seem clear that at low load intensities the smaller rolls give higher density at a given load. This is consistent with the higher specific pressure produced by a shorter arc of contact. The elongation is, however, greater; this also would be expected because of the greater curvature of the rolls.

The densities attained in this investigation are lower than expected. It may be that the application of strip tension during rolling contributes significantly to densification. If that is so then the use of smaller rolls would be expected to give higher densities not merely because of the higher specific pressure, but also because of the shear to which the strip is subjected.

This would have the disadvantage that a higher initial mass per unit area would be required for a given finished strip thickness, but it would also permit the use of coarser powder, giving the strip greater permeability and possible, by virtue of a wider size range, giving higher densities at all stages, reducing the roll loads necessary for densification. Furthermore, coarser powder would have a reduced specific surface and might permit a reduction in binder content.

D3.12 Properties of Strip that has been Sintered and Re-rolled

None of the properties reported in this section seem to be related systematically to the original particle size distribution of powders from which the various strips were made. It may, however, be significant that the finest powder made the softest strip at the lowest density.

A uniform grain size was achieved in the sintering operation and shows that considerable grain growth has taken place; in the case of the finer powders, the grain size is greater than the initial particle size and therefore some of the pores will be isolated within grains. As a result of this, there will be less densification in the next sintering stage in those strips made from fine powder.

The similar hardness numbers show that the extent of work hardening is similar in each case. This would be expected, as all the samples have been reduced in gauge by a similar proportion in the rolling operation, from about 18% porosity to about 5%. At this density level the hardness figures will not be depressed much by collapse of pores beneath the indenter.

D3.13 Properties of Strip that has been Sintered Twice

The method used for density determination is more accurate than measuring the specimen by micrometer and weighing it, particularly where the specimen is not uniform in thickness. To estimate the mean thickness using a micrometer on an irregular specimen it is necessary to take a large number of measurements. Nine readings on a sample of Strip P gave a standard deviation of measured thickness of 6μm, on a specimen 235μm thick. This gives a standard error of 0.8% resulting from variations in thickness alone: about 200 readings would be necessary to achieve the accuracy which is given by the flotation method. If a flat-ended micrometer is used on an irregular specimen it will indicate a greater thickness than is actually the case, because the measurement will be taken across the "high spots" of the specimen. Thus the calculated density will be lower than the true density. This is the case for all the density measurements reported in this thesis except those made on the strip which has been sintered twice. Hence the shrinkage in the second sintering operation is less than is indicated in Table 25.

There is some negative correlation between density and grain size, as shown in Fig.42. This would be expected if in the coarse grained samples many of the pores have been isolated within the grains. Micrographs of polished sections do not show this clearly, but it is noticeable that on fracture surfaces more pores are visible in the finer grained strip A, although the porosity content of S is higher (Fig.43).

The tensile tests are thought to be unreliable, particularly with spect to elongation. Because the variation in gauge has caused a number failures to occur near the end of the measured gauge length, some of the ongation will have taken place outside the gauge length. In this respect is noteworthy that the fracture surface of A shown in Fig. 43 appears to ve been far more ductile than that of S, but the measured elongation s 11% for A and 12% for S.

In some cases poor physical properties may be caused by defects the material. Fig.44 shows defects in strips Y and W, which appear to lamellar cracks in the plane of the strip. These may be caused by istering during the first sinter; although flattened during the second lling operation, they have not sintered together. The tensile test pieces of showed surface cracks which appeared to be laminations breaking through to e surface.

CONCLUSIONS

1. Steel strip can be made from iron powder by the BISRA process.
2. The processing conditions used in this investigation do not give satisfactory results with either exceptionally coarse water atomised powder or exceptionally fine water atomised powder.
3. The roll loading intensity necessary to produce a given green strip density can be calculated from the compressibility of the powder.
4. The density of the green strip produced at high roll loading intensity is limited by the volume of binder present and by the air trapped during rolling.
5. The probability of the formation of defects caused by the expansion of trapped air is increased by rolling at high roll loading intensity, rolling at high speed, and using strip of low permeability. Low permeability will normally be associated with powders of high specific surface and small mean particle size.
6. The density of the strip does not change much during the first sintering operation. Defects produced in the first rolling operation may lead to the formation of blisters during sintering.
7. High specific pressure is necessary to produce strip of low porosity in the second rolling operation without strip tension.
8. Considerable grain growth may occur in the second sintering operation.
9. Large grains are associated with relatively high porosity.

10. Some of the strip samples produced had mechanical properties comparable to those of strip produced by conventional methods.

References

1. U.K. Patent 1 257 032/1 257 033

2. W. G. Jaffrey, I. Davies, R. L. S. Taylor, Science Journal, 5A, (3), 61-67 September 1971

3. United States Steel Corporation, "The Making, Shaping and Treating of Steel", Seventh Edition, Pittsburgh, 1957

4. E. A. Bloch, G. Thym, Metals and Materials, 1972, 6, (2), 90-94

5. S. Slevolden, Metals and Materials, 1972, 6, (2), 94-96

6. J. D. Berwick, Metals and Materials, 1972, 6, (2), 72-73

7. Hidetaro Nemoto and Takaho Kawawa, J. Metals, 1969, 22, (8), 62-67

8. F. A. Koch, R. W. Vook, J. Appl. Physics, 1971, 42, (11), 4510-4511

9. "Sir Henry Bessemer, F. R. S. An Autobiography", 1905, Engineering, London

10. Siemens and Halske A. G., German Pat. 154 998

11. G. Naeser, F. Zirm, Stahl U. Eisen, 1950, 70, 995-1003

12. S. Storcheim, Metal Progress 70, (3), 120, 1956

13. D. N. Skinner, Ph.D. Thesis, Loughborough University 1971

14. G. Matsumura, S. Higuchi, M. Sasakai, Int. J. Powder Met. 1966 2, (1), 9

15. P. E. Evans & G. C. Smith, Powder Met. 1953, 3, 26

16. P. E. Evans, "Powder Metallurgy", Interscience, N.Y. 1961

17. German Federal Republic Patent 1 226 508

18. T. S. Daugherty, Powder Met., 1968, 22, (11), 342-357

19. U.K. Patent 1 258 214

20. H. H. Hirsch, 1970 International P.M. Conference, N.Y., July 12-16

21. H. S. Nayar, Powder Metallurgy Int. 1972, 4, (1), 30-36

22. P. Ramakrishnan, Powder Met. Conf. Supplement, 3rd European P.M. Conference, Brighton 1971

23. B. Kalling, S. Eketorp, S. Backstrom, Trans. AIME, 1957,209, 1440

24. U.K. Patent 1 243 649

25. C. H. Weaver, R. G. Butters, J. A. Lund, Int. J. of P.M., 1972, 8, (1), 3-15

26. A. R. E. Singer, Metals and Materials 1970, 4, (6), 246-250 and 257

27. Japanese Patent 45/7406

28. F. V. Lenel, Trans. AIME, J. of Metals, 1955, 6, 158

29. T. Sakai, Lecture given at L.U.T.,1973

30. D. K. Worn, R. P. Perks, Powder Met. 1959, (3), 45-71

31. D. G. Hunt, R. Eborall, Powder Met. 1960, 5

32. M. H. D. Blore, V. Silins, S. Romanchuk, T. W. Benz, V. N. Machin A. S. M. Metals Eng. Quarterly 1966, (6), 54-60

33. U.S.A. Patent 3 502 466

34. U.S.A. Patent 3 396 015

35. D. M. Stephens, G. Greetham, Powder Met. 1968, 11, (22), 330

36. G. I. Aksenova, G. A. Vinogradov, E. B. Lozhecnikov, G. F. Tikhonov Porosh. Met. 1967, 11, 9

37. U.S.A. Patent 3 501 277

38. M. V. Mal'tsev, V. G. Khromov, Z.N. Malyshkina, Tr. Gorkov, Polytechn. Inst. 1970, 26, (15), 33-40

39. G. M. Sturgeon, G. Jackson, V. Barker, G. M. H. Sykes, Powder Met. 1968, 11, (22), 314-329

40. S. R. Crooks, Iron and Steel Engineer, 1962, 72

41. Anon;. Stainless Steel 1971, 19, 13-15

42. U.K. Patent 1 153 932

43. U.S.A. Patent 3 489 555

44. U.S.A. Patent 3 433 632

45. I. Davies, W. M. Gibbon, A. G. Harris, Powder Met. 1968, 11, (22), 295

46. V. P. Severdenko, E. B. Lozhechnikov, V. I. Timofeev, S. N. Levitskii, Novaya Technika I. Progressivnaya Technologya, Minsk, 1969, 270-275, (Abstract in Metal Powder Report 25, (4), 58)

47. German Federal Republic Patent 1 295 965

48. P. E. Evans, Metals and Materials, 1968, 2, (8), 235-240

49. U.K. Patent 776 544

50. S. H. Williams, Ph. D. Thesis, Loughborough University 1973

51. G. J. Pearson, J. S. Hirschorn, Powder Met. Int. 1970, 2, (1), 1-4

52. A. V. Zborovskii, Porosh. Met. 1969, 84, (12), 5-9

53. G. M. Krishnamoorthy, Powder Met. 1971, 14, 179

54. M. J. Kockzak, A. Cawley, 1971 Fall Meeting, Met. Soc. of AIME, Detroit

55. S. Bhattacharyya, N. M. Parikh, Powder Met. 1971, 14, (28), 235

56. P. Costelloe, R. Jackson, B. Scarlett, D. Skinner, unpublished work

57. W. N. Hayden, J. D. Shaw, W. V. Knoppe, Met. Powder Ass., ASM Symposium Chicago 1957, (2), 82; (3), 145; (4) 193

58. P. J. James, Powder Met. Int. 1972, 4, Nos. 2-4

59. M. Stromgren, H. Astrom, K. E. Easterling, Powder Met. 1973, 16, (32), 155-165

60. G. Bockstiegel, "Modern Developments in Powder Metallurgy", Vol 1, Editor H. H. Hausner, Plenum Press, N.Y. 1966

61. K. Kawakita, Y. Tsutsumi, Jap. J. App. Phys. 1965, 4, (1), 56-63

62. K. Kawakita, Y. Tsutsumi, Bull. Chem. Soc. of Japan 1966, 39, (7), 1364-1368

63. K.Kawakita, K-H. Ludde, Powder Technology 1971, 4, 61-68

63a. C. Ballhausen, Arch. Eisenhüttenwesen 1951, 22, 185

63b. P. Murray, D. T. Livey, J. Williams, "Ceramic Fabrication Processes", Ed. W. D. Kingery, John Wiley & Son 1958, 147-171

63c. K. Konopicky, Radex Rundschau, 1948, 141

63d. A. L. Athy, Bull. Am. Assoc. Petrol. Geologists 1930, 14, 1

63e. K. Tanimoto, Trans. Jap. Soc. Civ. Eng. 1957, 43, 53

64. R. W. Heckel, Trans. Met. Soc. AIME 1961, 221, (5), 1001

64a. M. Yu Balshin, Vestnik Metalloprom 1938, 2, 124

64b G. B. Smith, Metal Ind. 1948, 72, 141

65. P. J. M. Chare, T. Sheppard, Powder Met. 1973, 16, (32), 437-458

66. J. L. Brackpool, M. Tech. Thesis, University of Loughborough, 1970

67. K. Kawakita, A. Otsuka, Y. Tsutsumi, K. Danjo, Y. Okada J. Japan Soc. Powder Met. 1965, 12, (3), 116-122

68. J. A. Hersey, J. E. Rees, Particle Size Analysis Conf., Bradford, 1970

69. P. J. James, Powder Met. Int. 1973, 5, (2), 80-84

70. P. J. James, Private Communication

71. F. J. Lohan, 4th International Powder Metallurgy Conf., Toronto, 1973

72. R. F. Mallender, C. J. Dangerfield, D. S. Coleman, Powder Met. 1972, 15, (30), 130-152

73. G. A. Vinogradov, V. P. Katashinskii, Porosh. Met. 1963, 3, (15),30-36

74. M. V. Maltsev, Porosh. Met 1971, 6, 19-24

75. Reuy-Shan Lee, E. G. Schwartz, Int. J. Powder Met, 1967, 3, (4) 83

76. V. P. Katashinskii, G. A. Vinogradov, Porosh. Met. 1965, (5), 9

77. R. S. Ioffe, Porosh. Met. 1971, 98, (2) 25-36

78. K. M. Radchenko, Porosh. Met 1971, 12, (9), 8-13

79. H. Hertz, "Uber die Beruhrung fester elastischer Korper", Gesammelte Werke Vol. 1, Leipzig 1895

80. K. M. Radchenko, Porosh. Met. 1972, 111, (3), 31-37

81. V. K. Sorokin, Porosh. Met 1970, 91, (7), 18-20

82. G. I. Aksenov, Porosh. Met. 1970, 89, (5), 23-28

83. G. I. Aksenov, Porosh. Met. 1970, 90, (6), 25-30

84. O. A. Katrus, R. L. Oganyan, Porosh. Met. 1971, (7), 12-18

85. J. H. Tundermann, A. R. E. Singer, Powder Met. 1968, 22, (11),261

86. O. A. Katrus, A. J. Otrok, Porosh. Met. 1971, (8), 36-40

87. A. M. Musikhin, G. A. Vinogradov, Porosh. Met. 1970, 90, (6), 17-24

88. J. H. Hitchcock, "Roll Neck Bearings", Report of A.S.M.E. Special Research Committee on Bearings, A.S.M.E. 1935

89. H. Ford, J.I.S.I. 1947, 156, 380

90. F. P. Bowden, D. Tabor, "The Friction and Lubrication of Solids", Clarendon Press, Oxford 1954

91. J. W. Golten, Ph.D. Thesis, U. of Wales (Swansea), 1969

92. Sherif D. El Wakil, R. Davies, Powder Met. 1973, 16, (31), 72-87

93. T. Satoh, N. Tajima, N. Kohtaki, T. Watanabe, J. Japan Soc. Pdr. and Powder Met. 1970, 16, (7), 15-19

94. Yu. G. Dorofeev, V. T. Prutsakov, Porosh. Met. 1970, 93, (9), 7-11

95. M. Carrol, A. C. Holt, J.A.P. 1972, 43, (2), 759-761,

96. M. Carrol, A. C. Holt, J.A.P. 1972, 43, (4), 1626-1635

97. W. Herrmann. J.A.P. 1969, 40, 2490-9

98. J. K. Mackenzie, Proc. Phys. Soc. B., 1950, 63, 2

99. R. F. Mallender, private communication

100. J. Williams, J.I.S.I., 1957, 9, 19-24

101. W. M. Long, I. R. Alderton, Powder Met. 1960, 6, 52-72

102. E. Klar, W. M. Shafer, Int. J. Powder Met. 1969, 5, (2), 5

103. E. Klar, W. M. Shafer, Int. J. Powder Met. 1969, 5, (4), 5

104. K. E. Easterling, A. R. Tholen, Powder Met. 1973, 16, (31), 112

105. F. T. Thummler, W. Thomma, J. Met. and Mat. 1967, 1, 69

106. R. L. Coble, J, Burke, "Progress in Ceramic Sciences" Vol. 3, Pergamon Press, Oxford, 1963

107. R. L. Coble, J. App. Phys. 1961, 32, 787

108. M. H. Tikkanen, M. Lahtinen, 4th Int. Powder Met. Conf.Toronto, Canada, 1973

109. P. S. Kisly, M. A. Kuzenkova, Porosh. Met. 1969, 83, (11), 21-25

110. G. Naeser, Int. J. Powder Met. 1970, 6, (2), 3-11

111. B. Ya. Pines, A. F. Sirenko, I. F. Ormelyanerko, Porosh. Met. 1970, (7), 43-48

112. K. E. Easterling, A. R. Tholen, Met. Sci. J. 1970, 4, 130-135

113. T. K. Gupta, J.Amer. Ceram. Soc. 1972, 55, (5), 276-7

114. S. C. Samantha, R. L. Coble, J. Amer. Ceram. Soc. 1972, 55, (11), 583

115. M. Stevanic, Physics of Sintering 1973, 5, (1), 25-30

116. J. R. Moon,Powder Met. International 1971, 3, (4), 194-9

117. H. Frydrych, Metalurgia Proskow, 1969, 12, 7-42, Abstract in Metal Powder Report 25, 4, 67

118. D. R. F. Spencer, Ph.D. Thesis, Loughborough University, 1969

119. R. L. Coble, J. Amer. Ceram. Soc. 1962, 45, 123

120. I. Amato, Mats. Sci.and Eng. 1971, 7, (1), 49-53

121. O. A. Katrus, A. V. Aleshina, Porosh. Met. 1971, 101, (5), 40-42

122. A. Nadai, J. App. Mech. 1939, 6, A54-A62

123. P. E. Evans, G. C. Smith, Powder Met. 1959, 3, 45

124. M. Eudier, Powder Met. 1962, 9, 278-290

125. R. Haynes, Powder Met. 1971, 14, (27), 64-70

126. J. H. Dudas, K. J. Brondyke, "Aluminium P/M parts - their properties and performance", Aluminium Company of America, 1970

127. H. Fischmeister, K. Easterling, L. E. Larsson, P-Å Nickolausson K. Heurling, L. Olsson, Report No. R96/71, Dept of Engineering Metals, Chalmers University of Technology, Gothenburg, Sweden.

128. P. E. Evans, G. C. Smith, Powder Met. 1959, 3, 1

129. G. H. Gessinger, H. Metzler, F. Esper, H. E. Exner, Powder Met. Conference Supplement 1, 1971, 289-310

130. A. Buch, S. Goldschmidt, Mat. Sci. Eng. 1970, 5, (2), 111-118

131. S. M. Kaufmann, Materials Engineering Congress Metal Show Conference Cleveland, 1972

132. H. Kuroki, Y. Tokunaga, J. Japan Soc. Powder & Powder Met. 1969 16, (6), 14-21

133. H. H. Bache, J. Amer. Ceram. Soc. 1970, 53, (12), 654-658

134. F. A. McClintock, J. Appl. Mechanics, ASME Trans. E. 1968, 35, 368-371

135. W. Rostoker, S.Y.K. Liu, J. Materials 1970, 5, (3), 605-617

136. S. H. Williams, R. Haynes, Powder Met. 1973, 16, (32), 387-404

137. S. M. Kajman, S. Mocarski, International J. Powder Met. 1971, 7, (3), 19-30

138. "Test Sieve Data", Endecotts (Filters) Ltd., London, 1970

139. Instruction Manual 56/2e, Alpine Multi-Plex Laboratory Zigzag Classifier 100 MZR, Alpine Aktiengesellschaft, Augsburg, Federal Republic of Germany, 1967

140. W. J. Rees and W. Hugill, Trans. Brit. Ceram. Soc. 1925, 24, 70

141. R. F. Mallender, C. J. Dangerfield, D. S. Coleman, Powder Met. International, 1974, 6, (4), 194-198

142 R. F. Mallender, Ph.D. Thesis, Loughborough University 1974

143. B. H. Kaye, A. G. Naylor, Seminar on Particle Technology, Madras, 1971

144. R. Charlier, W. Goossens, Powder Technology 1971, 4, (6), 351-359

145. P. E. Evans, G. C. Smith, Powder Met. 1959, 3, 1-25, 26-44

146 S. Miwa, K. Tasaka, J. Soc. Mat. Sci. Japan, 1971, 20, (213), 742

147. K. J. Scott, D. Mumford, South African C.S.I.R. Chem. Eng. Group Special Report CHEM 155, 1971

148. H. Suito, M. Arakawa, H. Mishima, S. Yano, S. Ishida, K. Hayashida, Int. Chem. Engineering 1971, (1), 134-139

149. C. Fisher, M. Cole, The Microscope, 1968, 16, (2), 81-94

150. M. J. Smith, The Microscope, 1968, 16, (2), 123-125

151. A. R. Dexter, D. W. Tanner, Nature Phys. Sci. 1972, 238, (90), 31-32

152. H. H. Hausner, International J. Powder Met. 1967, 3, (4), 7

153. B. S. 4359: Methods for Determination of the Specific Surface of Powders

154. C. Orr, J. M. Dallevalle, "Fine Particle Measurement", Macmillan, 1957

155. S. Brunauer, P. H. Emmett, E. Teller, J. Amer. Chem. Soc. 1938, 60, 309

156. D. Yarnton, Metallurgia, 1970, 82, (492), 159-160

157. H. J. Scullion, J. E. C. Harris, Powder Tech. 1971, 4, (3), 151-155

158. T. Allen, N. G. Stanley-Wood, Seminar on Particle Technology, Madras India, 1971

159. C. E. Underwood, "Quantitative Stereology", Addison Wesley, 1970

160. W. D. Harkins, G. Jura, J. Amer. Chem. Soc. 1944, 66, 1362-6

161. A. Morley, "Strength of Materials", Longmans, Green & Co. Ltd. London 11th Edition, 1961

162. S. Timoshenko, "Strength of Materials", Part 1, Van Nostrand-Reinhold, New York, 1969

163. S. Timoshenko, S. Woinowsky, "Theory of Plates and Shells", McGraw-Hill Book Co. Inc., New York, 2nd Edition, 1959

164. J. Bellis, B.S.C. Strip Mills Division, private communication

165. D. Pohl, Powder Met. International 1969, 1, (1), 26

166. I. Newton, Philosophiae Naturalis Principia Mathematicia, Royal Society, London 1686

167. A. Harris, B.S.C. Strip MillsDivision, private communication

168. M. Donnelly, R. Haynes, Powder Met. 1972, 15, (29), 11

169. J. Prescott, "Applied Elasticity", Longmans Green & Co. Ltd.,London 1924

170. M. D. Stone, Iron Steel Eng. 1953, 30. (2), 61

171. H. Ford and J. M. Alexander J.I.M., 1960, 88, (5), 193

172. D. R. Bland, Proc. Inst. Mech. Eng. 1950, 163, 141

173. E. Orowan, Proc. Inst. Mech. Eng. 1943, 150, 140

174. G. Petit Bois, "Tables of Indefinite Integrals", Dover Publications, Inc., New York, 1964

175. D. R. Bland, and H. Ford,J.I.S.I. 1952, 171, (3), 248

176. M. F. Spotts,"Design of Machine Elements", Prentice-Hall Inc. Englewood Cliffs, N.J. 1961.

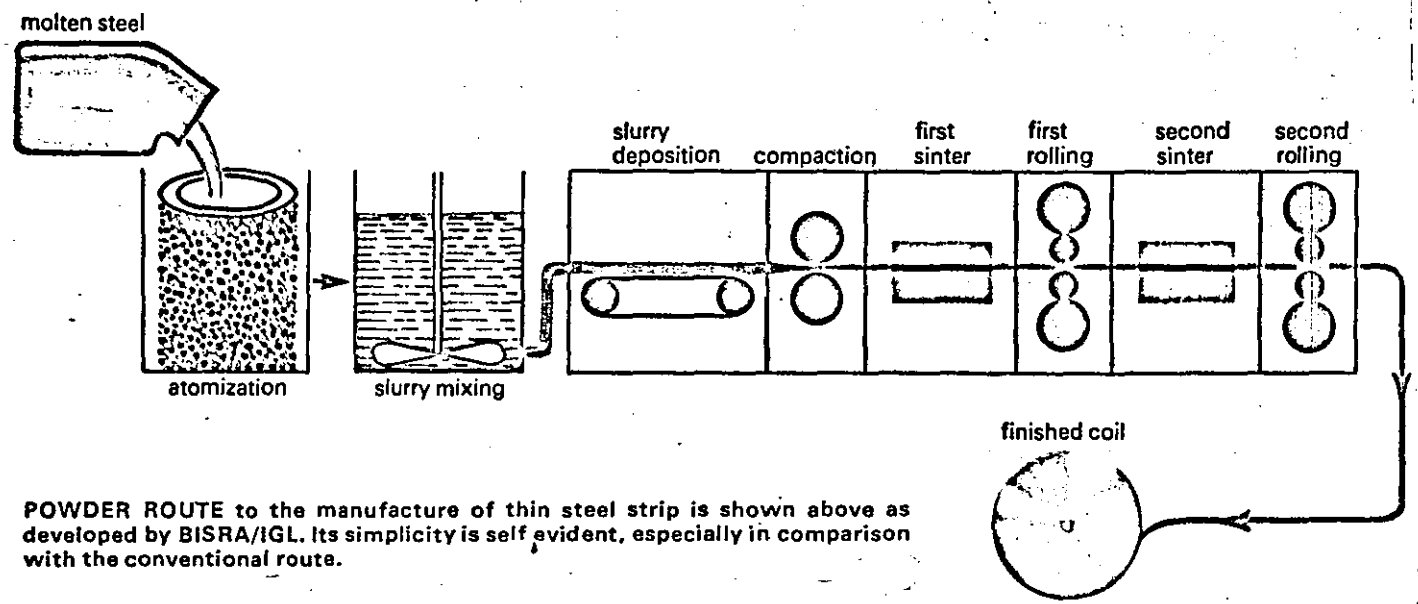

POWDER ROUTE to the manufacture of thin steel strip is shown above as developed by BISRA/IGL. Its simplicity is self evident, especially in comparison with the conventional route.

FIG. 1

Extract from Science Journal.

FIG. 2 STIRRING THE SLURRY

FIG. 3 THE ROLLER-COATER

FIG. 4 THE STRIP LINE AT SKETTY HALL

Photographs: B.S.C.

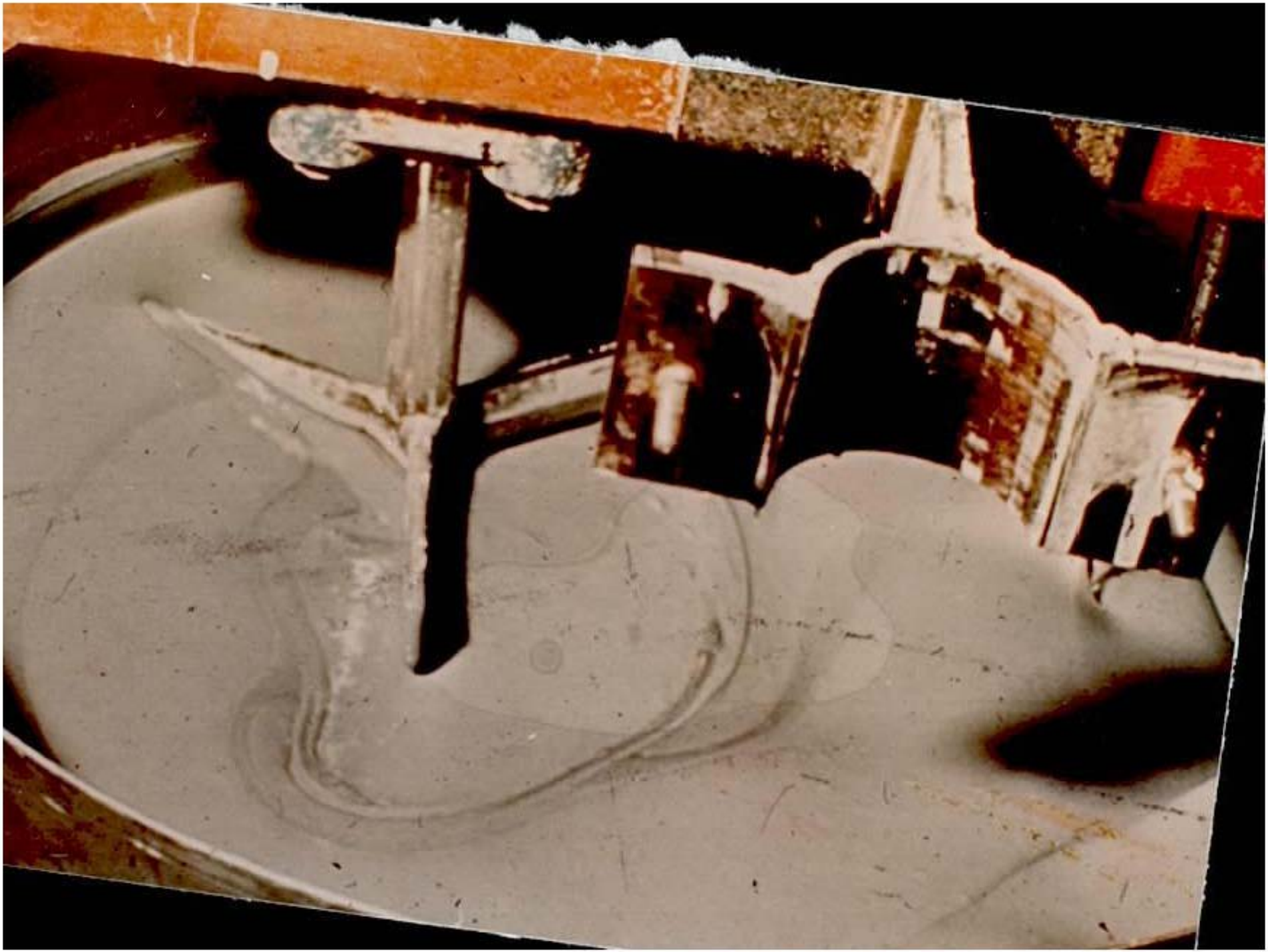

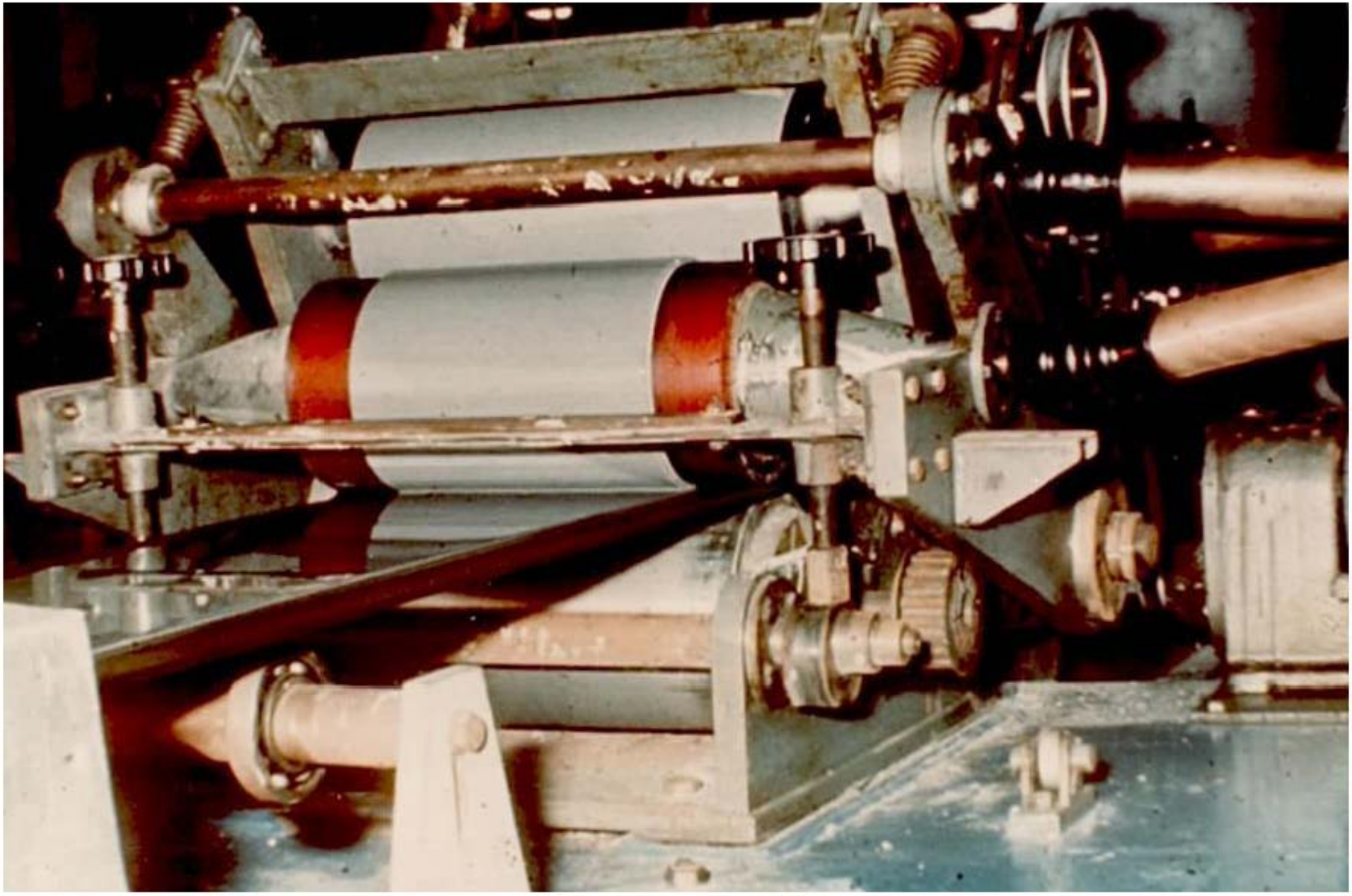

FIG. 5 TRIMMING FLEXISTRIP

FIG. 6 THE FIRST ROLLING OPERATION

Photographs: B.S.C.

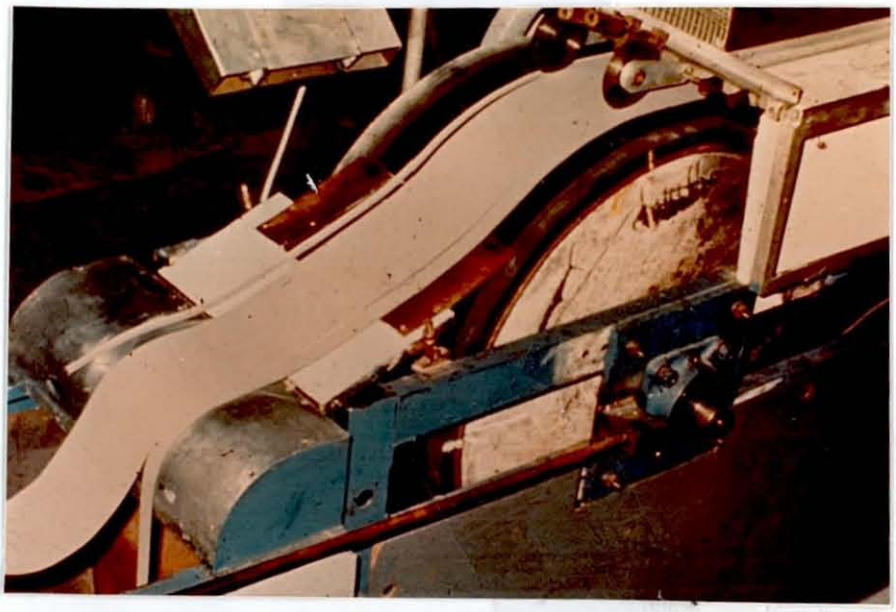

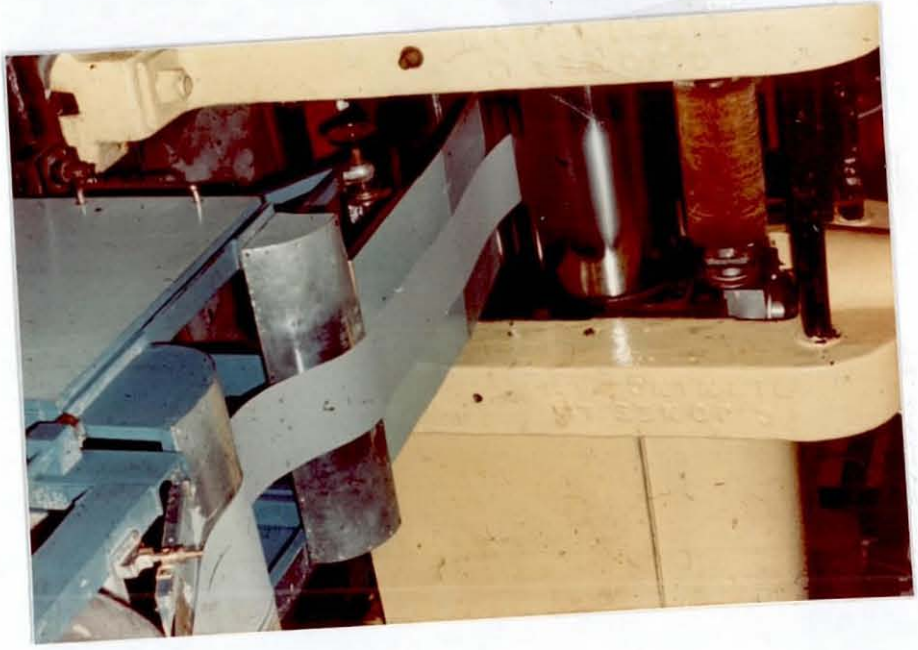

FIG. 7 GREEN STRIP ENTERING THE FURNACE

FIG. 8 SINTERED STRIP LEAVING THE FURNACE

Photographs: B.S.C.

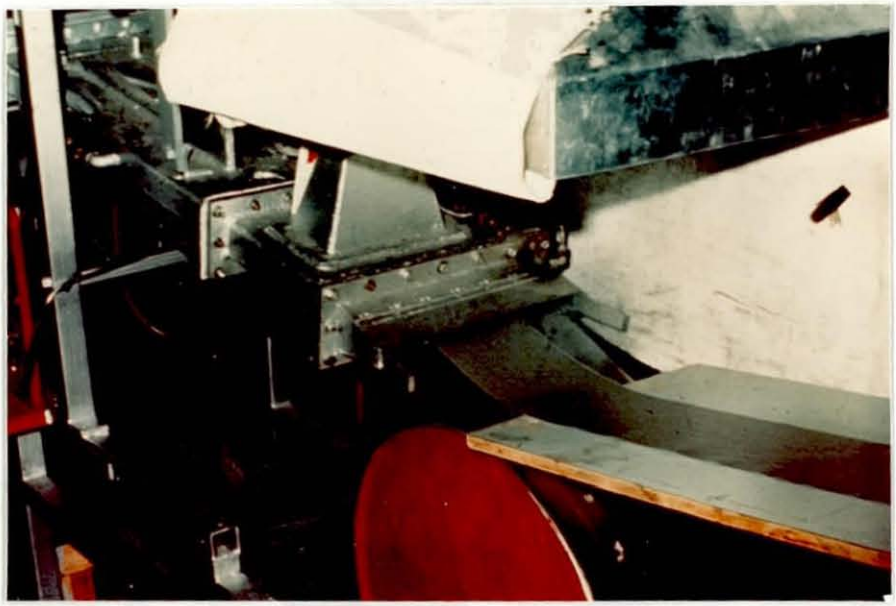

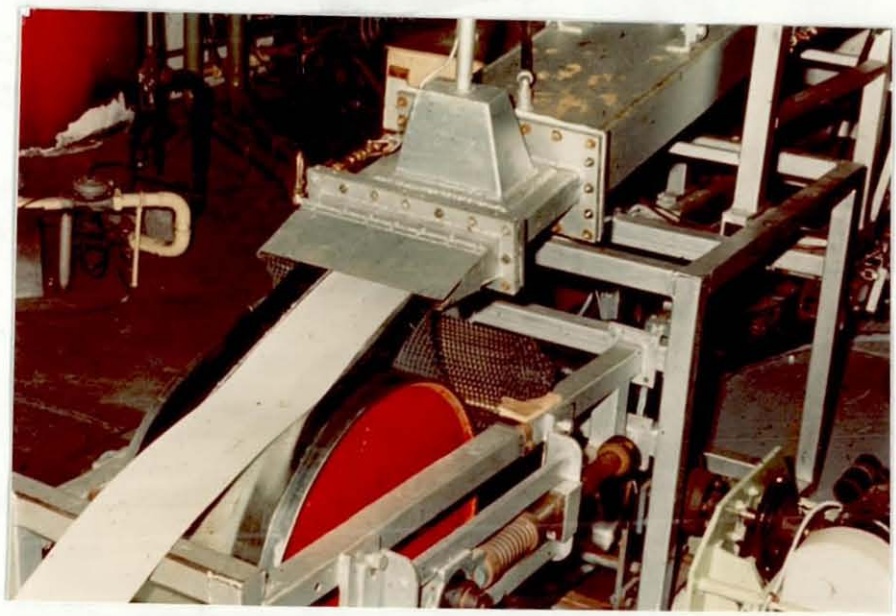

FIG. 9 THE SECOND ROLLING OPERATION

FIG. 10 COILING AFTER THE SECOND SINTER

Photographs: B.S.C.

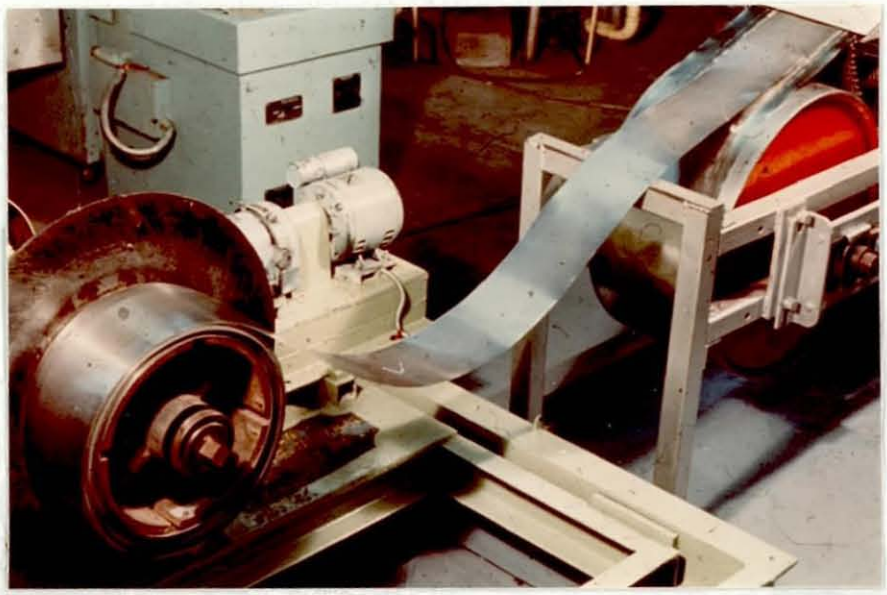

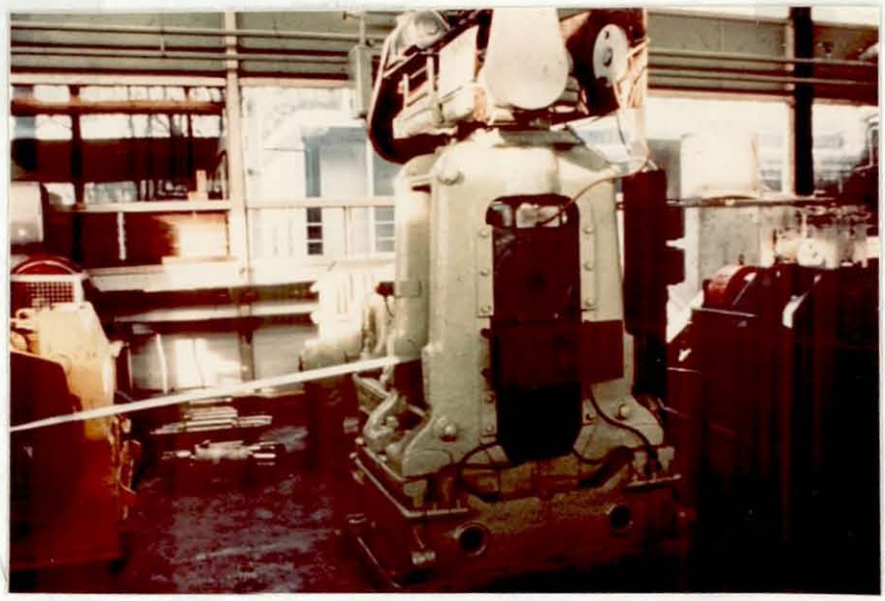

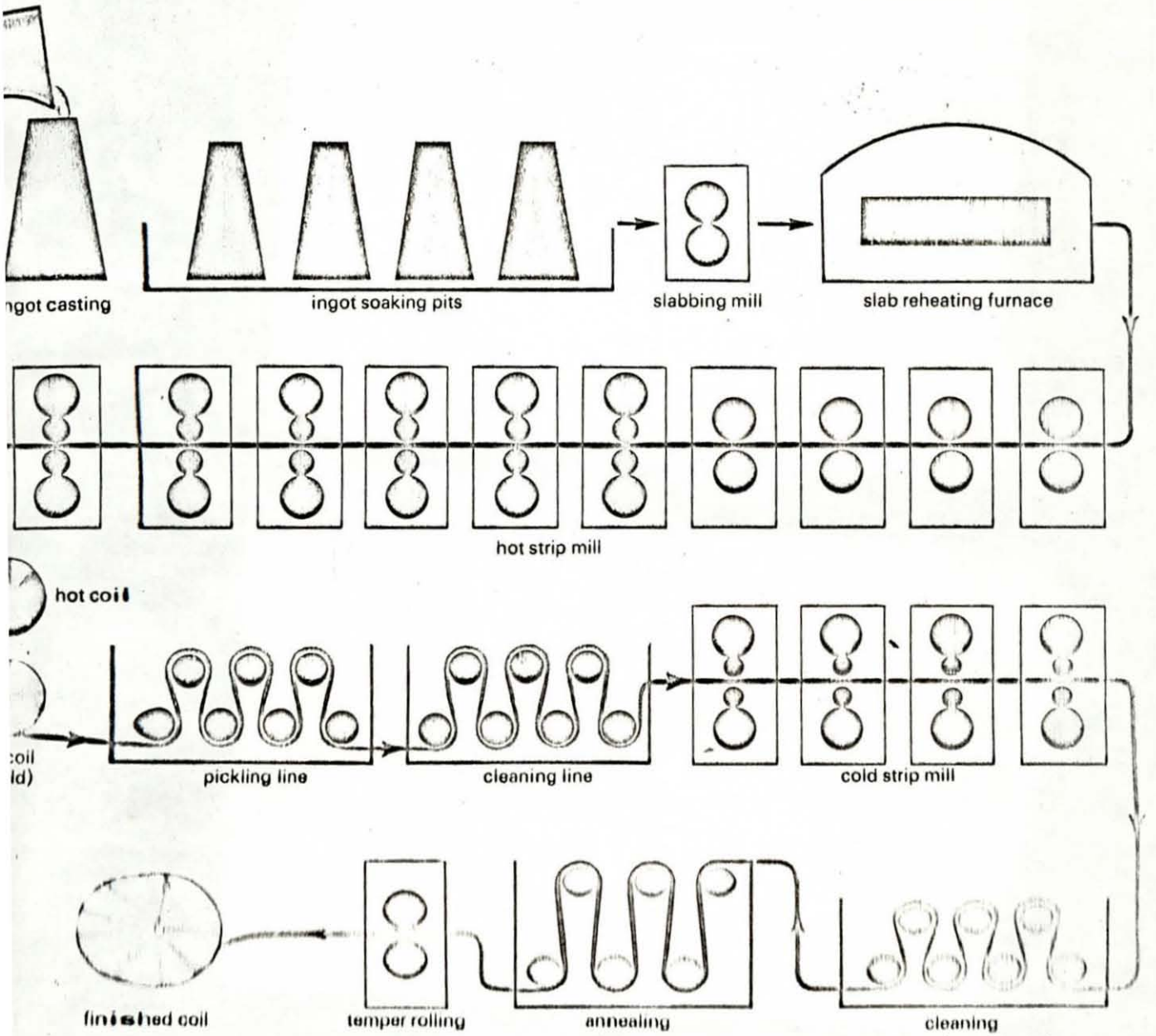

FIG. 11

THE CONVENTIONAL PROCESS FOR THE PRODUCTION OF STEEL STRIP.

Extract from Science Journal.

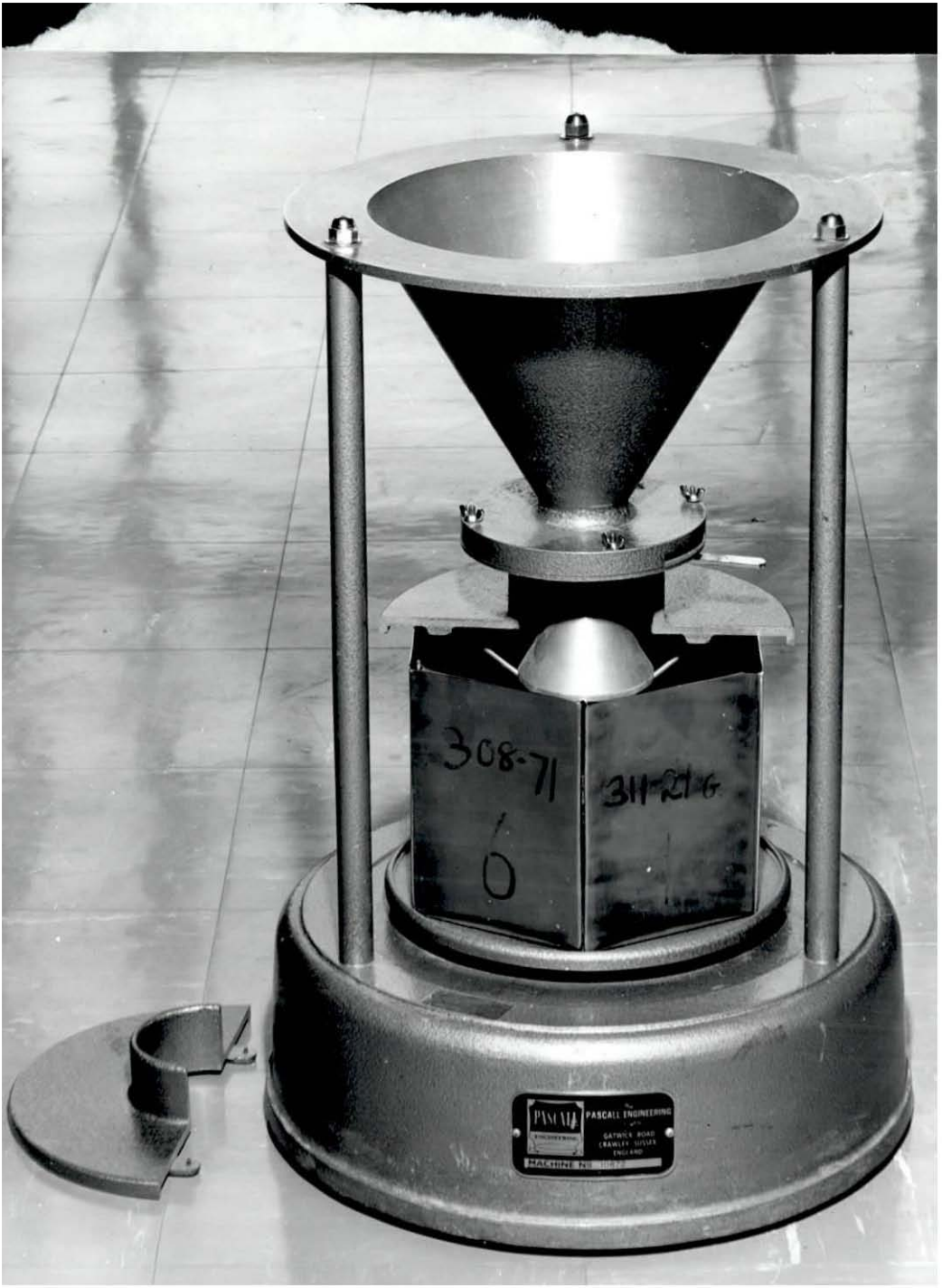
308-71
311-21G
PASCALL
PASCALL ENGINEERING
GATWICK ROAD
CRAWLEY SUSSEX
ENGLAND
MACHINE NO

. THE PASCAL POWDER SAMPLE DIVIDER

FIG. 12

(a) ASSEMBLED VIEW

(b) THE SAMPLE DIVIDING HEAD

FIG. 13 THE SPINNING RIFFLER

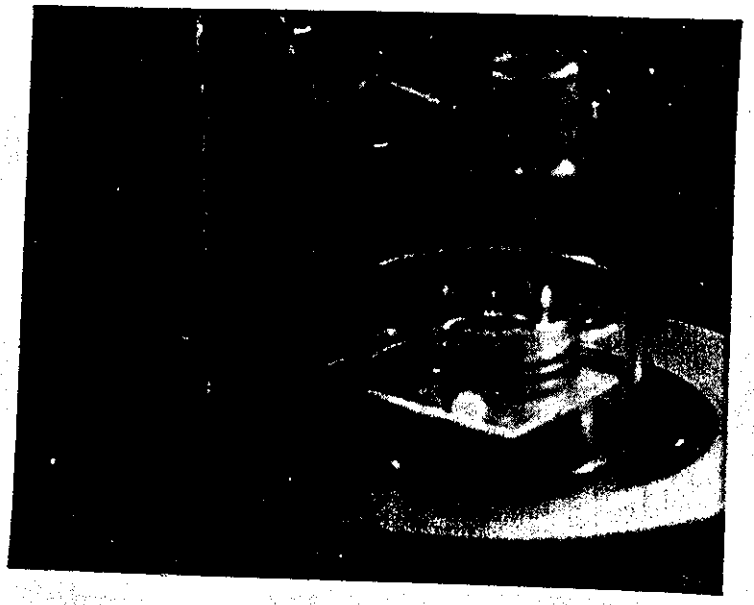

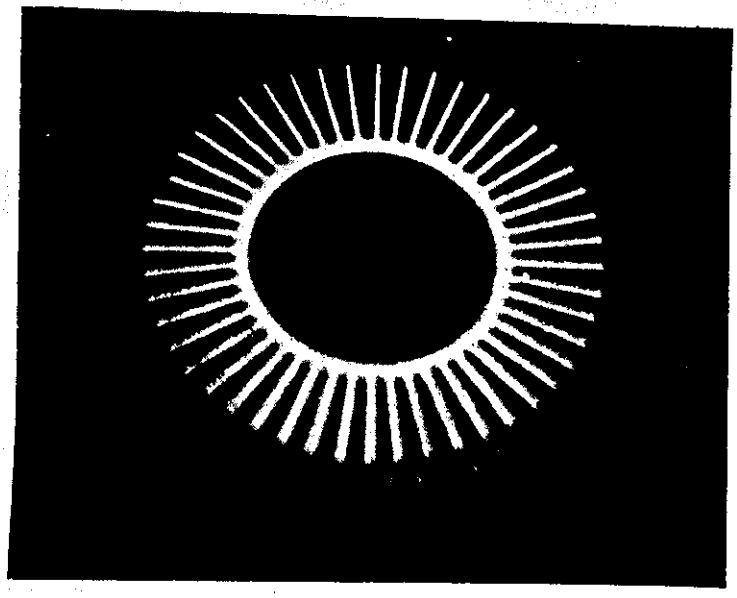

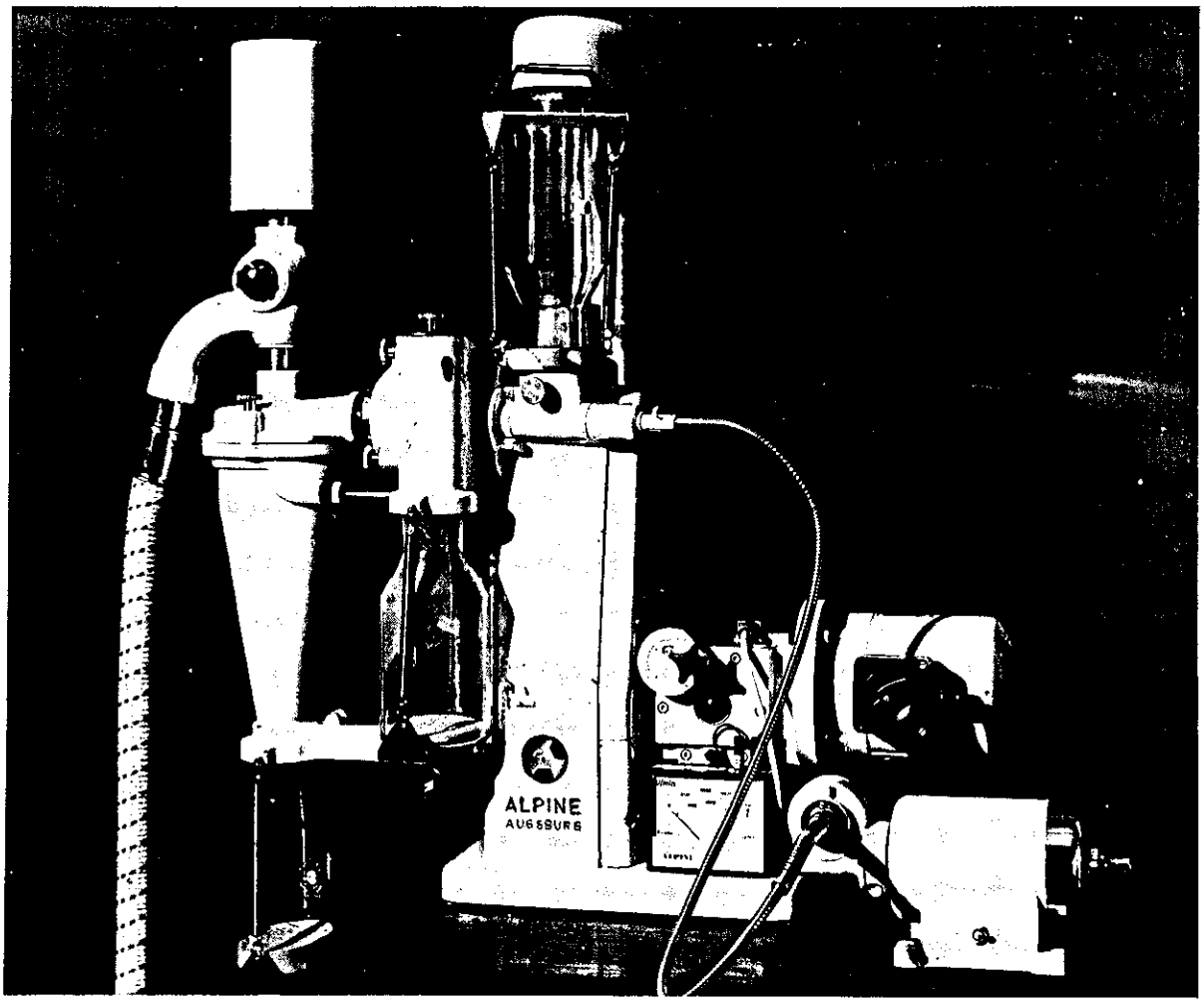

THE ALPINE ZIG-ZAG POWDER CLASSIFIER

FIG. 14

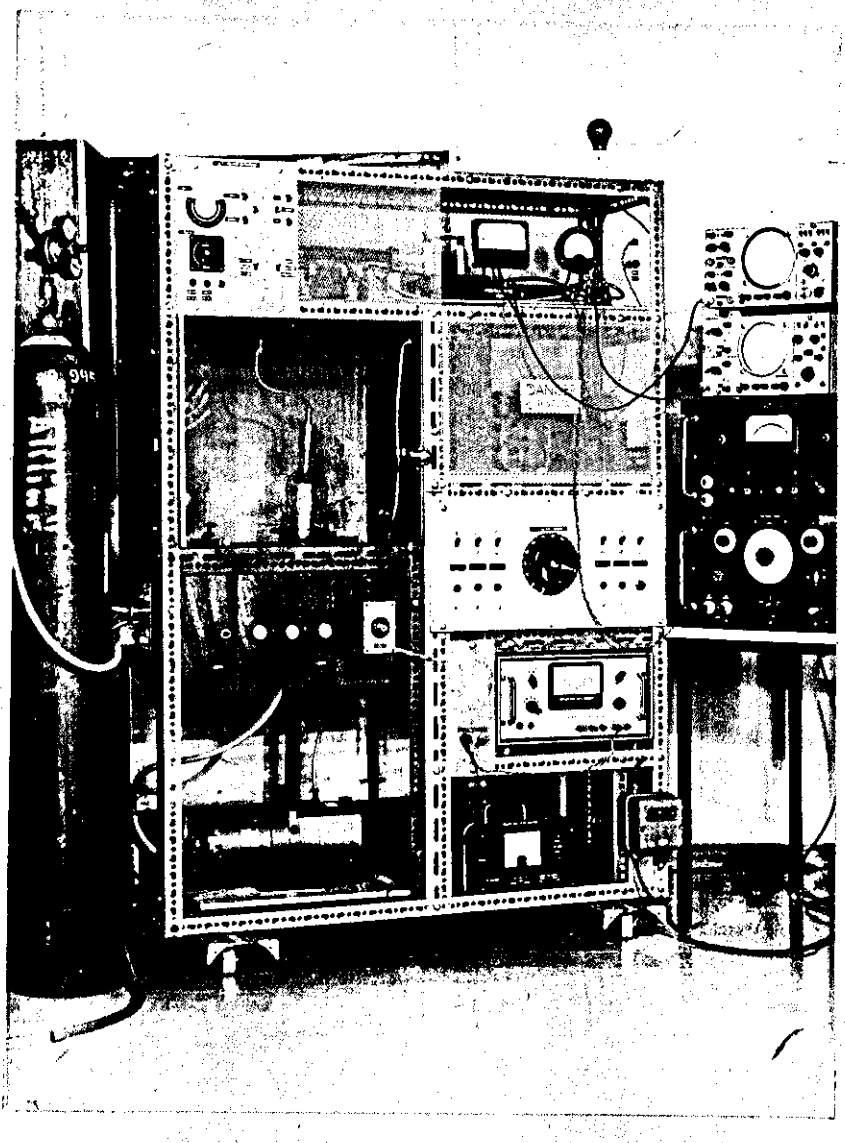

FIG. 15 THE ION ETCHING APPARATUS

Photograph: D.Tomkins

FIG. 16

MATERIAL :-

B.S.A. WATER ATOMISED

N9481/83

COMPOSITION :-

POWDER Q.

FROM :-

TREATMENT :-

TEST PIECE :-

0.2717 g.

RESULTS :-

REMARKS :-

L1 = Length of powder fill.

L2 = Length of compact.

SIGNATURE :-

BEAM :- | GRIPS :-

MAGNIFICATION :- 16XXXXXXX1

DATE :-

FIG.16 TENSOMETER CHART FOR COMPRESSIBILITY TEST.

TEST REF. No. :-

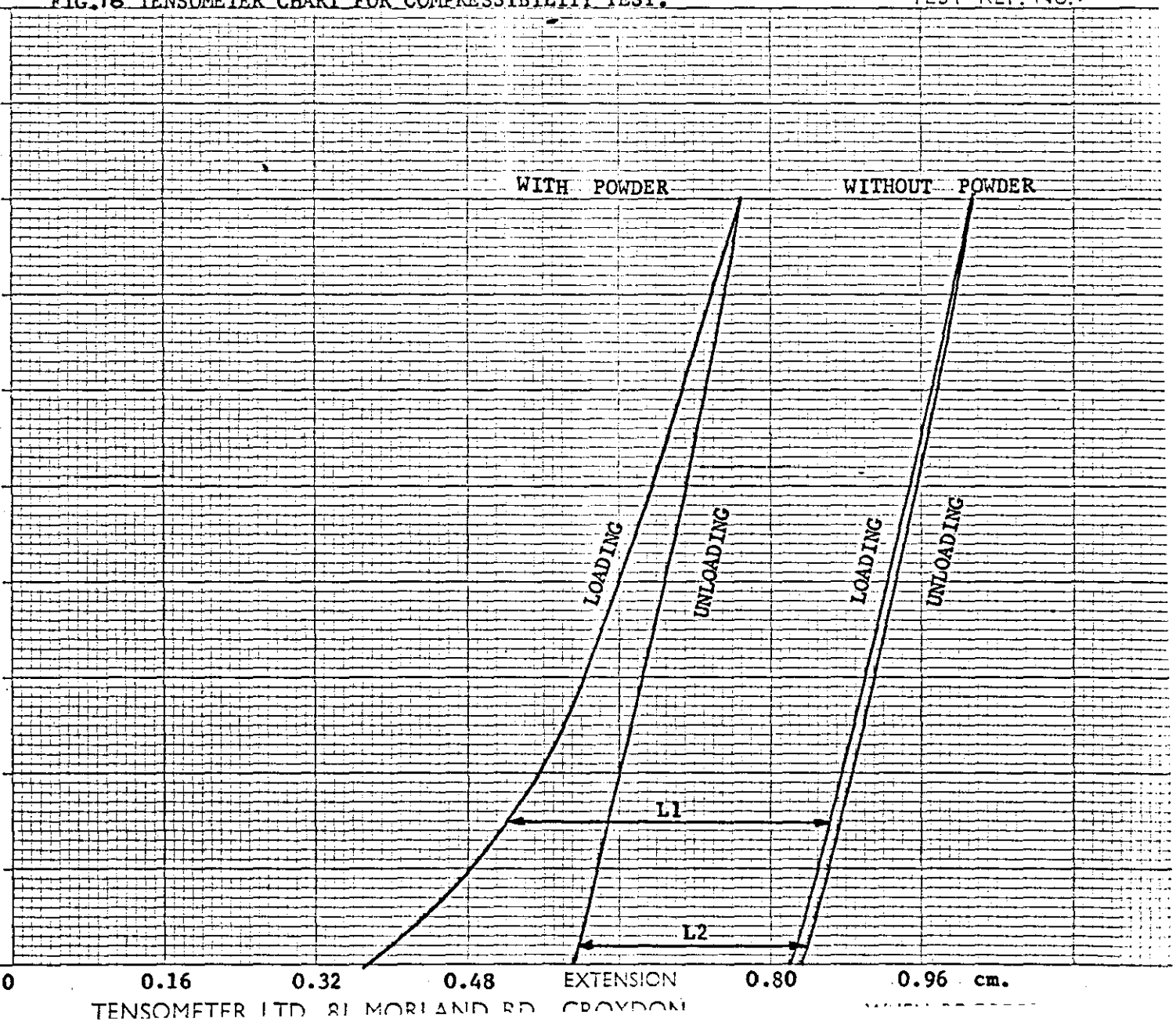

TENSOMETER LTD. 81 MORLAND RD. CROYDON

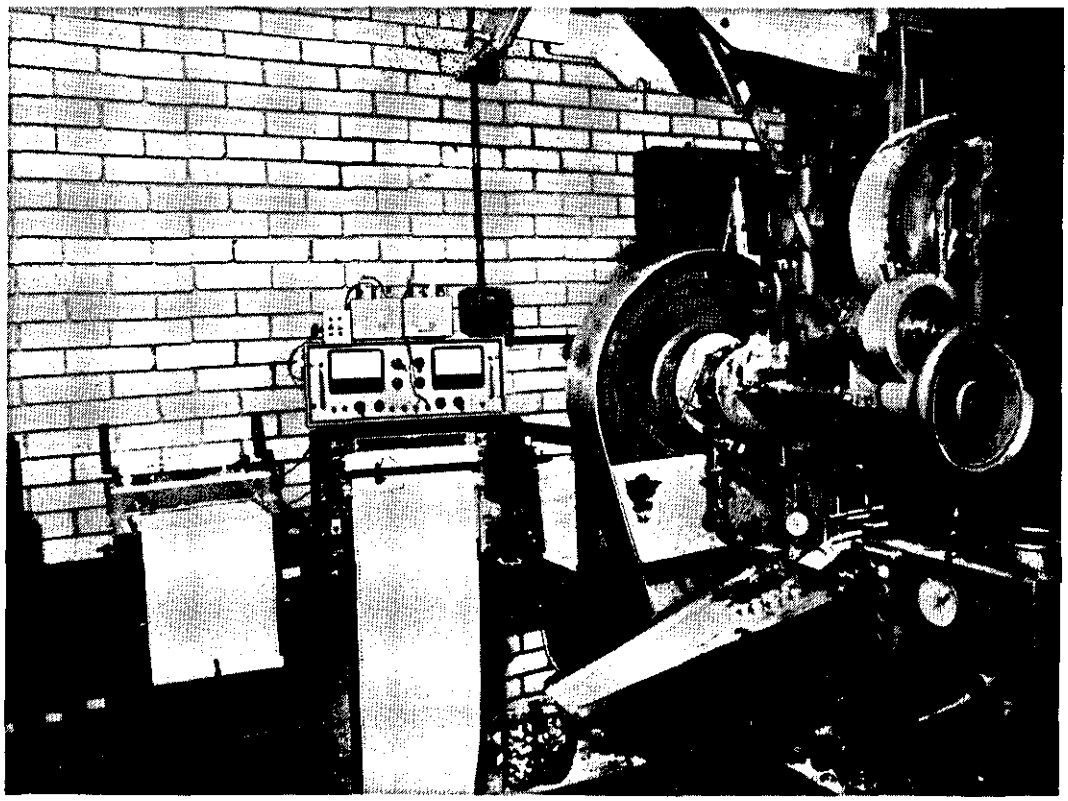

Figure 17 Press instrumentation for pilot plant pressing studies.

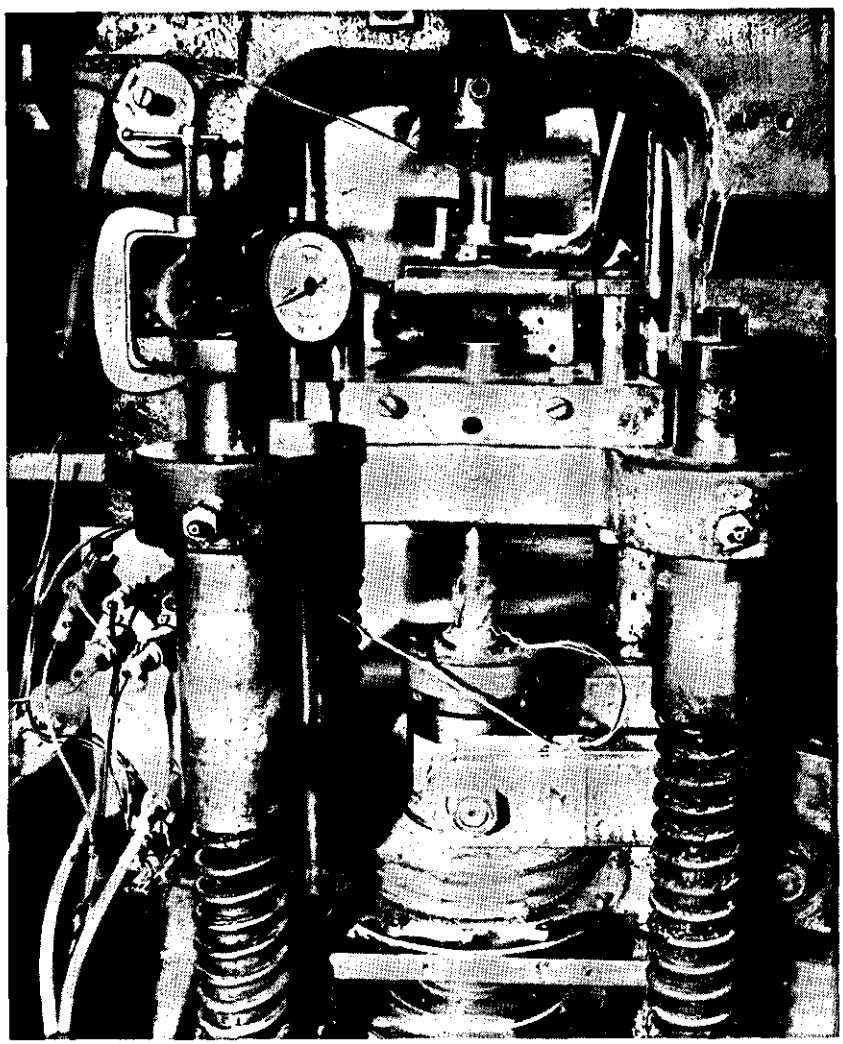

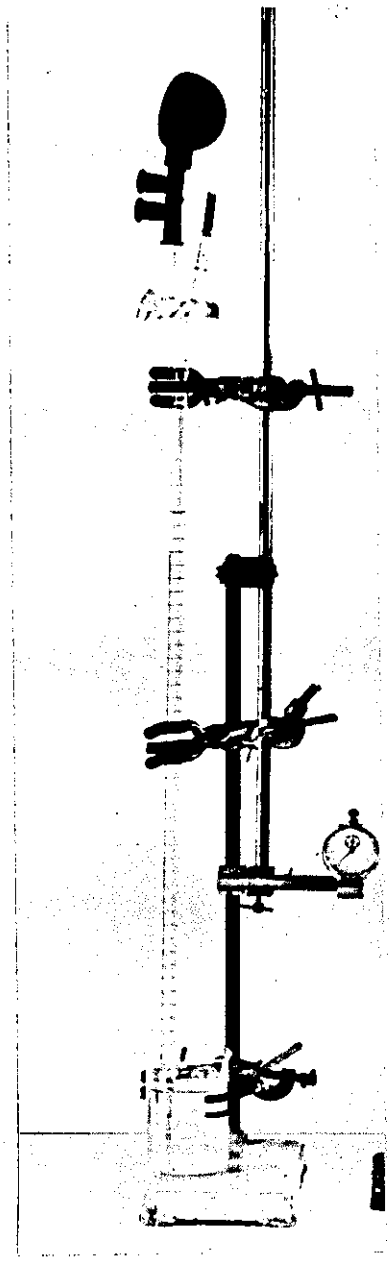

FIG. 18 THE PERMEAMETER

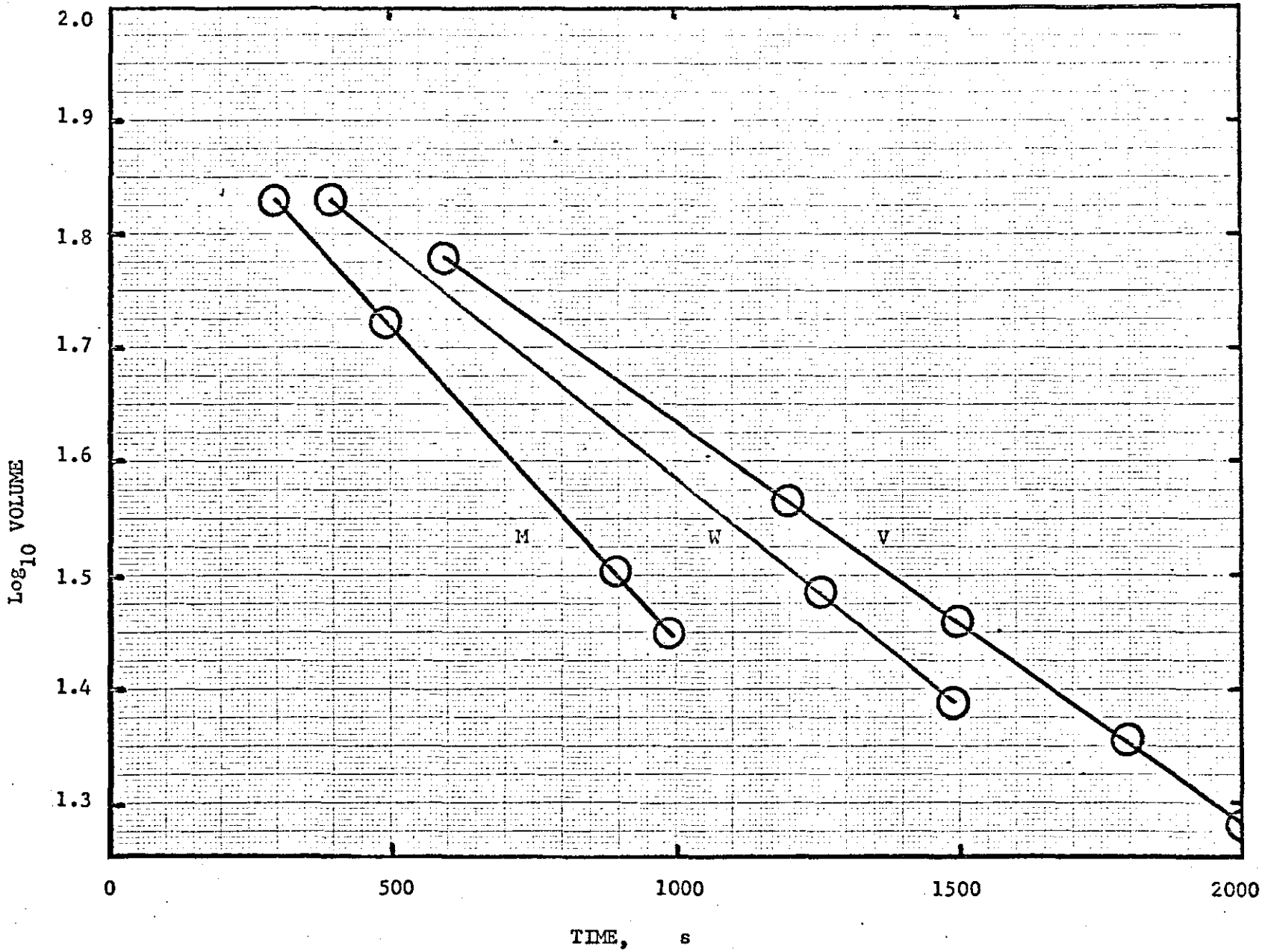

FIG. 19.

SURFACE AREA BY FALLING PRESSURE PERMEAMETRY

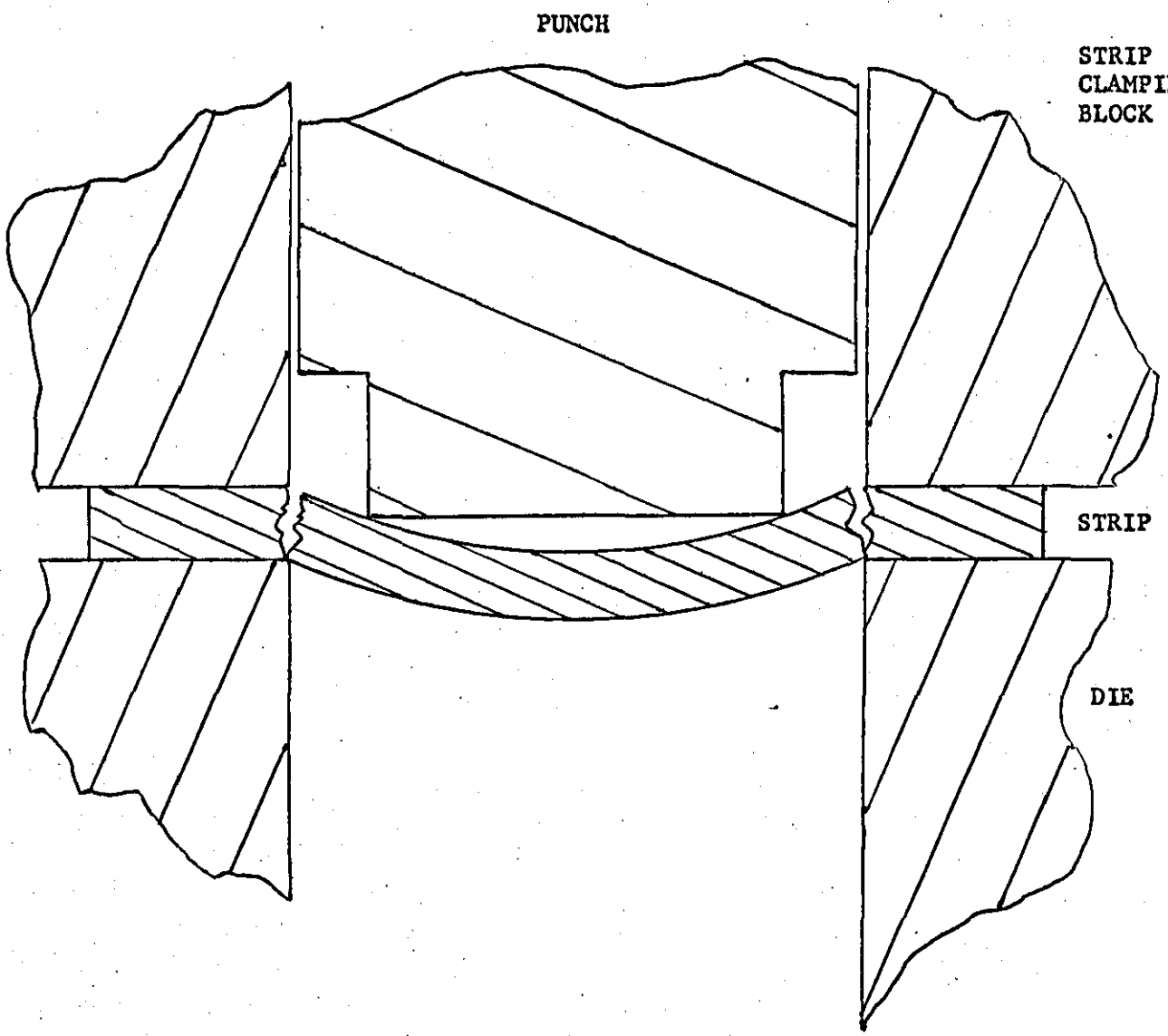

SECTION THROUGH TOOL USED IN ANNULAR BEND TEST

FIG. 20

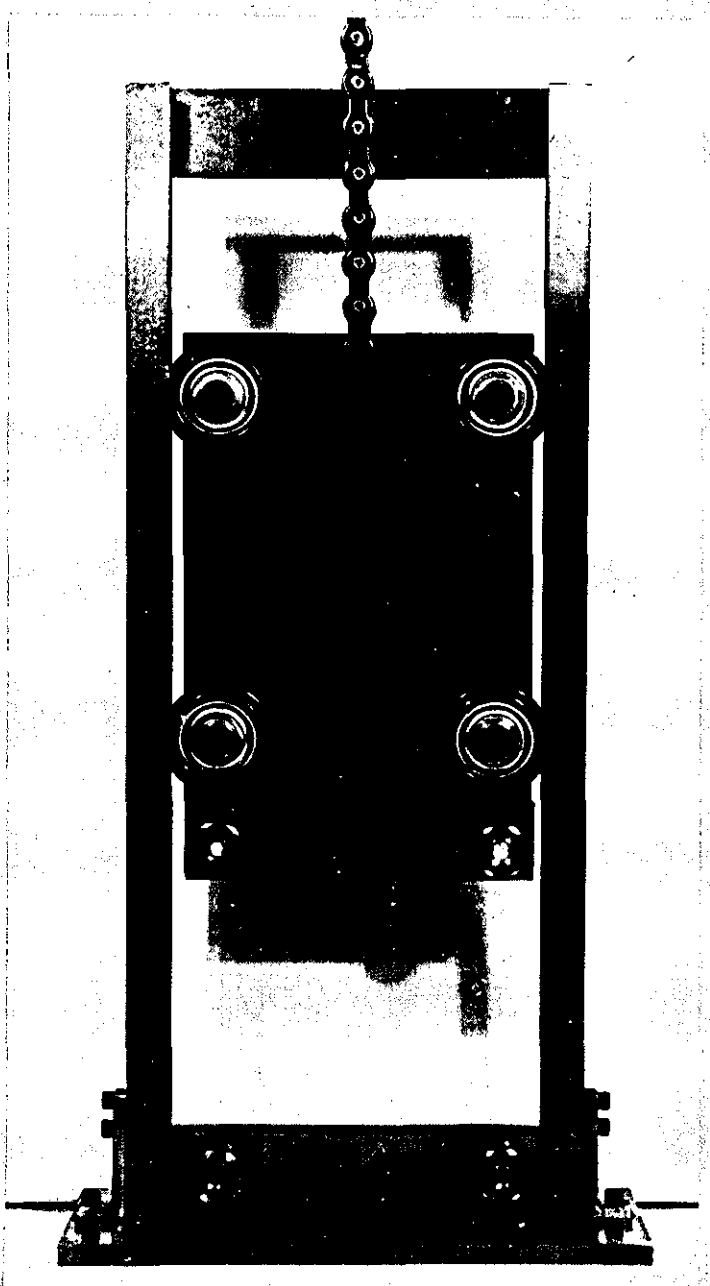

FIG. 21 THE TENSILE TEST JIG

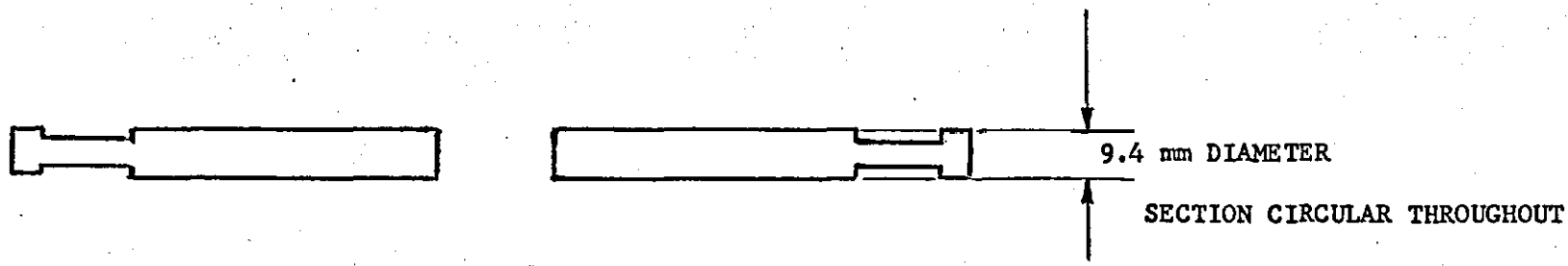

GRIPS

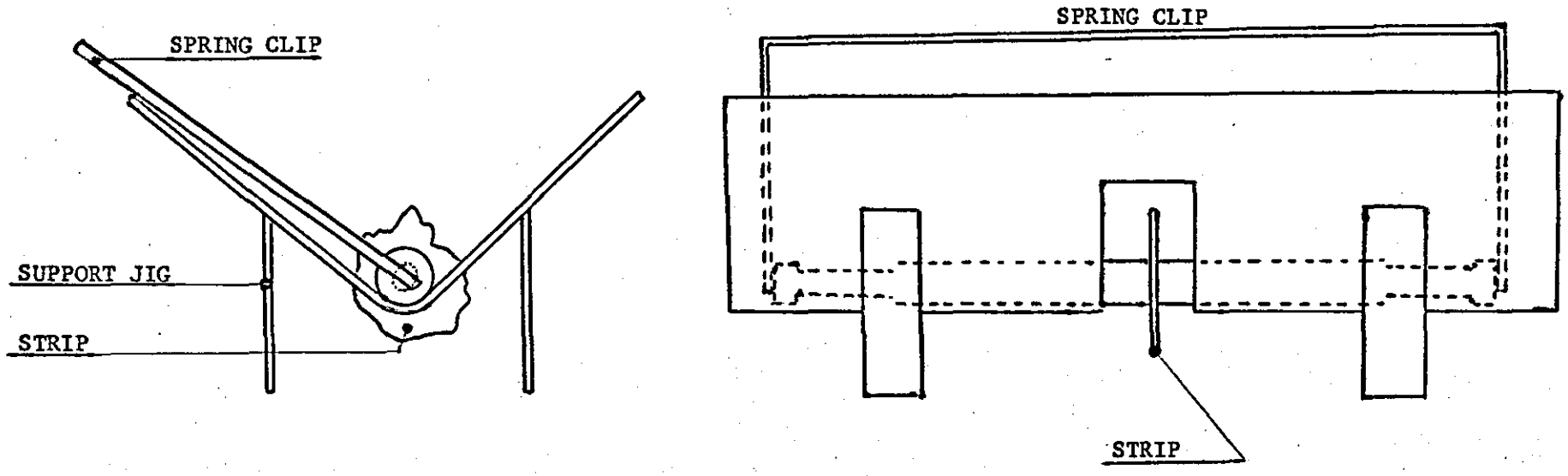

CURING ASSEMBLY

FIG.22 TENSILE TESTING APPARATUS

FOR TEST NORMAL TO PLANE OF STRIP

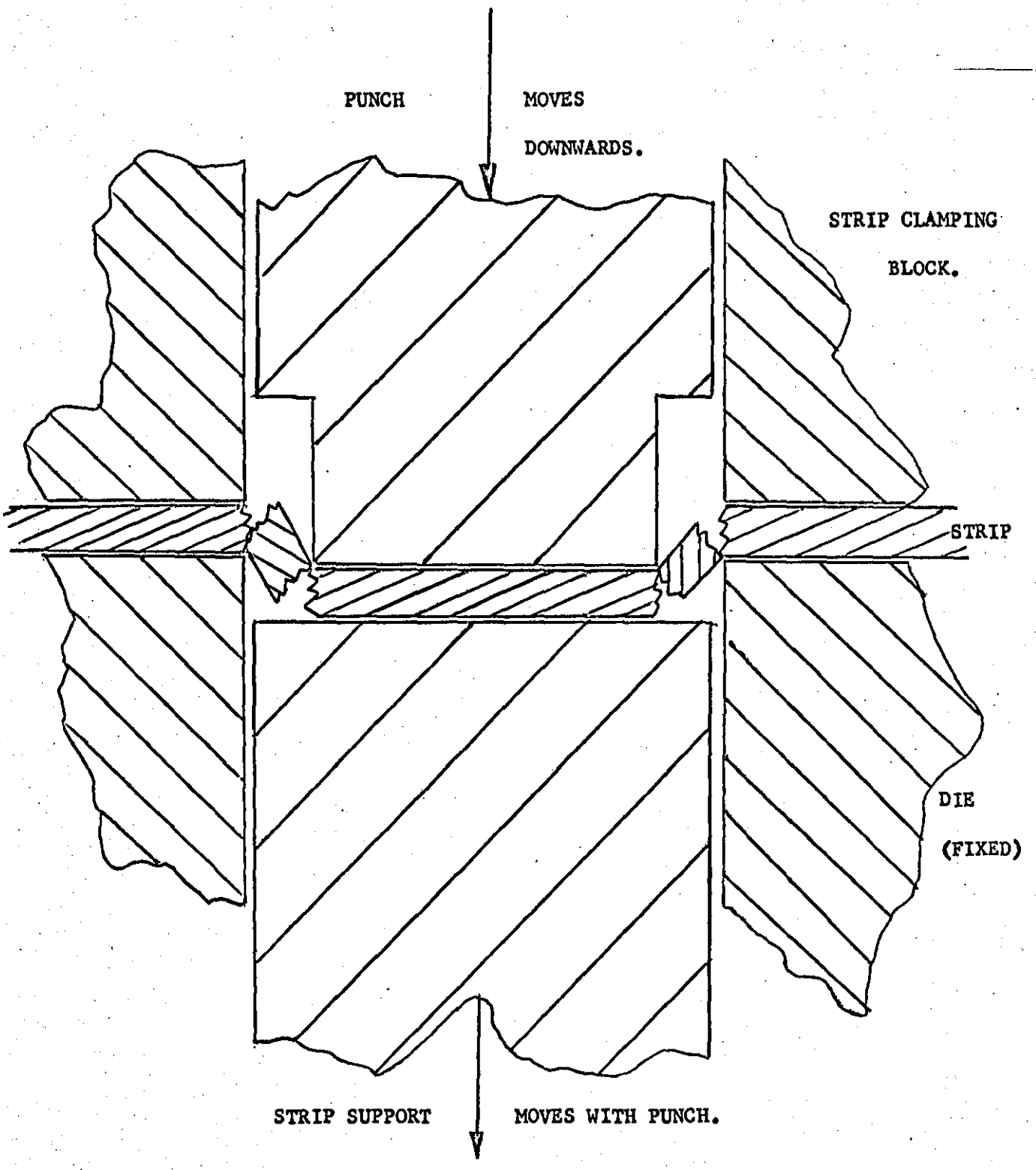

FIG. 23 : SECTION THROUGH GREEN SHEAR TOOL AND BROKEN STRIP.

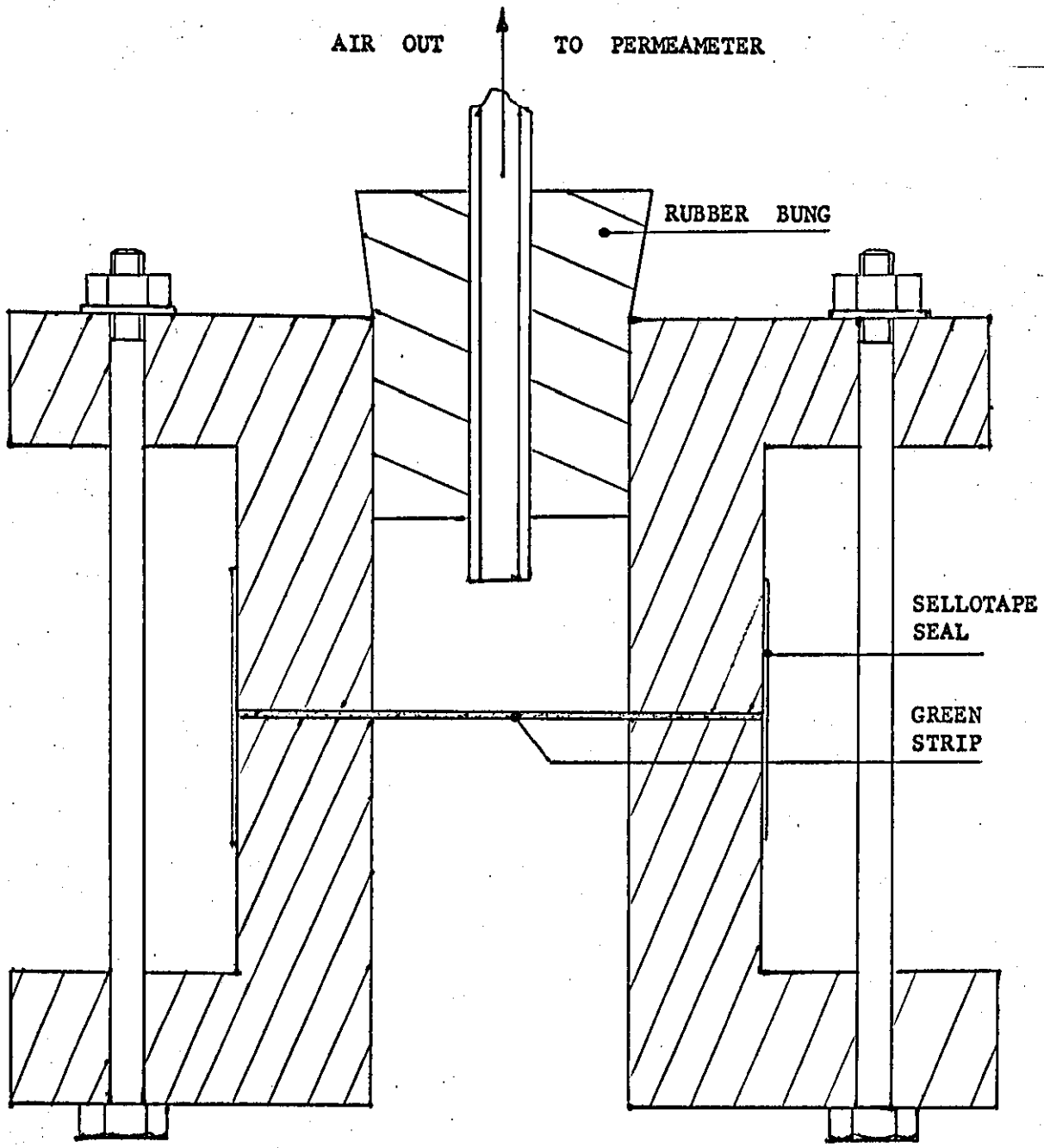

SECTION THROUGH CELL USED TO MEASURE PERMEABILITY OF GREEN STRIP

FIG. 24

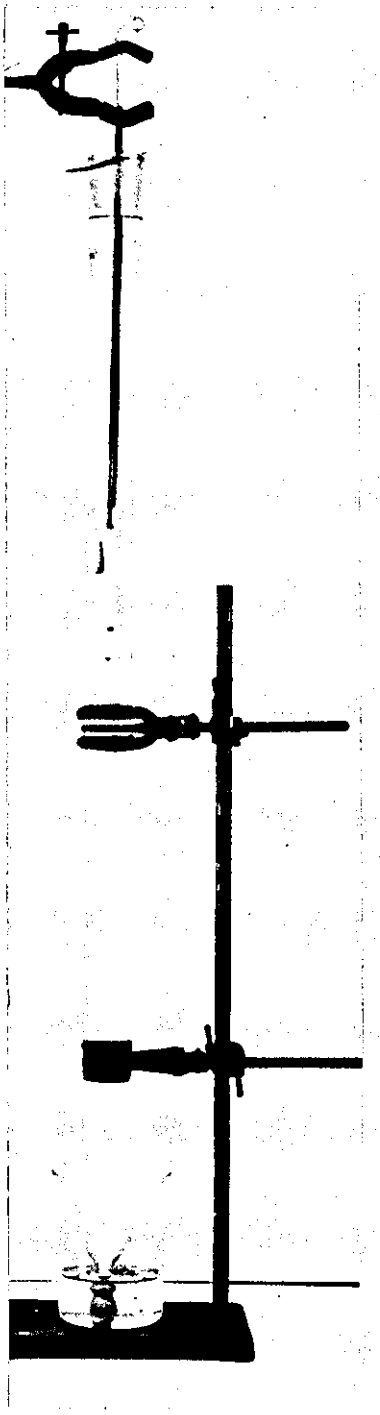

FIG. 25 THE TEMPERATURE GRADIENT COLUMN

(a) WATER ATOMISED POWDER, x 800

ETCHED IN 2% NITAL

(b) SPONGE POWDER, x 800

ARGON ION ETCH

FIG. 26 PHOTOMICROGRAPHS OF THE AS-RECEIVED POWDERS

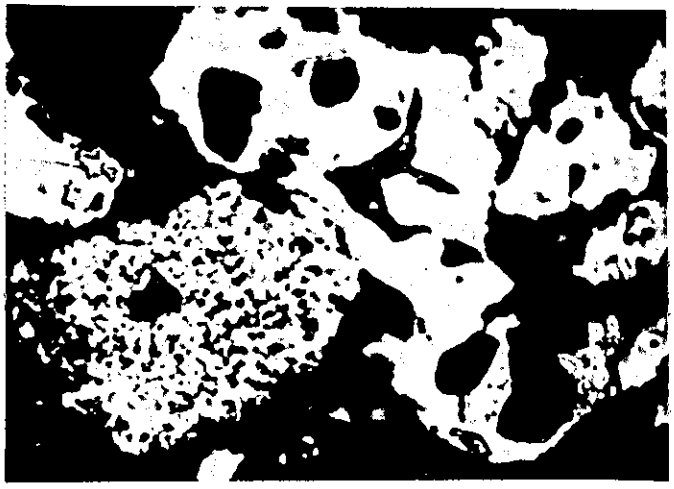

(a) x 500

(b) x 2000

(c) x 5000

(d) x 5000

FIG. 27 SCANNING ELECTRON MICROGRAPHS OF POWDER

(a) - (d) WATER ATOMISED POWDER

(e) x 500

(f) x1000

(g) x 2000

(h) x 10 000

FIG. 27 SCANNING ELECTRON MICROGRAPHS OF POWDER

(e) - (h) SPONGE POWDER

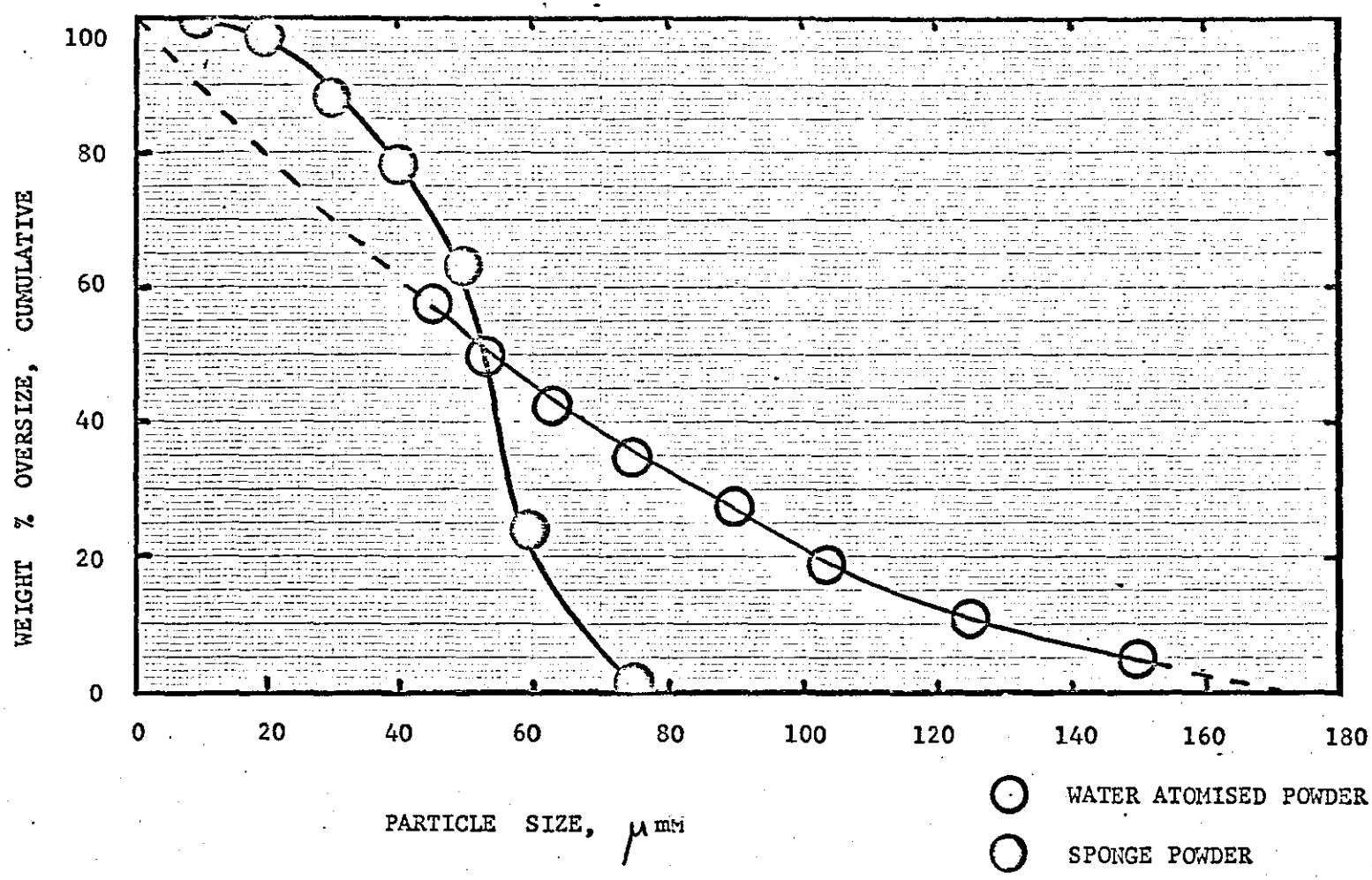
100
80
60
40
20
0
WEIGHT % OVERSIZE, CUMULATIVE
0
20
40
60
80
100
120
140
160
180
PARTICLE SIZE, μm
WATER ATOMISED POWDER
SPONGE POWDER

FIG. 28

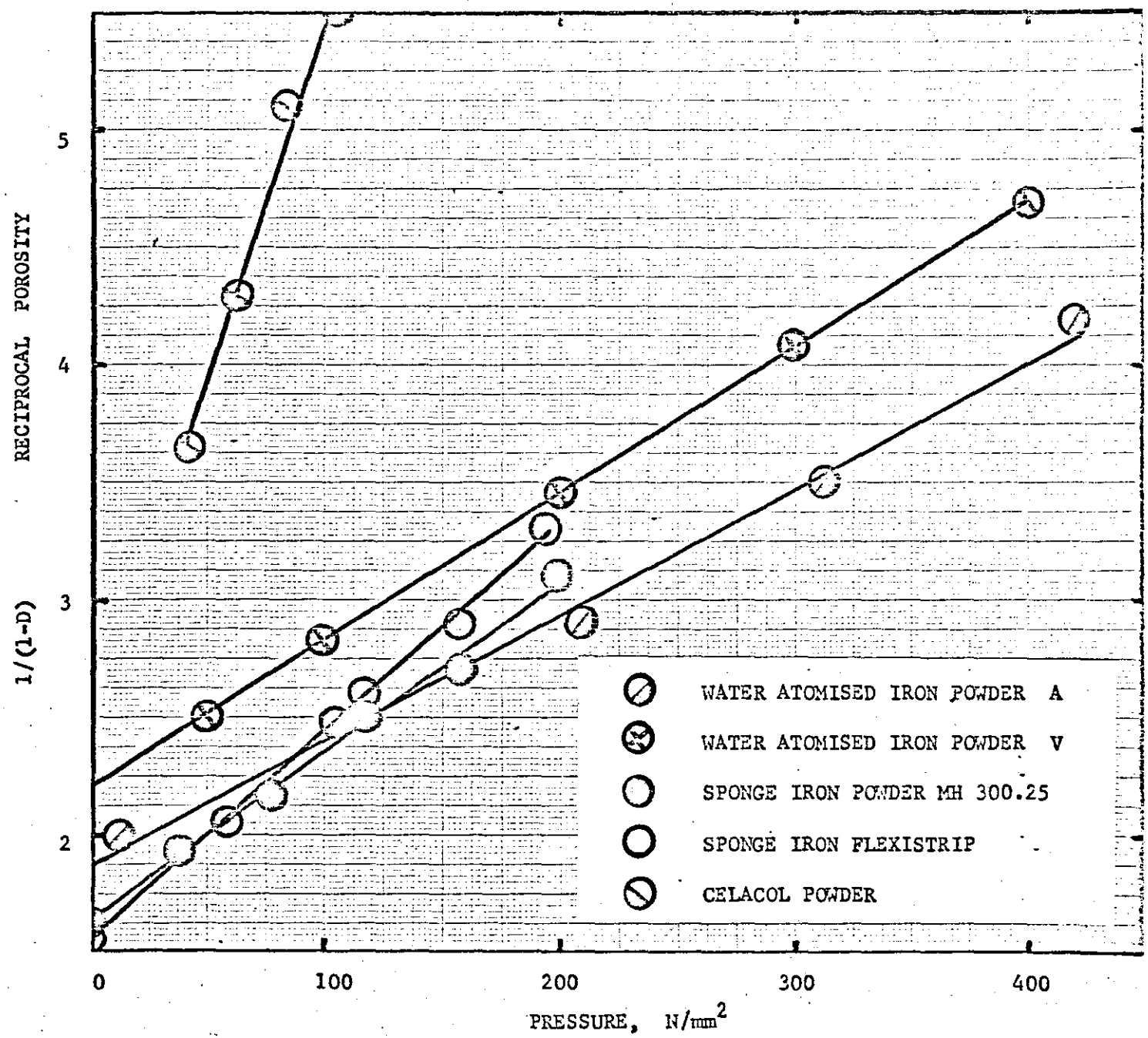
RECIPROCAL POROSITY
1/(1-D)
5
4
3
2
0
100
200
300
400
PRESSURE, N/mm²
WATER ATOMISED IRON POWDER A
WATER ATOMISED IRON POWDER V
SPONGE IRON POWDER MH 300.25
SPONGE IRON FLEXISTRIP
CELACOL POWDER

FIG. 29

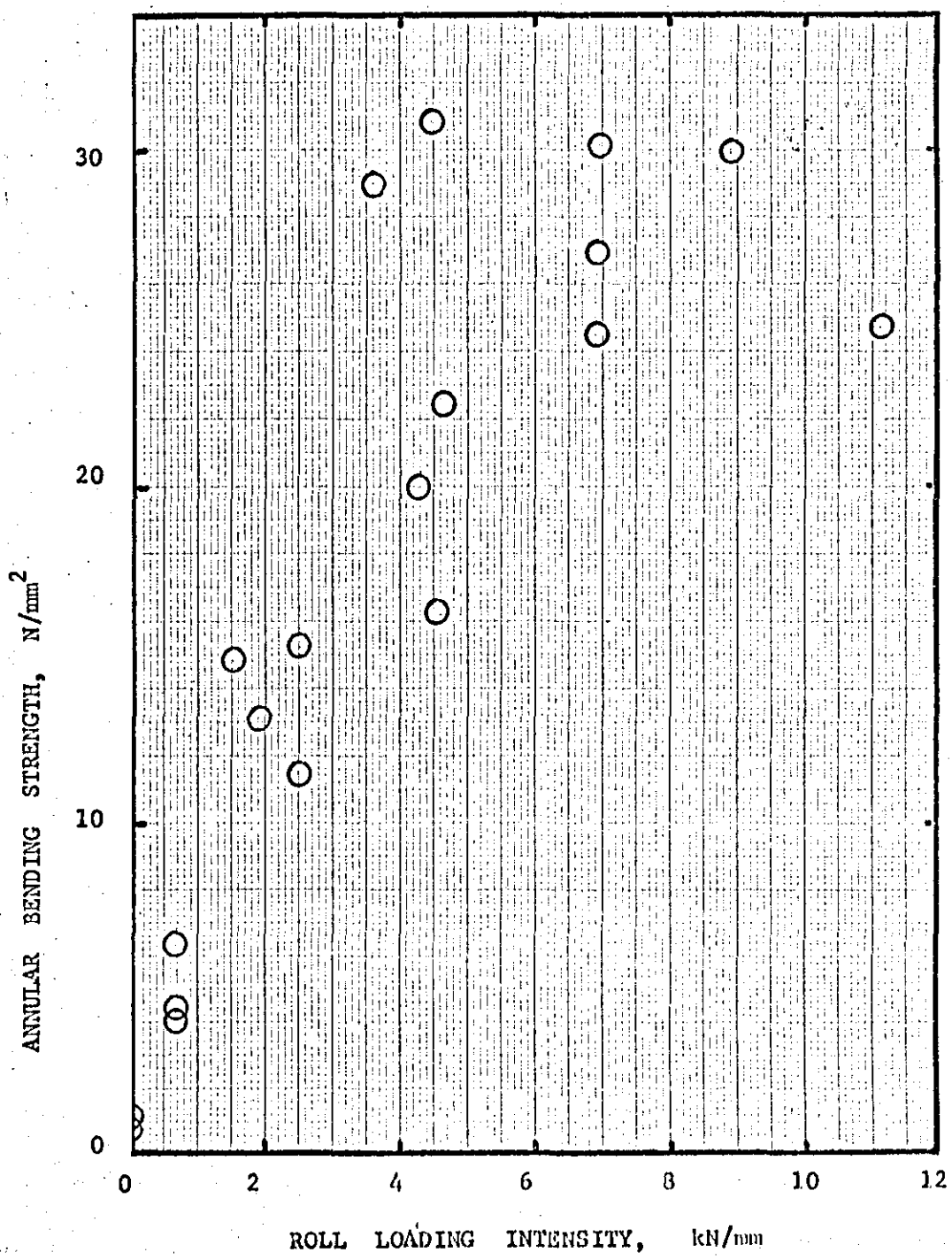
ANNULAR BENDING STRENGTH, N/mm^2
0
10
20
30
0
2
4
6
8
10
12
ROLL LOADING INTENSITY, kN/mm

WATER ATOMISED POWDER

FIG. 31

WATER ATOMISED POWDER

FIG. 32

SPONGE POWDER

FIG. 33

(a) x 1100

(b) x 220

FIG. 34 FRACTURE SURFACE IN THE PLANE OF GREEN STRIP

Strip made from sponge iron powder

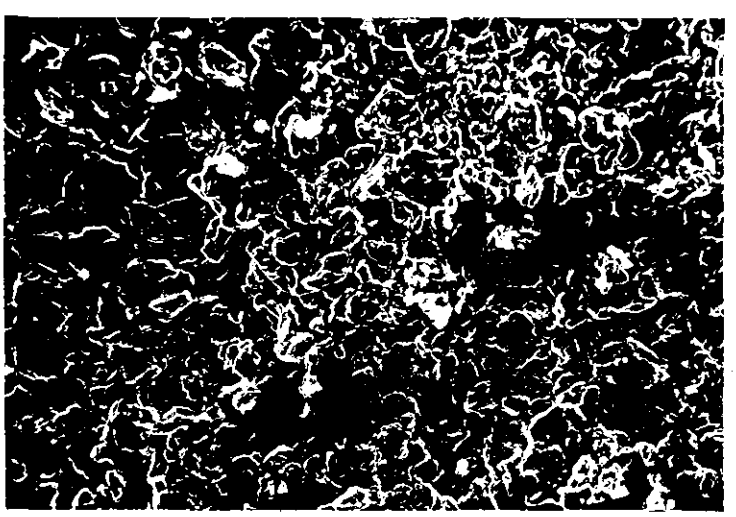

(a) x 800

(b) x 200

FIG. 35 TRANSVERSE FRACTURE SURFACE OF GREEN STRIP MADE FROM WATER ATOMISED POWDER

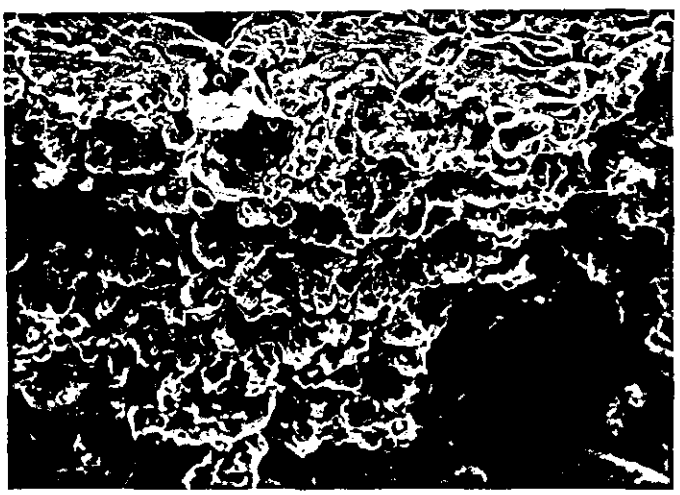

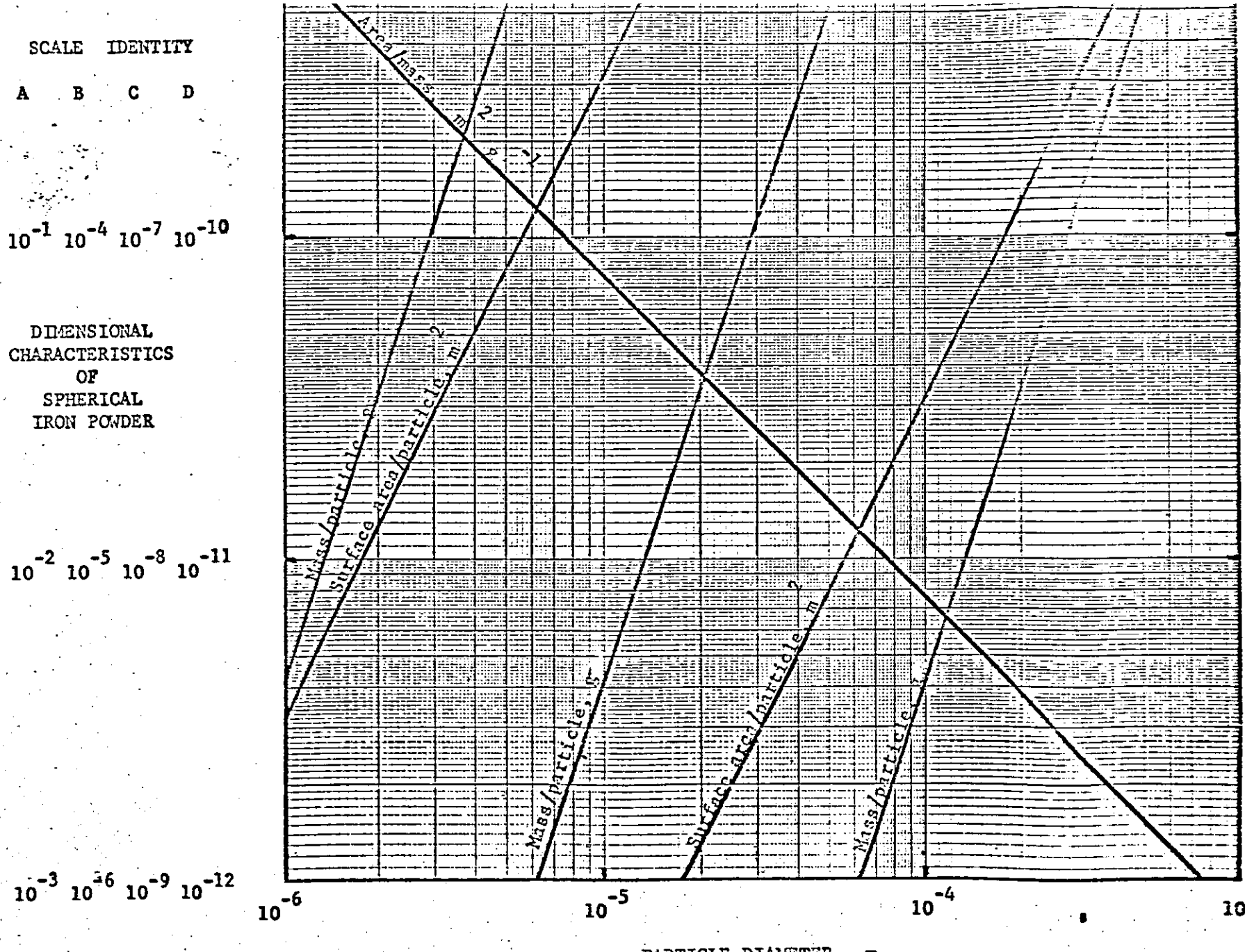
SCALE IDENTITY
A B C D
10^{-1} 10^{-4} 10^{-7} 10^{-10}
DIMENSIONAL CHARACTERISTICS OF SPHERICAL IRON POWDER
10^{-2} 10^{-5} 10^{-8} 10^{-11}
10^{-3} 10^{-6} 10^{-9} 10^{-12}
Area/mass, m^2/g
Surface Area/particle, m^2
Mass/particle, g
Surface area/particle, m^2
Mass/particle, g
10^{-6}
10^{-5}
10^{-4}
10^{-3}
PARTICLE DIAMETER, m

FIG. 36

(a) FRACTURED FLEXISTRIP, x 550

SURFACE IS UPPER REGION OF PHOTOGRAPH

(b) SURFACE OF STRIP REMOVED FROM ROLL GAP, x 1 000

ROLLED STRIP ON LEFT

(c) FRACTURED GREEN STRIP, x 550

SURFACE IS UPPER REGION

FIG. 37 SCANNING ELECTRON MICROGRAPHS OF THE FILM OF BINDER ON THE SURFACE OF WATER ATOMISED STRIP

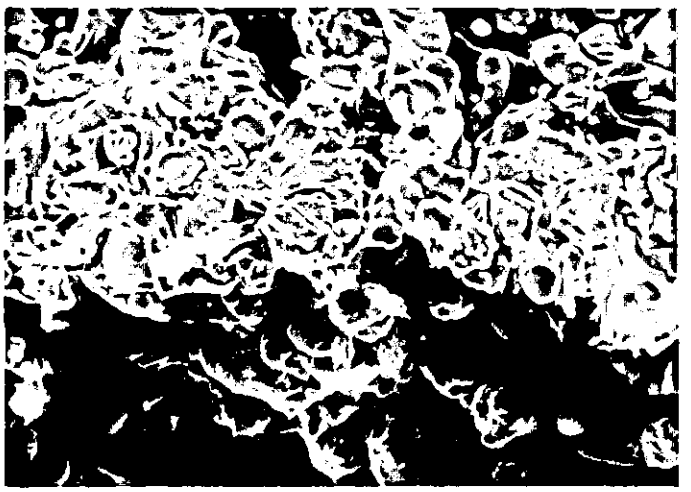

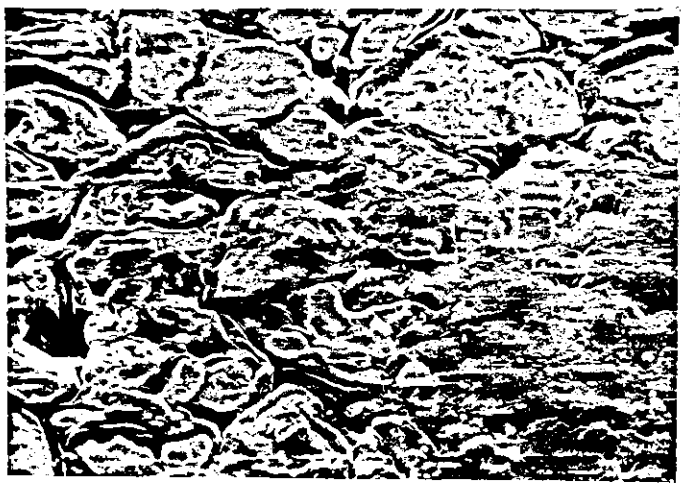

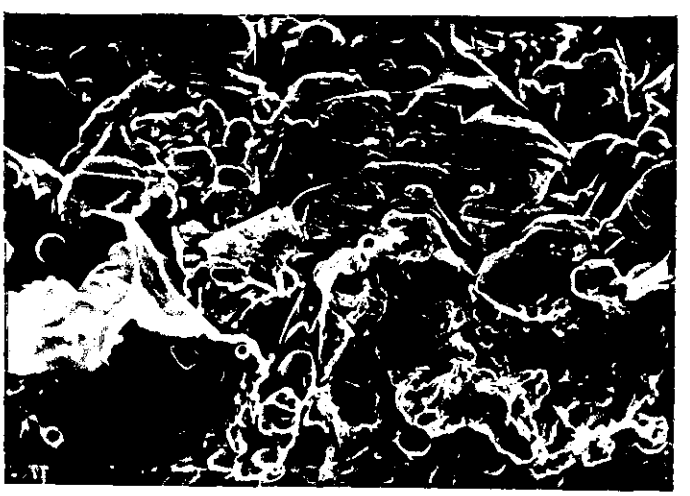

(a) WATER ATOMISED, x 550 STRIP SURFACE AT TOP OF PICTURE

(b) WATER ATOMISED, x 550 STRIP SURFACE AT TOP OF PICTURE

(c) SPONGE, x 550

FIG. 38 SCANNING ELECTRON MICROGRAPHS OF FILMS OF BINDER IN FLEXISTRIP

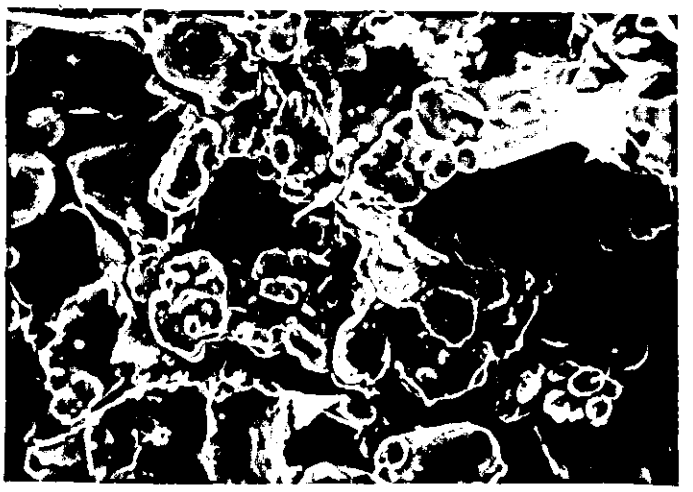

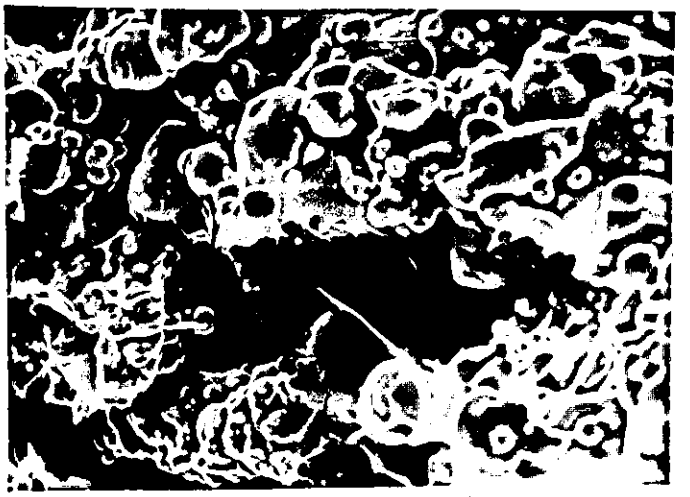

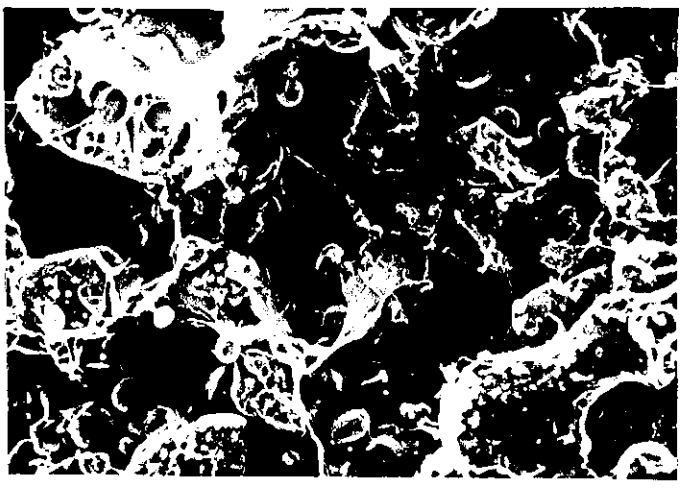

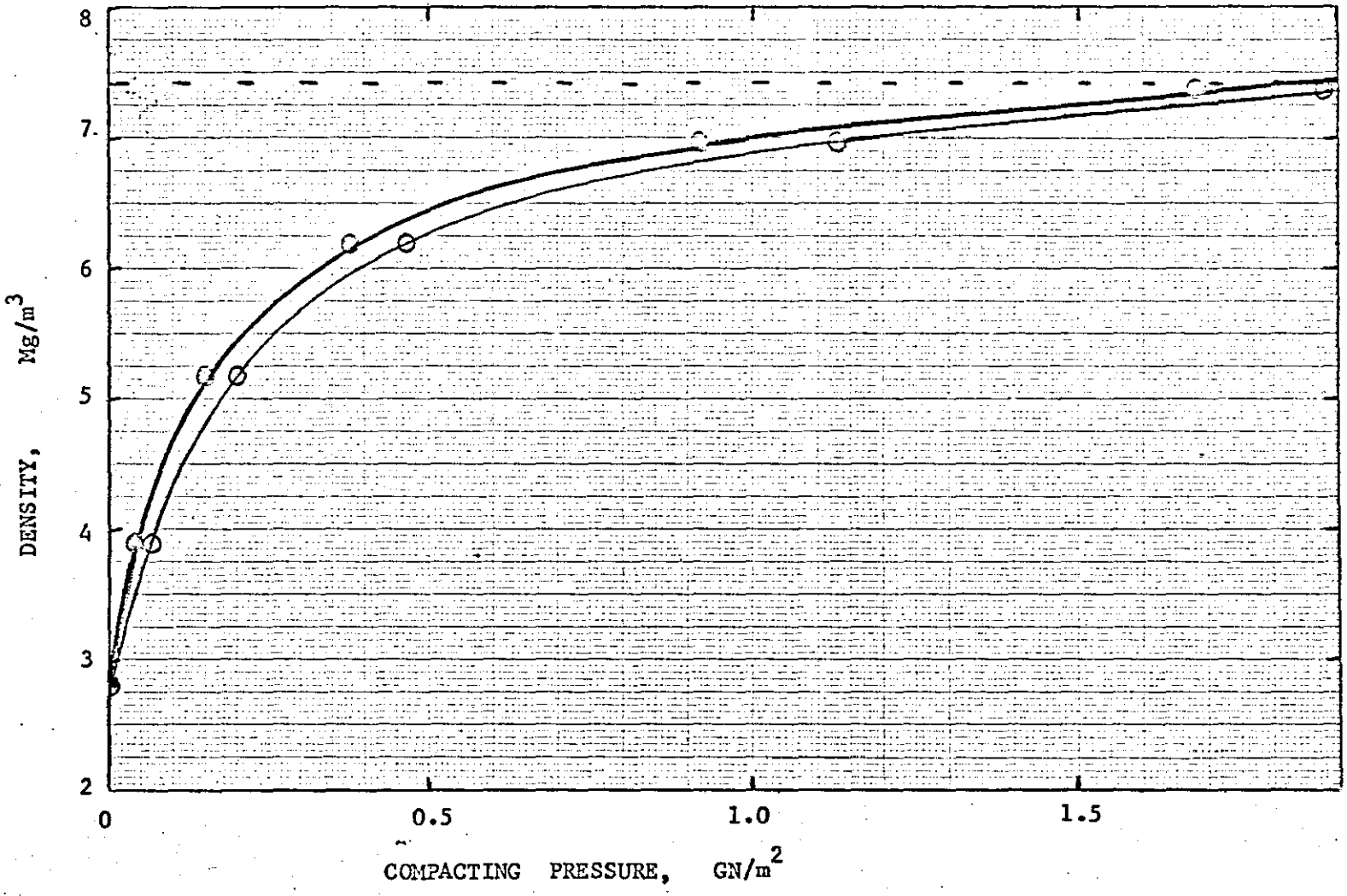

FIG. 39

From compressibility of flexistrip

From compressibility of MH 300. 25

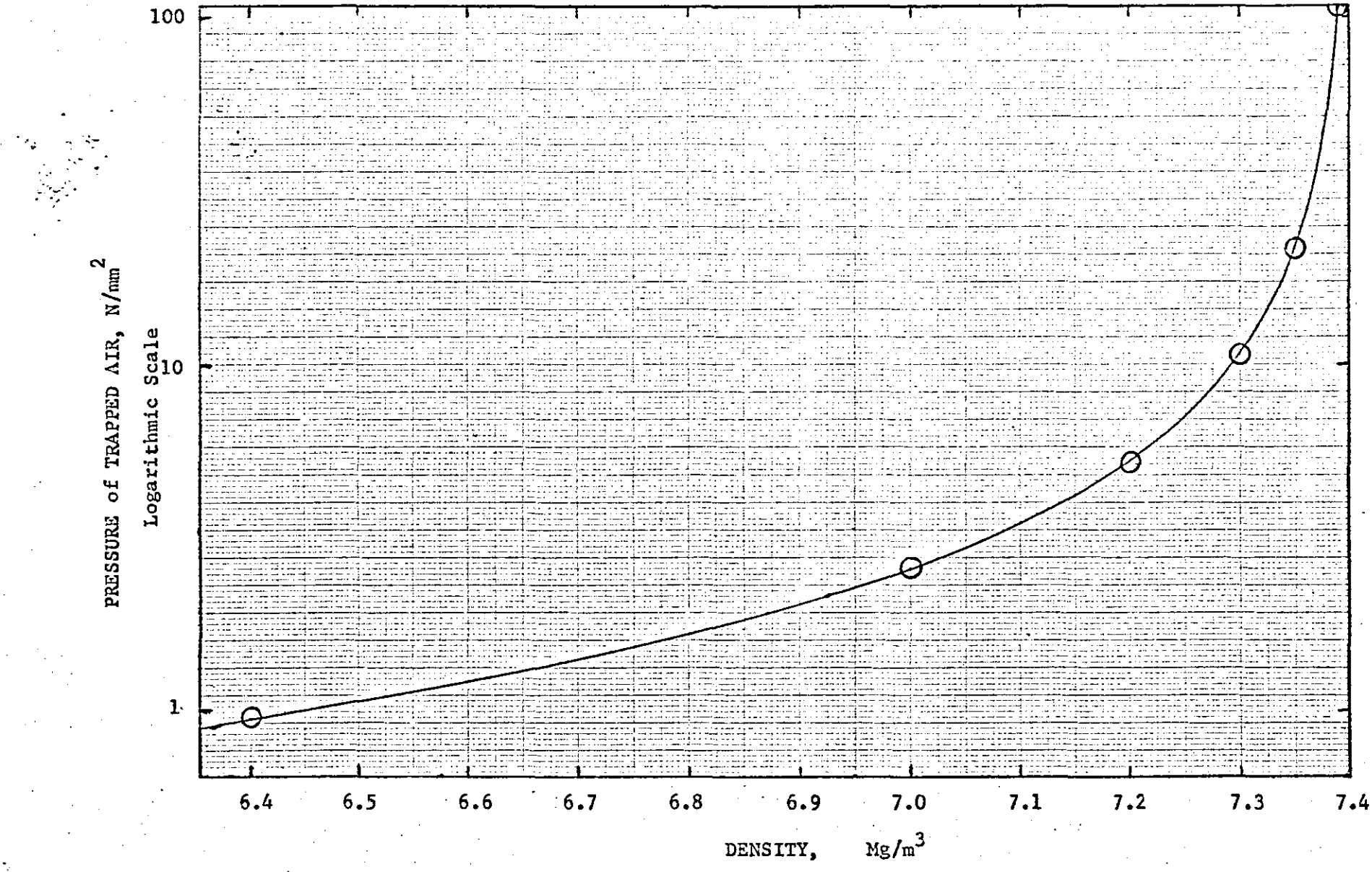
100
10
1
PRESSURE of TRAPPED AIR, N/mm^2
Logarithmic Scale
6.4
6.5
6.6
6.7
6.8
6.9
7.0
7.1
7.2
7.3
7.4
DENSITY, Mg/m^3

FIG. 40

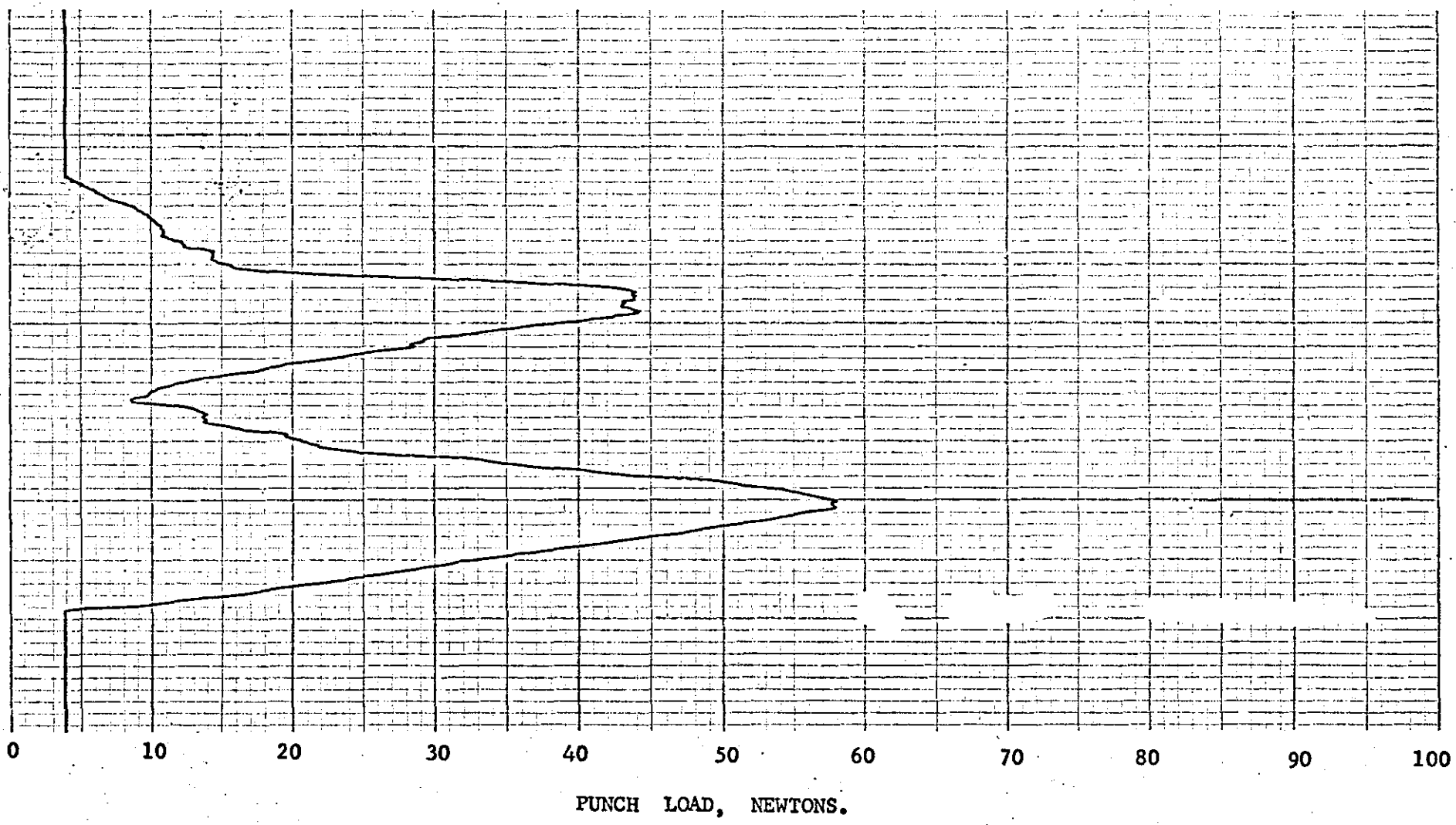

INSTRON CHART FOR ANNULAR BEND TEST SPECIMEN I1. CHART STRAIN MAGNIFICATION 100 : 1

INITIAL LOAD REPRESENTS PUNCH WEIGHT. SECOND PEAK (TOP OF CHART) IS ATTRIBUTED TO FAILURE OF THE INNER SEGMENT OF THE ANNULUS.

FIG. 41

MEAN LINEAR INTERCEPT, μm
20
18
16
14
12
10
8
7.66
7.70
7.74
7.78
7.82
STRIP DENSITY, Mg/m3

FIG. 42

(a) Strip made from powder A, x 1 000

(b) Strip made from powder S, x 1 000

FIG. 43 SCANNING ELECTRON MICROGRAPHS OF FRACTURE SURFACES OF LONGITUDINAL CENTRE TENSILE TEST PIECES

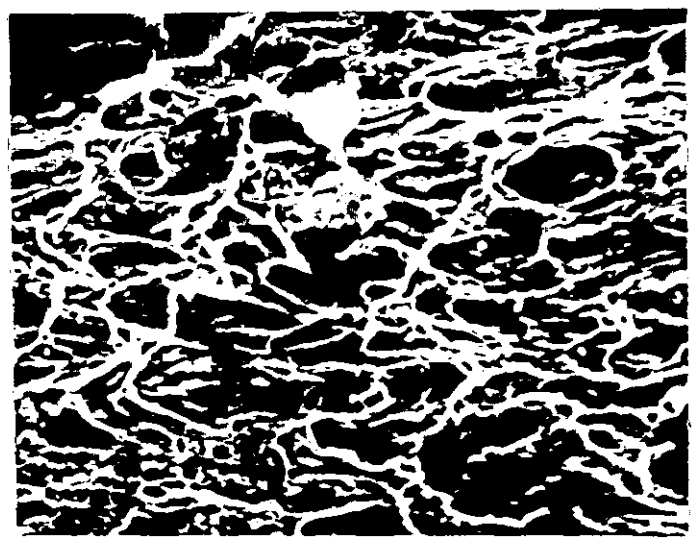

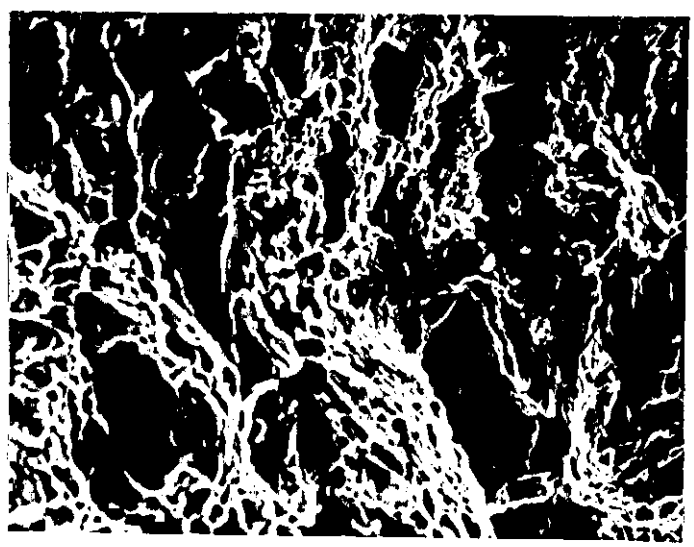

(a) Strip made from powder Y, x600

(b) Strip made from powder W, x600

FIG. 44 CROSS SECTIONS THROUGH FINISHED STRIP

as polished, showing defects

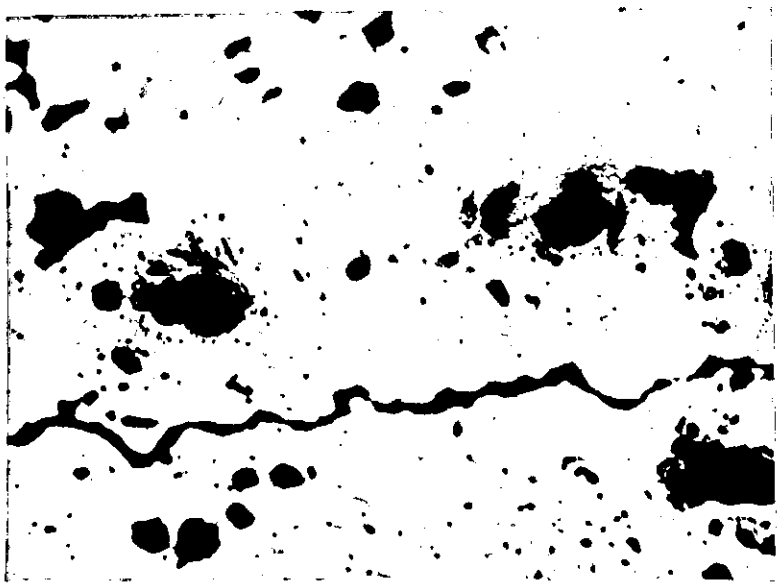

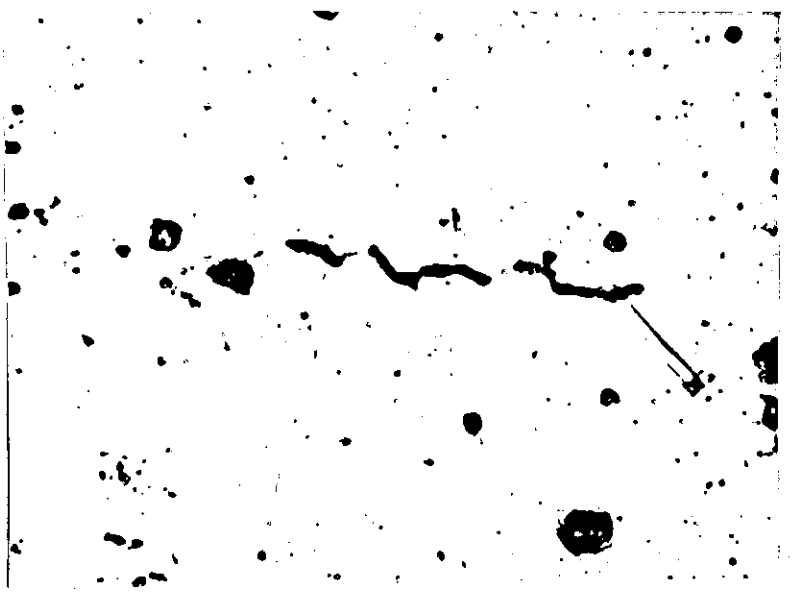

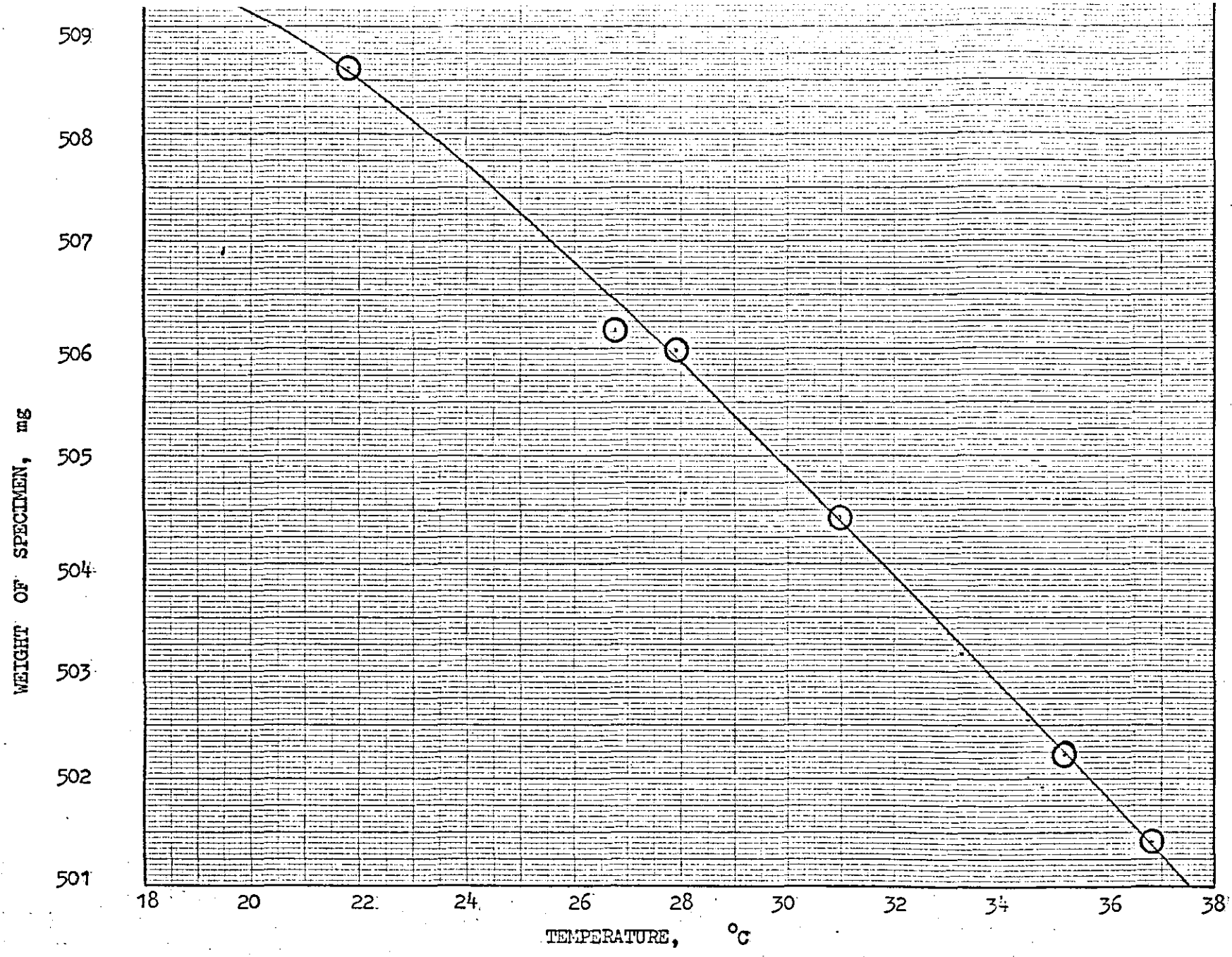

FIG. 45 SPECIMEN WEIGHT V. FLOTATION TEMPERATURE

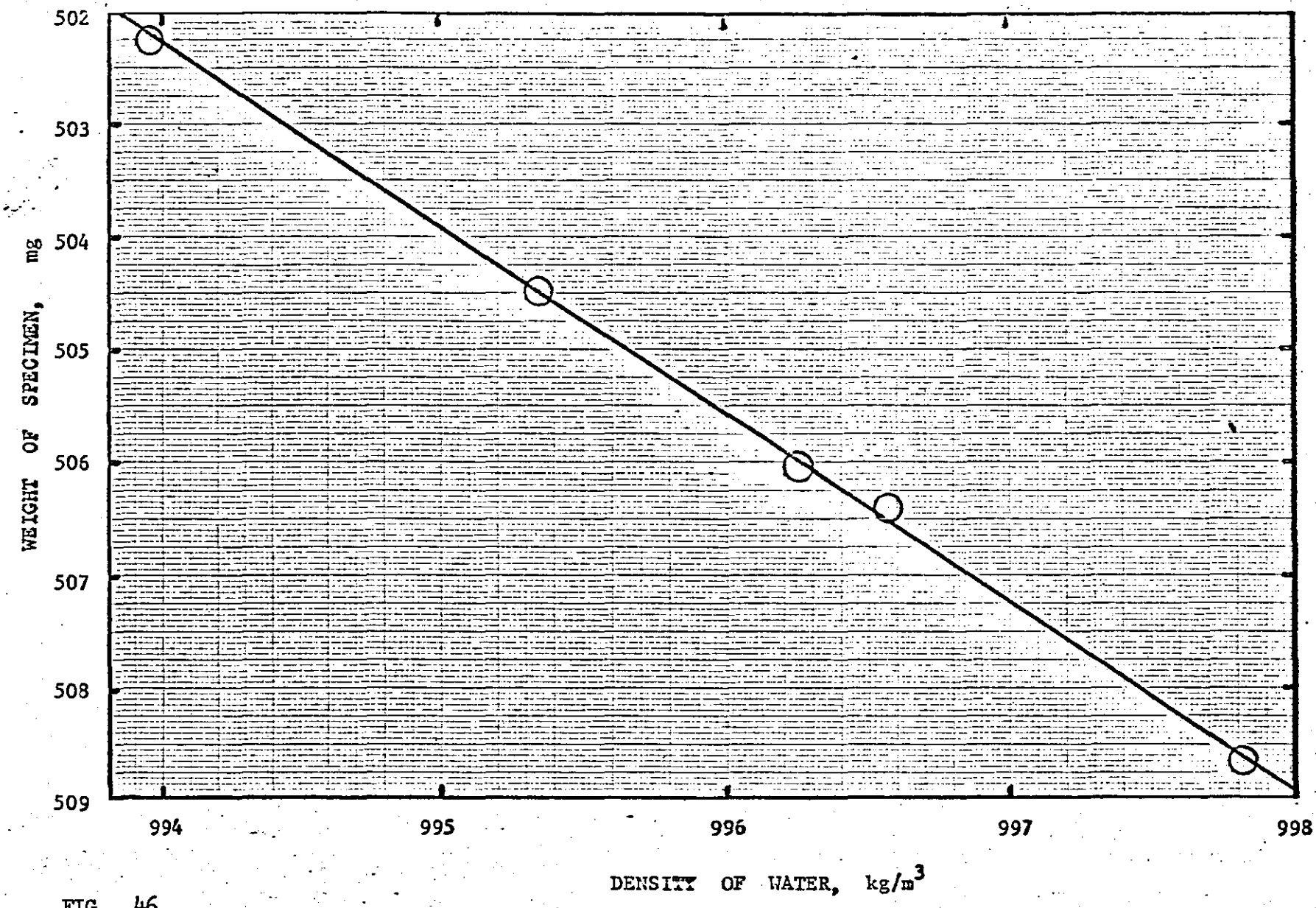
502
503
504
505
506
507
508
509
WEIGHT OF SPECIMEN, mg
994
995
996
997
998
DENSITY OF WATER, kg/m3

FIG. 46

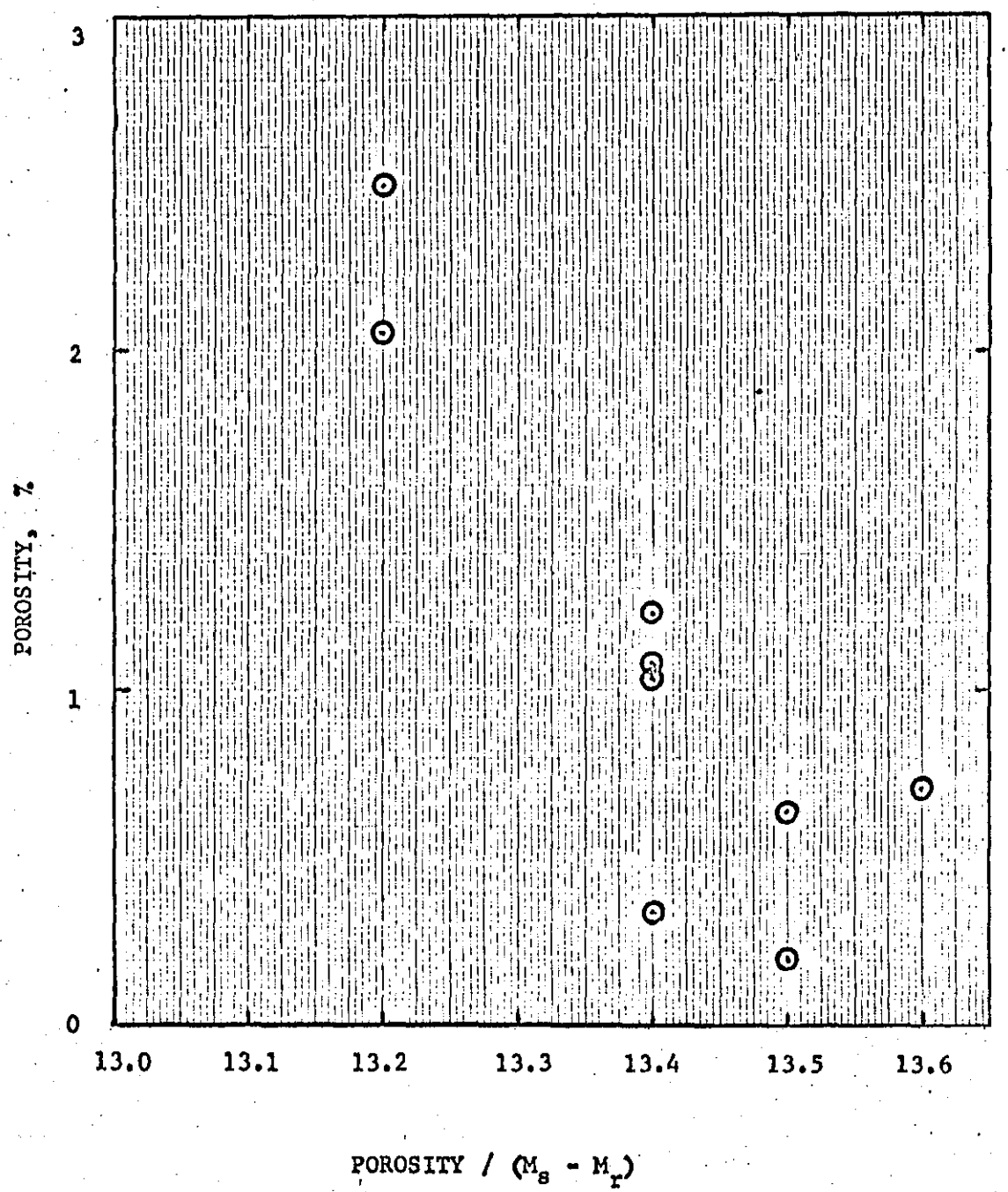

FIG. 47

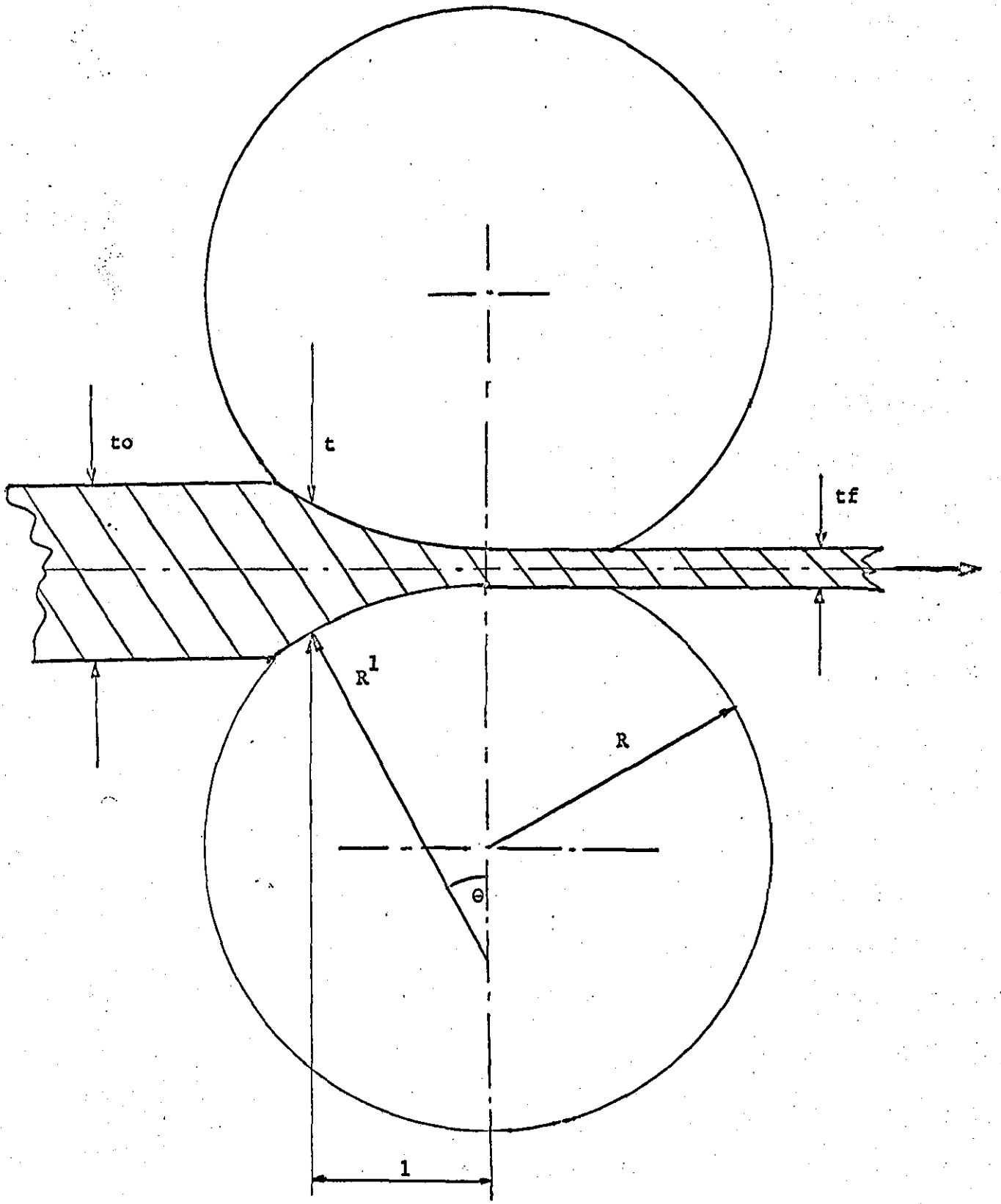

DEFORMED SHAPE OF ROLLS

FIG. 48

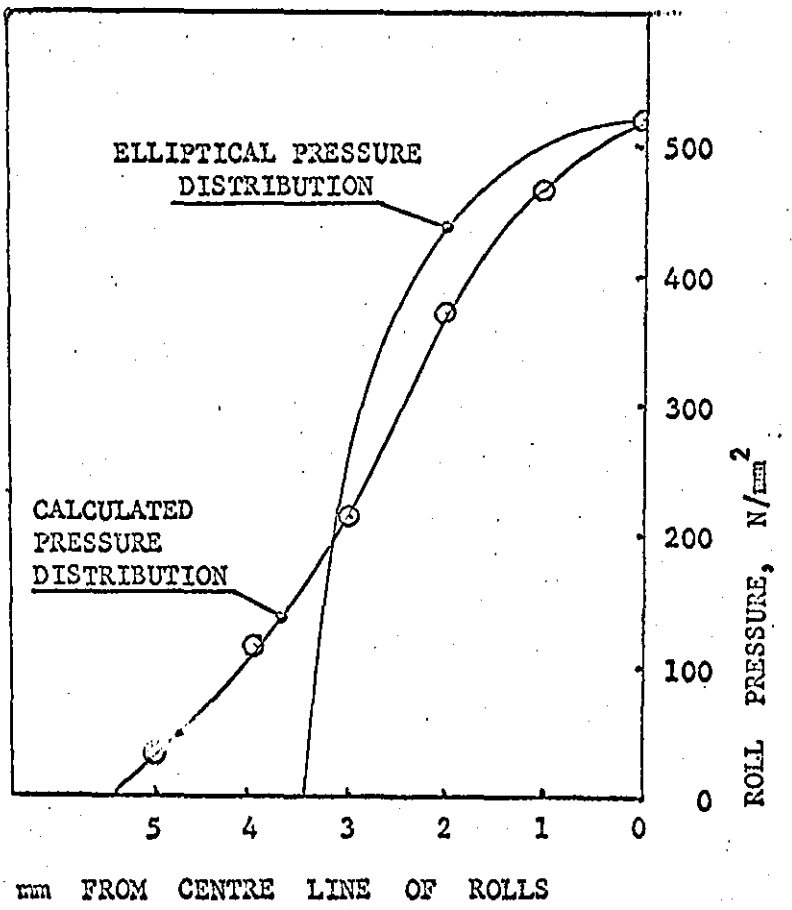

FIG. 49

COMPARISON OF ELLIPTICAL PRESSURE DISTRIBUTION WITH THE PRESSURE DISTRIBUTION WHICH WOULD BE PRODUCED BY A CIRCULAR ARC OF CONTACT.

TOTAL FORCE AND MAXIMUM PRESSURE ARE THE SAME FOR BOTH CURVES.

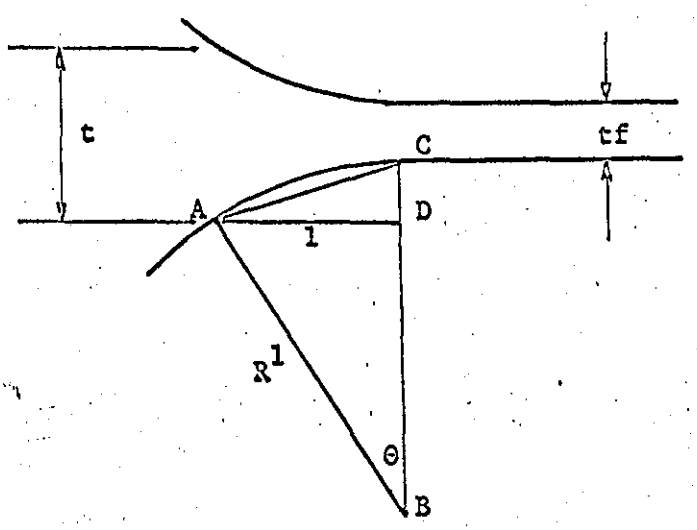

From triangle ABC,

BAC = BCA = $(180^\circ - ABC)/2$

From triangle ADC,

CAD = 90° - ACD

Therefore

CAD = ABC/2 = $\theta/2$

$t = tf + 2l\sin\theta/2$

FIG. 50

Powder Identity	Lower Cut size	Powder Identity	Lower Cut Speed	Calculated Particle Size
A	As received	J	35 rev/s	0.064 mm
B	0.150 mm	K	50 rev/s	0.037 mm
C	0.125	L	66 rev/S	0.019 mm
D	0.104	M	100 rev/s	0.010 mm
E	0.090	N	133 rev/s	0.0064mm
F	0.075	O	-	0
G	0.063			
H	0.053			
I	0.045			

TABLE 1 : Identification of classified fractions of B.S.A. water-atomised powder

Powder Identity	Composition Equal Parts by Weight (except Y)
P	E,F,G
Q	C,D,E,F,G,H,I
R	B,C,D,E,F,G,H,I,K,L
S	2 x B, C,D,E,F,G,H,I,K,L,M,N,O
T	H,I,K.
U	F,G,H,I,K,L,M
V	D,E,F,G,H,I,K,L,M,N,O
W	L,M,N
X	I,J,K,L,M,N,O
Y	45g N, 105g M

TABLE 2: Composition of blends of B.S.A. water-atomised powder

	C	S	P	Mn	Si	N	Hydrogen Loss
B.S.A.Water Atomised Powder Manufacturer's Analysis	0.032			0.10	0.02		
B.S.C.Analysis	0.022	0.020	0.010	0.12	0.019	0.003	0.6
Hoganas Sponge MH 300.25 Manufacturer's Typical Analysis	0.01						0.2
B.S.C.Analysis	0.005	0.002	0.003	0.02	-	0.0026	0.2

TABLE 3 : Chemical composition of as-received powders, weight %

	Grain Size	Microhardness	Particle Density Mg/m^3
B.S.A.Water-Atomised Powder	= particle size (40%) = 0.0025 mm* (60%)	HV/0.02 222 Min 299 Mean 484 Max	7.65
Hoganas Sponge MH300.25	Particle size	HV/0.01 116 Min 170 Mean 257 Max	7.77

TABLE 4 : Particle grain size, microhardness and density

* Mean linear intercept

B.S.A. Water-Atomised Powder		Hoganas Sponge MH300.25	
Nominal Sieve Aperture, μm	Cumulative Weight % Oversize	Nominal Sieve Aperture, μm	Cumulative Weight % Oversize
150	4.6	152	0.0
125	10.9		
104	18.2	106	0.2
90	27.1		
75	34.4	75	1.0
63	42.0	64	1.1
53	49.3	53	1.8
45	57.1	45	4.8
0	100.0	0	100.0

TABLE 5 : Particle Size Distribution by Weight

Minimum Chord, μm	Cumulative Number Percentage of Particles Oversize				
	MH300.25	M	W	X	Y
60	3.6				
50	13		0.1	0.1	0.1
40	20	0.2	0.6	0.3	0.2
30	30	2.4	2.1	0.6	0.6
20	54	4.7	8.7	1.9	3.2
10	86	51	41	14	19
0	100	100	100	100	100

TABLE 6 (a) :Particle Size Distribution by Number

Minimum Chord, μm	Cumulative Number Percentage Oversize				
	B	P	Q	R	S
230	13				
210	17				
190	35				
180		0.1		0.8	
170	69	0.3		0.9	
160		0.3		1.0	
150	88	0.5	0.1	1.2	
140		0.9	0.2	1.8	
130	100	1.5	0.7	2.7	
120		2.0	1.5	3.1	0.1
110		2.1	2.6	5.3	0.1
100		2.9	2.9	6.1	0.1
90		4.1	5.3	6.6	0.3
80		7.9	8.5	8.7	0.4
70		12	13	12	0.8
60		19	17	18	1.8
50		22	21	21	2.9
40		28	28	33	4.2
30		29	36	35	7.2
20		39	37	53	14
10		43	46	67	32
0		100	100	100	100

TABLE 6 (b) Particle Size Distribution by Nunber

Minimum Chord, μm	Cumulative Number Percentage of Particles Oversize				
	A	I	T	U	V
150	0.2				
140	0.3				
130	0.5				
120	0.7				
110	0.8		0.2		
100	1.2	0.3	0.3	0.2	
90	2.0	0.6	0.8	0.4	0.1
80	4.2	2.0	2.8	1.0	0.3
70	7.5	2.6	4.2	1.7	0.6
60	11	13	7.0	2.5	0.7
50	16	15	13	4.5	1.5
40	24	18	17	6.6	1.9
30	35	24	27	12	3
20	53	31	51	28	7
10	72	51	70	63	25
0	100	100	100	100	100

TABLE 6 (c) Particle Size Distribution by Number

Minimum Chord, μm	Weight % Oversize Cumulative
60	24
50	63
40	78
30	88
20	97
10	100
0	100

TABLE 7: Size Distribution of MH300.25 converted from number % to weight %

POWDER IDENTITY	WEIGHT MEAN DIAMETER, μm	STANDARD DEVIATION, μm	STANDARD DEVIATION / MEAN DIAMETER
B	168	19	0.11
F	82	6.5	0.08
P	83	14	0.17
Q	87	31	0.36
R	84	43	0.52
S	73	54	0.71
I	49	3.2	0.07
T	49	8.5	0.17
U	49	23	0.48
V	51	37	0.72
M	14.5	4.0	0.28
W	17	10	0.60
X	27	19	0.69
Y	6.7	2.4	0.36

TABLE 8 Statistical analysis of synthetic size distributions of B.S.A. Powder.

POWDER IDENTITY	SEGREGATION RANKING ORDER 1= GOOD, 15=BAD	COMPACTIBILITY	WEIGHT SPECIFIC SURFACE. m^2/g
MH300.25	-	GOOD	0.045
A	12	SATISFACTORY	0.030
B	2	SATISFACTORY	0.015
F	10	SATISFACTORY	0.031
P	8	SATISFACTORY	0.022
Q	14	BAD	0.021
R	11	SATISFACTORY	0.022
S	15	POOR	0.031
I	4	SATISFACTORY	0.033
T	13	POOR	0.029
U	9	POOR	0.031
V	9	SATISFACTORY	0.046
M	5	BROKE ON EJECTION	0.066
W	7	POOR	0.067
X	6	BROKE ON EJECTION	0.065
Y	3	BAD	0.156

TABLE 9 : Segregation, compactibility and specific surface

POWDER IDENTITY	APPARENT DENSITY Mg/m^3	TAP DENSITY Mg/m^3	COMPRESSIBILITY		DENSITY OF PELLET @ MAX.LOAD Mg/m^3
			INTERCEPT DENSITY Mg/m^3	SLOPE m^2/GN	
MH300.25	2.7	3.4	2.2	7.3	
A	3.2	4.0	3.7	3.3	
B	2.5	2.8	3.3	4.0	5.48
F	3.1	3.5	3.5	4.6	5.76
P	2.9	3.5	3.2	4.4	5.59
Q	3.0	3.4	3.2	4.2	5.56
R	3.1	3.8	3.6	4.2	5.64
S	3.5	4.4	4.2	5.1	6.00
I	3.2	3.5	3.9	3.5	5.56
T	3.2	3.9	3.6	3.7	5.53
U	3.4	4.2	4.0	4.1	5.78
V	3.4	4.7	4.2	6.1	6.18
M	3.4	3.9	3.7	4.9	5.89
W	3.4	4.3	4.0	4.7	5.87
X	3.4	4.6	4.5	4.8	6.03
Y	2.7	3.8	3.8	4.7	5.81
MH300.25	LARGE SAMPLE		3.0	7.5	
A	LARGE SAMPLE		3.8	4.7	

TABLE 10 Apparent density, tap density and compressibility

NUMBER OF LAYERS	1	2	3	4	6	MEAN STRENGTH IN TENSILE TESTING, N/mm^2
CALCULATED MAXIMUM STRESS N/mm^2	0.58	0.48	0.42	0.43	0.51	0.27

TABLE 11 Strength of flexistrip made from Hoganas powder

	INTERCEPT DENSITY Mg/m^3	SLOPE m^2/GN	CORRELATION COEFFICIENT
FLEXISTRIP MADE FROM MH300.25	2.80	9.1	0.99895
CELACOL	0.72	33	0.99035

TABLE 12 Compressibility of flexistrip and Celacol

ROLL LOAD INTENSITY M N/m	ANNULAR BEND STRENGTH, N/mm^2	DENSITY Mg/m^3	ELONGATION %
0	1.0	2.9	0
0	0.95	2.9	0
0	0.81	2.6	0
0	0.80	2.7	0
0.66	6.3	-	-
0.66	4.1	-	-
0.66	4.3	5.4	-
0.7 MEAN	-	-	6
1.5	15	6.5	-
1.9	13	6.4	-
2.5	15	6.4	15
2.5	11	6.3	15
3.6	30	7.2	-
4.2	20	6.6	-
4.4	31	7.3	19
4.5 MEAN	-	-	12
4.6	22	6.8	10
4.6	16	6.5	10
6.0 MEAN	-	-	13
6.9	30	7.0	12
6.9	27	6.8	12
6.9	25	7.0	12
7.0 MEAN	-	-	12
8.8 MEAN	-	-	9
8.9	30	7.2	-
11	25	6.8	-
17	25	6.9	-

TABLE 13 Effect of roll loading on green strength, density and elongation of

POWDER IDENTITY	THICKNESS OF ROLLED STRIP , mm	CALCULATED ROLL LOAD INTENSITY, MN/m
B	0.28	4.5
F	0.28	3.8
P	0.31	4.2
Q	0.38	4.7
R	0.29	3.9
S	0.33	4.5

TABLE 14 Roll loads for B,F,P, Q,R and S water atomised powder blends, calculated from Appendix V11.

Speed of strip entering rolls	57.1 mm/s
Peripheral speed of rolls	59.6 mm/s
Speed of strip leaving rolls	58.4 mm/s

TABLE 15 Speed of Strip during Rolling: Sponge Iron Powder

COMPACTED THICKNESS mm	DENSITY Mg/m^3	COMPACTING ENERGY J/g
0.57	2.4	0
0.42	3.3	3
0.36	3.4	6
0.28	3.8	19
0.23	5.1	30

TABLE 16 Energy expended in impact compaction of MH300.25 flexistrip

	MEAN	STANDARD DEVIATION	STANDARD ERROR
TENSILE STRENGTH LONGITUDINAL, N/mm^2	4.55	0.44	0.14
TENSILE STRENGTH TRANSVERSE, N/mm^2	3.12	0.75	0.24
TENSILE STRENGTH NORMAL, N/mm^2	7.63	0.61	0.19
ANNULAR BENDING STRENGTH, N/mm^2	17.0	1.34	0.42
MASS PER UNIT AREA kg/m^2	1.48	0.06	0.02
DENSITY Mg/m^3	6.4	0.11	0.03

TABLE 17 Mechanical properties of green strip made from Hoganas MH300.25 Powder

STRIP IDENTITY	DENSITY Mg/m^3	THICKNESS mm	ANNULAR BENDING STRENGTH, N/mm^2	MACROHARDNESS HV/5	SEGREGATION INDEX $\epsilon\sqrt{N}/I^2, \mu m^{-1}$	CALCULATED WEIGHT SPECIFIC SURFACE m^2/g
B	6.4	0.27	16	101	1.11	0.114
F	6.5	0.29	12	104	0.83	-
P	6.4	0.33	17	100	0.77	-
Q	6.4	0.39	8	132	0.55	0.178
R	6.4	0.31	15	76	1.36	-
S	6.8	0.35	19	104	1.57	-
I	6.5	0.39	7	112	0.98	0.123
T	6.5	0.36	7	102	0.87	-
U	6.5	0.40	7	109	0.76	-
V	6.6	0.41	15	102	1.68	-
M	6.5	0.33	11	92	1.36	-
W	6.5	0.33	7	83	1.43	0.305
X	6.7	0.35	7	92	1.62	-
Y	6.4	0.36	6	-	0.87	0.458

TABLE 18 Properties of green strip made from B.S.A. water-atomised powder

STRIP IDENTITY	DENSITY Mg/m^3	HV / 1		
		EDGE HARDNESS	CENTRE HARDNESS	MEAN HARDNESS
A	6.3	82	86	84
B	6.4	77	77	77
F	5.8	67	71	69
P	6.4	77	79	78
Q	6.6	86	79	82
R	6.3	91	83	87
S	6.5	77	84	80
I	6.3	94	78	86
T	6.1	68	80	74
U	6.7	85	82	84
V	6.6	83	81	82
M	6.5	60	83	72
W	6.5	62	68	65
X	6.6	74	83	79
Y	6.3	69	70	69
WEIGHT SPECIFIC SURFACE OF P = 0.063 m^2/g				

TABLE 19 Properties of first-sintered strip made from B.S.A. powder

PRESSURE N/mm^2	DENSITY Mg/m^3		
	MH300.25	B.S.A. "A"	B.S.A. "A"
0	6.78	6.62	6.60
26	6.78	6.62	
53	6.78	6.78	
106	6.80	6.82	
158	6.87	6.82	
212	6.90	6.89	
264	6.93	6.89	
317	6.97	6.89	
368	7.09	6.89	
422	7.10	6.89	
475	7.14	7.00	
528	7.30	7.11	
580	7.34	7.13	
390			7.02
790			7.17
1180			7.29
1580			7.35
1970			7.20
2360			7.04

TABLE 20 The compressibility of first-sintered strip. The second test on the B.S.A. as-received powder was done in the stronger tool set.

ROLL LOAD INTENSITY MN/m	300 mm DIA.ROLLS		350mm DIA. ROLLS	
	DENSITY Mg/m^3	ELONGATION %	DENSITY Mg/m^3	ELONGATION %
0	6.75	0	7.06	0
0.3	6.80	1.0		
0.4			6.99	0
1.1	6.99	2.0		
1.2			7.19	0.2
1.5	7.01	1.5		
1.8			7.19	0.5
2.1	7.26	2.0		
2.4	7.32	2.7		
2.7			7.09	0.4
3.1	7.42	2.2		
3.6	7.26	3.8		
3.7			7.15	0.8
4.5			7.37	1.5
4.6	7.42	2.8		
5.2			7.44	0.8
6.2			7.16	1.6
7.0			7.33	2.1
8.0			7.52	2.1
8.1			7.24	1.2
10.3			7.48	2.4

TABLE 21 The effect of roll loading on the density and elongation of first - sintered MH300.25 strip.

STRIP IDENTITY	MEAN LINEAR INTERCEPT μm	HARDNESS HV/1			DENSITY Mg/m^3
		EDGE	CENTRE	MEAN	
A	-	203	187	195	7.3
B	8.5	184	192	188	7.4
F	-	233	216	224	7.2
P	8.0	212	201	207	7.3
Q	8.4	218	215	217	7.5
R	8.2	203	195	199	7.3
S	8.1	203	196	200	7.3
I	8.1	192	215	204	7.4
T	7.7	210	215	213	7.4
U	8.2	237	229	233	7.5
V	7.9	199	199	199	7.3
M	-	206	206	206	7.6
W	-	211	213	212	7.3
X	7.7	216	203	210	7.3
Y	-	187	197	192	7.2

TABLE 22 Properties of second compacted strip made from B.S.A. powder

STRIP IDENTITY	MEAN LINEAR INTERCEPT μm	HARDNESS HV/1			DENSITY Mg/m^3		
		EDGE	CENTRE	MEAN	EDGE	CENTRE	MEAN
A	11.3	114	116	115	7.82	7.80	7.81
B	13.2	-	104	(104)	-	7.77	(7.77)
F	12.5	124	125	125	7.79	7.80	7.80
P	13.2	131	141	136	7.78	7.83	7.81
Q	11.1	117	124	121	7.79	7.78	7.79
R	13.9	116	122	119	7.79	7.77	7.78
S	18.9	109	107	108	7.75	7.68	7.72
I	11.6	126	141	133	7.79	7.77	7.78
T	13.2	111	121	116	7.80	7.76	7.78
U	12.0	127	125	126	7.80	7.78	7.79
V	12.1	112	117	114	7.78	7.80	7.79
M	10.4	127	118	122	7.82	7.76	7.79
W	9.6	112	137	125	7.76	7.82	7.79
X	17.2	111	123	117	7.79	7.76	7.78
Y	20.1	98	93	95	7.68	7.65	7.67

TABLE 23 Grain size, hardness and density of second-sintered strip made from B.S.A. powder

STRIP IDENTITY	YIELD STRESS, N/mm^2				ULTIMATE STRESS, N/mm^2				ELONGATION % MEAN
	TRANSVERSE	LONGITUDINAL EDGE	LONGITUDINAL CENTRE	MEAN	TRANSVERSE	LONGITUDINAL EDGE	LONGITUDINAL CENTRE	MEAN	
A	261	300	298	286	364	374	363	366	13
B	240	-	246	243	258	-	254	256	3
F	293	357	277	309	377	418	336	377	11
P	300	306	295	300	377	368	324	356	12
Q	251	-	278	265	339	-	278	308	12
R	252	367	293	304	331	379	321	344	12
S	207	217	235	220	316	218	293	270	12
I	298	362	304	321	385	447	377	397	15
T	273	314	300	296	317	380	344	347	16
U	257	283	267	269	350	321	325	332	12
V	314	320	348	327	395	406	414	405	14
M	293	295	307	298	381	382	384	382	16
W	272	295	284	284	346	381	335	354	11
X	237	263	227	242	338	371	362	357	18
Y	164	199	176	180	268	326	291	295	13

TABLE 24 Tensile properties of second sintered strip made from B.S.A.Powder

IDENTITY	FRACTIONAL POROSITY						
	APPARENT	TAP	INTERCEPT	GREEN	1ST SINTER	2ND COMPACTION	2ND SINTER
A	0.58	0.49	0.52	-	0.18	0.07	0.005
B	0.68	0.64	0.58	0.18	0.18	0.06	0.010
F	0.61	0.55	0.56	0.18	0.26	0.08	0.006
P	0.63	0.55	0.59	0.18	0.19	0.07	0.005
Q	0.61	0.56	0.59	0.18	0.16	0.05	0.008
R	0.60	0.51	0.54	0.19	0.19	0.07	0.009
S	0.55	0.43	0.47	0.14	0.17	0.07	0.017
I	0.59	0.55	0.51	0.18	0.20	0.05	0.009
T	0.59	0.49	0.54	0.18	0.22	0.05	0.010
U	0.57	0.46	0.49	0.18	0.15	0.04	0.007
V	0.56	0.40	0.46	0.16	0.16	0.07	0.007
M	0.56	0.50	0.53	0.17	0.18	0.03	0.007
W	0.56	0.45	0.49	0.17	0.18	0.07	0.007
X	0.56	0.41	0.43	0.14	0.16	0.07	0.009
Y	0.65	0.51	0.52	0.18	0.19	0.09	0.023

TABLE 25 The densification of strip made from B.S.A. water-atomised powder shown as reduction of porosity

APPENDIX I

OLIVETTI PROGRAMME FOR MEAN, STANDARD DEVIATION AND STANDARD ERROR, DATA NOT GROUPED.

1. Enter programme.
2. Press V.
3. Enter reading.
4. Press S.
5. Enter next reading, press S.

Repeat until all readings are entered.

6. Press Z.

Machine prints:

1. Mean.
2. Variance.
3. Standard deviation.
4. Variance of mean.
5. Standard error.
6. Number of entries.

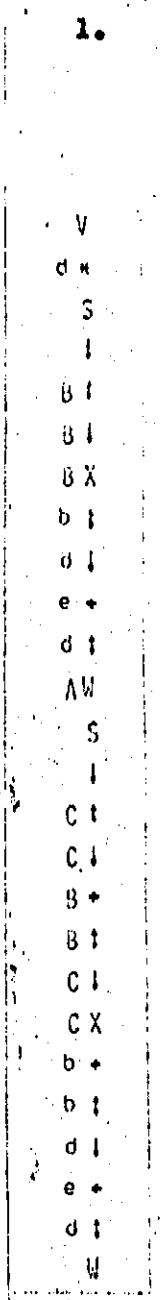

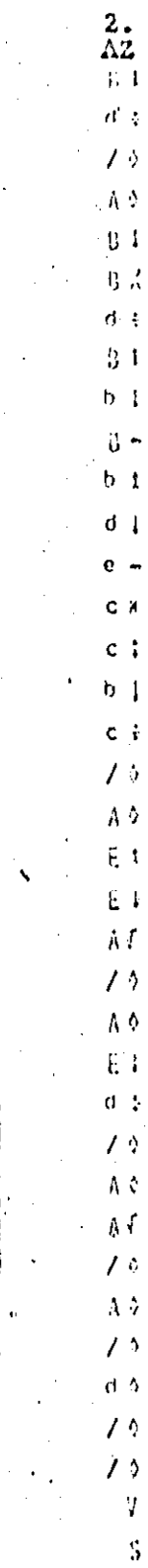

APPENDIX II

OLIVETTI PROGRAMME FOR FITTING A STRAIGHT LINE BY THE METHOD OF LEAST SQUARES.

To find "m" and "c" in the equation $y = mx + c$, group the data in pairs of y and corresponding x values.

1. Enter programme.
2. Press V.
3. Enter 1st y.
4. Press S.
5. Enter corresponding x, press S.
6. Enter 2nd y, press S.
7. Enter 2nd x, press S.

Continue until all pairs are entered.

8. Press Z.

Machine prints "c", "m".

1.	2.
	AZ
	D ↓
AV	D X
S	b ↑
c ↑	E ↓
S	B X
C ↑	b −
d ↓	b ↑
c +	e ↓
d ↑	D X
D ↓	C ↑
C +	d ↓
D ↑	E X
C ↓	C −
c X	b ÷
e +	A ◊
e ↑	D ↓
C ↓	d X
C X	C ↑
E +	e ↓
E ↑	B X
C ↓	C −
C ÷	b ÷
B +	A ◊
B ↑	B ×
V	b ×
	d ×
	D ×
	e ×
	E ×
	AV

APPENDIX 111 Weight Specific Surface

An air permoameter to operate at atmospheric pressure has been constructed (Fig18). It consists of a 100 ml. burette inverted over a beaker of deionised water, on top of which is a cell 35mm long and 6.23mm diameter.

(1) Cell Preparation

Two discs of filter paper 6mm diameter are made using an office punch. A ring of p.v.c. tubing 6.3mm diameter is pushed into one end of the cell, and a disc of filter paper is pushed through from the other end of the cell to rest on the p.v.c. ring. The powder to be tested is poured into the cell, taking care to avoid segregation; if necessary it is lightly compacted to give a porosity of about 50%. The remaining filter paper and p.v.c. ring are fitted to the open end. The cell is weighed to determine the weight of powder; the length of cell occupied by powder is measured (in the present case, by ruler) to establish the effective cell volume.

(2) Operation

Water is sucked up the burette using a pipette filler, to just below the tap, which must be kept well greased to prevent admission of air; the tap is then closed. The cell is connected to the top of the burette by a rubber tube, so that air entering the burette must do so via the cell. The tap is opened, and the water level in the burette falls, sucking air in through the cell. The time elapsed as the water falls past the 100 ml. mark, and at 10 ml. intervals, is noted. A graph of the time v. $\log_{10}$ volume is plotted. The relationship of head of water to volume indicated by the burette is measured.

APPENDIX 111 Weight Specific Surface

(2) Operation cont'd

The weight specific surface is calculated from the equation:

$$Sw^2 = \frac{1}{K\eta\rho^2 L} \frac{\left[1 - \frac{4W}{\rho\pi D^2 L}\right]^3}{\left[\frac{4W}{\rho\pi D^2 L}\right]^2} \frac{T_2 - T_1}{\log_{10}V_1 - \log_{10}V_2} \frac{\rho_w g\pi D^2}{4.\ 2.303} \frac{H}{V} \quad \ldots(1$$

Where S_w = weight specific surface, m^2/g

W = weight of powder, kg

ρ = density of powder, kg/m^3

D = diameter of cell, m

L = length of powder column, m

$(T_2-T_1)\ (\log_{10}V_1 - \log_{10}V_2)$ = slope of graph of time in seconds v. volume in m^3

ρw = density of water, kg/m^3

g = gravitational constant, m/s^2

V/H = volume of water (m^3) per m.water head in burette

K = aspect factor, assumed = 5

η = viscosity of air, Ns/m^2

(3) Theory

Equation (1) is derived from Kozeny's equation [177]

$$Sw^2 = \frac{1}{K\eta\rho^2 u} \frac{e^3}{(1-e)^2} \frac{\Delta p}{L} \quad \ldots\ (2)$$

where e = porosity

Δp = pressure drop across cell

u = volumetric flow rate/cross-sectional area of cell

e = (volume of cell) - (volume of metal)

$$= 1 - \frac{4W}{D^2 L \rho\pi} \quad \ldots\ (3)$$

(3) Theory cont'd

$$u = \frac{dV}{dT} \quad \frac{4}{\pi D^2} \qquad \ldots\ (4)$$

$$\Delta p = H \rho_w g \qquad \ldots\ (5)$$

from (2), (4), and (5)

$$\frac{dV}{dT} = \frac{H \rho_w g \pi D^2}{4K \rho^2 L \, Sw^2 \eta} \quad \frac{e^3}{(1-e)^2} \qquad \ldots\ (6)$$

$$\int_{V_2}^{V_1} \frac{dV}{H} = \int_{T}^{T_1} \frac{dT \, \rho_w \, g \, \pi D^2 \, e^3}{4K\eta \, \rho^2 L \, Sw^2 \, (1-e)^2} = \int_{V_2}^{V_1} \frac{dV}{V} \quad \frac{V}{H} \qquad \ldots\ (7)$$

$\frac{V}{H}$ is a constant for the burette and beaker used; see section (4) below.

$$\frac{V}{H} \log_{10} (V_1/V_2) \quad 2.303 = \frac{(T_2 - T_1) \rho_w \quad g \quad e^3 \pi D^2}{4K \rho^2 L \, Sw^2 \, (1 - e)^2 \, \eta} \qquad \ldots\ (8)$$

Rearranging,

$$Sw^2 = \frac{(T_2 - T_1)}{(\log_{10} V_1 - \log_{10} V_2)} \quad \frac{g \rho_w e^3 \pi D^2}{4K \rho^2 L \eta (1 - e)^2 \, 2.303} \quad \frac{H}{V} \qquad \ldots\ (9)$$

Substituting for e from equation (3) gives equation (1).

(4) Experimental Details

For the beaker and burette used, H/V was found to vary from 6720 to 6770 because of taper in the beaker. A mean value of 6730 was used. The variation is not significant in view of the errors attributable to segregation - an error of -3% has been measured. The experiments were carried out at temperatures ranging from 21°C to 26°C; in calculation, $\rho_w = 997.5$, and $\eta = 0.0000182$ were used. ρ was taken as 7 840. The graphs of $\log_{10}V$ v. T are shown in Fig. 19.

APPENDIX 1V

Determination of Mean Linear Intercept by Quantimet B, and Calculation of Degree of Segregation.

1. Mean Linear Intercept

Theory.

The mean linear intercept is the length of a line divided by the number of timesit is intercepted in that length. In the present case of a section through green strip, which is porous, the desired figure will represent the mean length of a line lying within a particle. This modified intercept figure is given by:

$$\frac{\text{length of line}}{\text{number of particles}} \qquad \text{---------- (1)}$$

The Quantimet operates by means of a television camera linked to a computer, which scans the field and detects those areas either lighter or darker than an adjustable threshold. Among the output data are the area A, of the field lighter than the threshold (this corresponds to the area of metal, as distinct from pore), and the number of times the horizontal lines of the television camera have entered regions lighter than the threshold setting.

1. Mean Linear Intercept cont'd.

This figure is described as the projection P, because it represents the projected total height of all the areas detected.

The length of line lying in particles can now be defined as:

$$\frac{\text{number of lines per frame x width of frame x area detected}}{\text{area of field}}$$

$$= \text{PoWA/Ao} \qquad \text{---------- (2)}$$

where Po = number of lines per frame

and Ao = area of frame

The method of operation of the Quantimet is such that the projection reading is higher than the number of intercepts. This is because fractional particles are counted as whole particles (a fractional particle is one which is partly outside the field examined). When both ends of a scanning line lie in pore, rather than metal, the reading is correct.Where a line starts or finishes within a particle, the length of the additional intercept measured is, on average, half its true length. Thus whenever a line has one of its ends lying within a particle, the projection reading is high by plus one half. The probability of this happening is twice the ratio of area detected to total area of field (because each line has two ends). Hence the total projection figure is higher than the number of intercepts by $\frac{1}{2}.2.\text{Po}.A/Ao = \text{Po } A/Ao$.

Therefore the number of intercepts is $P - \text{Po } A/Ao$ ----------(3)

Thus the mean linear intercept from (1), (2) and (3) is given by

$$\frac{\text{Po W A/Ao}}{P - \text{Po A/Ao}}$$

$$= \frac{W}{P\ Ao/Po\ A - 1}$$

1. Mean Linear Intercept cont'd.

Procedure

A x 10 objective was used. The area of the frame was set at 1000 units, 100 lines high. The length of the frame was measured by stage micrometer and was 87 microns. The threshold was set by comparing the direct image on the monitor screen with the image of the detected area, switching from one to the other and continually adjusting the threshold until both images were the same. The instrument was set to examine 50 fields along a transverse section of the strip. The mean linear intercept was calculated separately for each field, as

$$\frac{87 \text{ microns}}{10P/A - 1} = I$$

$$(Po = 100, \quad Ao = 1000)$$

The mean value $\bar{I}$ for the fifty fields was then calculated.

2. Segregation

Any field having in it a large number of small particles will have a low mean linear intercept; with few small particles, it will have a high mean linear intercept. Thus if the mean particle size varies from field to field, as in a segregated piece of strip, the mean linear intercept will vary . The standard deviation, σ, of the mean linear intercept, was calculated for each strip examined. For similar size distributions σ is a measure of segregation; it will be high for segregated strip and low where the size distribution is uniform. In the present case the size distribution varies from strip to strip. It may be shown that the standard deviation is inversely proportional to the square root of the number of frames measured; and also to the square root of the average number of intercepts per frame. Hence a better measure of segregation, independent of the number of frames or the number of intercepts per frame, is $\sigma\sqrt{N}$, where N is the total number of intercepts counted.

2. Segregation cont'd

There is also a scale effect: a standard deviation of five microns represents a greater degree of segregation for an average particle size of ten microns than for an average particle size of a hundred microns. The expression $\sigma\sqrt{N}/\bar{I}$ allows for this. The ratio of frame size to particle size also has an effect: where the particle size is of the same order of magnitude as the frame size, the variation from frame to frame will be far larger than where the powder is relatively fine. It might be possible to calculate the mean contribution of this effect, to the deviation of each reading of I from $\bar{I}$, and subtract it, before calculating the value for σ. However it was observed from the values of $\sigma\sqrt{N}/\bar{I}$ for the single cut sizes B,F,I,M,N that the magnitude of this effect was proportional to $\bar{I}$. Hence $\sigma\sqrt{N}/\bar{I}^2$ was taken as a measure of segregation. The size of field and number of fields counted was such that the average value recorded was about 1. A high degree of segregation would give a figure of 2 or more. In fact the highest obtained was 1.7 (powder V). This shows that all the powders were relatively homogeneous.
The calculation of $\bar{I}$ and σ was done using an Olivetti Programma 101 programmable calculator.

APPENDIX V

Density determination by neutral buoyancy

Small samples of strip prepared by the slurry process are not always uniform in gauge . On such samples density determination by measuring and weighing may lead to errors of up to several percent. Methods based on Archimedes' principle are unsatisfactory for specimens of volumes of the order of 100 mm^3 because exceptional care and considerable time is ne cessary to minimise the effects of temperature variation and surface tension.

Density determination by neutral buoyancy cont'd.

A method has therefore been devised which eliminates surface tension effects and takes advantage of the effects of temperature variation. This method has been described in "Powder Metallurgy" in a paper [168] which is included in this appendix.

Figure, table, reference and equation identification numbers quoted in that paper refer solely to the contents of the paper and not to the main body of this thesis.

MEASUREMENT OF THE DENSITY AND POROSITY OF SMALL SPECIMENS BY A FLOTATION METHOD

by M.Donnelly and R.Haynes.

ABSTRACT

A flotation method is described which enables the density and porosity of small specimens to be measured accurately by comparing the densities of reference and unknown specimens. The method uses the subtle but accurately known variation of the density of water with temperature to bring about the flotation of a specimen-float composite. Measurements can be made easily and quickly and the expressions derived for density and porosity are readily evaluated numerically.

1. INTRODUCTION

The determination of the porosity of a sintered material involves the accurate measurement of its density and knowledge of the density of the pore-free material (i.e. the 'theoretical density'). For large specimens, satisfactory results are obtained by the use of methods based on Archimedes principle, or the use of a volumenometer or pyknometer, provided that precautions are taken to prevent ingress into the pores of the specimen of the immersion fluid.

1. INTRODUCTION cont'd.

Indeed methods have been described which enable small changes in density to be determined to a very high degree of accuracy [1,2]. However, these methods are unsatisfactory when both the sample size and total porosity content are small because small differences in density produce changes in volumes and masses that are difficult to measure.

Therefore, a comparative method using a flotation technique has been developed to measure the densities of small samples containing only small amounts of porosity. Moreover, by the use of suitably coated specimens, the densities of more porous specimens can be measured with little loss of accuracy. The method was developed as part of an investigation of the production of thin high-density strip by powder rolling, but also should be of value for the study of any phenomenon which is accompanied by small changes in density.

2. Theory

When a solid specimen is immersed in a fluid in which it remains suspended showing no tendency either to rise or sink, its density is equal to that of the fluid. Thus if the density of the fluid is known, that of the solid is also known.

In practice, transparent fluids with densities greater than about 4.3 g/ml are not available [3], so that the direct measurement of the densities of the majority of metals and alloys by flotation is not possible. However, if a specimen is attached to a suitable float its density can be determined by comparison with a reference specimen, preferably of pore-free material if porosity content is to be determined.

2. Theory cont'd

Consider a system in which flotation is occurring at constant temperature. Let Ms, Mr and Mf represent the masses of the unknown specimen (s), reference specimen (r) and float (f); ρ_s ρ_r, ρ_f and ρ_L the densities of the unknown specimen, reference specimen, float and liquid (L): and Vsf and Vrf the volume occupied by the unknown specimen plus float and reference specimen plus float respectively.

When flotation of the unknown specimen occurs:

$$\frac{Ms}{\rho_s} + \frac{Mf}{\rho_f} = Vsf \qquad \text{----------(1)}$$

and $$Ms + Mf = Vsf\rho_L \qquad \text{----------(2)}$$

thus $$\frac{Ms}{\rho_s} + \frac{Mf}{\rho_f} = \frac{Ms + Mf}{\rho_L} \qquad \text{----------(3)}$$

Similarly for the reference specimen

$$\frac{Mr}{\rho_r} + \frac{Mf}{\rho_f} = Vrf \qquad \text{----------(4)}$$

and $$Mr + Mf = VrfPL \qquad \text{----------(5)}$$

Thus $$\frac{Mr}{\rho_r} - \frac{Mf}{\rho_f} = \frac{Mr + Mf}{\rho_L} \qquad \text{----------(6)}$$

Sub tracting (6) from (3)

$$\frac{Ms}{\rho_s} - \frac{Mr}{\rho_r} = \frac{Ms}{\rho_L} - \frac{Mr}{\rho_L} \qquad \text{----------(7)}$$

Rearranging

$$\rho_s = \frac{Ms}{\frac{Ms - Mr}{\rho_L} + \frac{Mr}{\rho_r}} = \frac{Ms\,\rho_L\,\rho_r}{Ms\,\rho_r + Mr(\rho_L - \rho_r)} \qquad \text{----------(8)}$$

Further the fractional porosity is given by

$$1 - \frac{\rho_s}{\rho_r} = \frac{(Mr - Ms)(\rho_L - \rho_r)}{Ms\rho_r + Mr(\rho_L - \rho_r)} \qquad \text{----------(9)}$$

if the reference specimen is of pore-free material.

2. Theory cont'd

Values for density can be corrected to a standard temperature e.g. 20°C by application of an appropriate correction for thermal expansion. However, it is noteworthy that porosity is independent of temperature.

3. EXPERIMENTAL PROCEDURE AND TYPICAL RESULTS

A glass float with a hook is prepared from glass tubing. The reference specimen is hooked to the float and immersed in a beaker of distilled water at ~22°C ensuring that no air bubbles are attached to either float or specimen*. The weight of the specimen is adjusted by filing until the specimen-float composite just sinks. Then the water is cooled until the specimen-float composite neither sinks nor rises when released by tweezers beneath the surface of the water. The uniformity of the temperature of the water is checked and, if necessary, it is gently stirred. No problem is caused by the slight turbulence arising from stirring, due to the relatively large size of the float. The temperature at which flotation occurs is measured to the nearest 0.1°C and the specimen is weighed to an accuracy of ± 0.0001g.

About 0.0005 g. of material is removed from the specimen by filing, the specimen reweighed and the new somewhat higher temperature of flotation is determined. The temperature of the water is conveniently raised by using the hands as a heat source. This procedure is repeated several times until the flotation temperature exceeds 30°C and a graph of flotation temperature versus mass of reference specimen is plotted, e.g. Fig.1. The specimen of unknown density is adjusted in weight until its flotation temperature falls within the range 20-30°C and the flotation temperature and specimen weight are measured.

* Formation of air bubbles can be largely avoided by preheating the water to 40°C and cooling to room temperature immediately before making the density measurements.

3. Experimental Procedure and Typical Results cont'd

The density of the unknown specimen is calculated from equation 8 or the porosity content from equation 9, using a value for the mass of the reference specimen at the same flotation temperature interpolated from the graph, and the density of the water at the flotation temperature [4], Table 1.

The method as described is suitable for determining the porosity contents of materials containing only closed porosity, say up to total porosity contents of a few percent. It can be extended to include more porous materials containing interconnecting porosity by coating the specimens with polystyrene laquer (saturated solution of polystyrene in xylene) and drying at a temperature of $\sim 150^{o}C$ for a few minutes prior to the density determination.

Once a calibration curve has been determined using the reference specimen the densities and porosities of unknown specimens can be easily and quickly measured.

Density and, where relevant, porosity values of specimens of several different materials, Table II, have been obtained using as a reference specimen a wrought AlSl type 304 stainless steel strip, whose density had been accurately determined on a large specimen using a method based on Archimedes' principle. The variation of flotation temperature of the reference specimen - float composite, with specimen mass is shown in Fig.1, using a float weighting 0.9g and having a volume of $1.4cm^3$.

4. ACCURACY

The main sources of error in the method lie in the measurement of the weights of the reference and unknown specimens and in the measurement of the temperature of the water, since over the temperature range used,

4. ACCURACY cont'd

the variation in the density of water is known to about one part in ten million and the presence of dissolved air affects the density value to the extent of the less than one part per million[4]. Thus, if the maximum error in the measurement of weights is 0.0001 g. and in the measurement of temperature is 0.1°C, the sensitivity of $\Delta\rho/\rho$ is 0.00134 for a metal such as iron ($\rho \sim 7.8$ g/cm^3).

If greater accuracy is required weighing to 0.00001 g and measuring temperature to 0.01°C should increase the sensitivity of $\Delta\rho/\rho$ to 0.00014.

5. CONCLUSION

A flotation method for the accurate measurement of density and porosity of small specimens has been devised. The method employs a specimen - float composite and brings about flotation through the subtle but accurately known variation of the density of water with temperature. Measurements are easily and quickly made. A sensitivity of $\Delta\rho/\rho = 0.0013$ is readily attained.

ACKNOWLEDGEMENTS

The work was carried out in the Materials Technology Department, Loughborough University of Technology and was supported by the Sketty Hall Research Laboratories of the British Steel Corporation. The authors wish to thank Professor I.A.Menziesfor the provision of laboratory facilities.

REFERENCES

1. G.A.Bell, Australian J. of Appl.Sci. 1958, 9, 236
2. R.T.Ratcliffe, Brit.J.Appl.Phys., 1965, 16, 1193
3. E.L.Simons, Analytical Chemistry, 1963, 35, 3, 407.
4. P.R.Bigg, Brit.J.Appl.Phys. 1967, 18, 521
5. Metals Handbook, 7th edition p.22 and 566, 1948, American Society for Metals, Metals Park, Ohio.

TABLE 1

Density of Pure Air-Free Water *

Temperature ^{o}C	Density g/cm^3
20	0.9982033
21	0.9979918
22	0.9977700
23	0.9975382
24	0.9972964
25	0.9970450
26	0.9967840
27	0.9965137
28	0.9962341
29	0.9959456
30	0.9956482
31	0.9953420
32	0.9950273

* The data is reproduced from the paper by Bigg[4]. (The original paper reports density values for temperature intervals of $0.1^{o}C$).

TABLE II

Typical Density and Porosity Values

Determined by the Flotation Method

Material	Weight of Specimen	Flotation Temperature °C	Density @ Flotation Temperature g/cm^3	Linear * Expansion Coefficient cm/cm/°C x 10^{-5}	Density @ 20°C g/cm^3	Porosity %
Reference AISI Type 304 Stainless steel (wrought)	0.5074	24.5		1.62	7.906**	
AISI Type 430 Stainless steel (Wrought)	0.5057	32.1	7.721	0.90	7.724	
AISIType 430 Stainless steel (sintered strip)	0.5104	23.6	7.612	0.90	7.613	1.43
Copper foil	0.4967	30.0	8.931	1.65	8.936+	-
Commercially pure aluminium sheet	0.7010	24.2	2.714	2.39	2.714+	-
Sintered Sherritt-Gordon Nickel bar	0.5061	32.0	7.685	-	-	13.65++ ± 0.25

* Data reproduced from Metals Handbook seventh edition [5]

** Density determined on a large sample and used as reference value

\+ Values are in good agreement with those quoted in Metals Handbook

++ Density of pore-free nickel assumed to be 8.90 g/cm^3

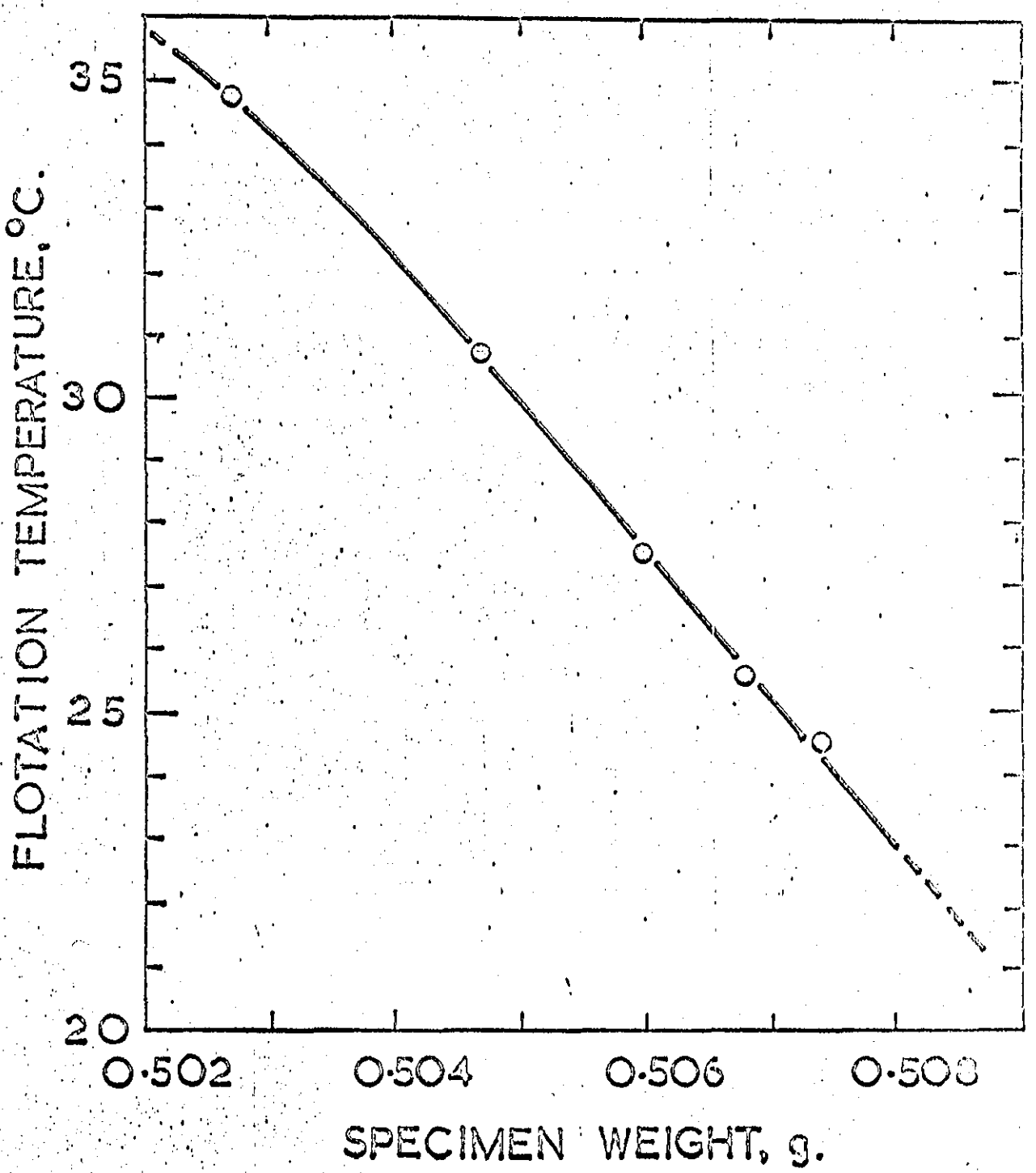
FLOTATION TEMPERATURE, °C.
35
30
25
20
0·502
0·504
0·506
0·508
SPECIMEN WEIGHT, g.

FIG. 1

APPENDIX V

Theory: Reference 168 is appended.

A suitable piece of wrought mild steel strip of the same composition as the powder was not available. A piece of commercial mild steel strip of unknown composition was therefore used as the standard. Microexamination indicates that it is reasonably clean.

The density of a 2o g piece of this strip was determined by weighing in air and water. The density of the strip was calculated from the equation:

$$\rho_s = \frac{W_A \rho_w - W_w \rho_A}{W_A - W_w}$$

where ρ_s = density of specimen

ρ_w = density of water

ρ_A = density of air

W_A = weight of specimen in air

W_w = weight of specimen in water

The density of air was calculated from the equation:

$$\rho_A = \rho_D (H - 0.378p) / H$$

where H = the atmospheric pressure

p = the water vapour pressure

ρ_D = density of dry air

The calculated density was 7.846(6) Mg/m^3 at 21.05 C

A mean value of 35.4×10^{-6} for the coefficient of volumetric thermal expansion was calculated from values for the coefficient of linear thermal expansion quoted in "Metals Handbook". Table 26 shows calculated values of the densities of the specimen used as standards, together with the weights and flotation temperatures ; Fig. 45 shows the graph.

APPENDIX V cont'd

Test specimens were cut to weigh between 0.5 g and 0.51 g. They were on average 20mm x 10mm with a 6mm diameter hole, made with a punch designed for punching holes in paper. They were not treated in any way to prevent oxidation or to keep water out of any open porosity. They were washed in alcohol and acetone; immediately after testing they were again washed in alcohol and acetone. The water used was deionised and distilled once. Densities and porosities were calculated using an Olivetti Programma 101.

In the course of the density investigations, the following points have become clear:

(a) if specimen weight is plotted against water density, rather than temperature, when determining density by the flotation method, a substantially straight line results, rather than the curve obtained when plotting against temperature. This makes interpolation more accurate; the equation of the line can be determined (Fig.46).

(b) where great precision is not required, the equation

$$\varepsilon = \frac{(M_R - M_S)\ (\rho_L - \rho_R)}{M_s \rho_R + M_R \rho_L - M_R \rho_R} \qquad \text{----------(1)}$$

where ε = fractional porosity

M_R = mass of reference specimen

M_S = mass of specimen under investigation

ρ_R = density of reference specimen

ρ_L = density of flotation liquid

can be simplified to give the approximate relationship

APPENDIX V cont'd:

$$\varepsilon = \frac{(M_R - M_S)\ (\rho_L - \rho_R)}{M_R \rho_L} \qquad \text{----------(2)}$$

In the present case, $\rho_R - \rho_L = 6.85\ Mg/m^3$

$$M_R \rho_L = 0.505\ kg^2/m^3 \text{ (average)}$$

$$\therefore \quad \varepsilon = 13.6\ (M_S - M_R) \qquad \text{----------(3)}$$

This approximate relationship becomes more accurate as the porosity decreases: it has been tested in a number of cases and the constant found to lie in the range 12.8 to 13.6, the former at 6% porosity and the latter at 0.7% porosity (Fig.47).

(c) Polystyrene lacquer does not necessarily seal all the pores in porous specimens.

Temperature C	Weight of Specimen g	Density of Specimen Mg/m^3
18.35	.50953	7.8474
21.80	.50861	7.8464
26.75	.50632	7.8450
27.90	.50598	7.8447
30.95	.50443	7.8439
35.20	.50221	7.8427
36.85	.50142	7.8422

In all cases the last figure quoted above is only a "best estimate".

TABLE 26 Flotation temperatures and corresponding densities of reference specimens of various weights.

APPENDIX V1

Transformation of Kawakita's Equation

Kawakita's equation as published [61, 62, 63] is

$$\frac{Vo - V}{Vo} = \frac{abP}{1 + bP} \qquad \text{---------- (1)}$$

where the symbols are as defined in section L2.1.

By definition,

$$D = \frac{Vs}{V} \qquad \text{----------(2)}$$

and

$$Do = \frac{Vs}{Vo} \qquad \text{---------- (3)}$$

where Vs = the volume of solid material (i.e. pore free) having the same mass as the compact. From (2) and (3)

$$\frac{Do}{D} = \frac{V}{Vo} \qquad \text{----------(4)}$$

From (1) and (4)

$$1 - \frac{Do}{D} = \frac{abP}{1 + bP} \qquad \text{----------(5)}$$

Putting $a = 1 - Do$ ----------(6)

and $b = \frac{c\,(1 - Do)}{Do}$ ----------(7)

From (5), (6) and (7)

$$(D - Do)\left(1 + \frac{(1-Do)\,cP}{Do}\right) = \frac{D}{Do}(1 - Do)^2 cP \quad \text{----(8)}$$

$$D - Do = \frac{(1 - Do)}{Do} cP \left[D\,(1 - Do) + Do - D\right] \qquad \text{----------(9)}$$

$$\frac{D - Do}{(1-Do)(1-D)} = cP \qquad \text{----------(10)}$$

$$\therefore \quad \frac{1}{1 - D} - \frac{1}{1 - Do} = cP \qquad \text{----------(11)}$$

APPENDIX V1

Transformation of Kawakita's Equation cont'd

This is the form in which Kawakita's equation is used in this thesis. To transform this to Aksenov's equation[82], the following substutitions are made:

$$D = \frac{Z}{Zo} \qquad \text{----------} \quad (12)$$

$$Do = \frac{1}{Zo} \qquad \text{----------} \quad (13)$$

From (11), (12) and (13),

$$\frac{Zo}{Zo - Z} - \frac{Zo}{Zo - 1} = cP \qquad \text{----------} \quad (14)$$

or

$$\frac{1}{Zo - Z} - \frac{1}{Zo - 1} = d\,P \qquad \text{----------} \quad (15)$$

where d is a constant. This is Aksenov's equation.

APPENDIX V11

A Proposed Relationship between Roll Load and Green Strip Density

It is proposed that the rolls deform under load to the shape shown in Fig. 48. This shape is such that

(i) Maximum pressure gives maximum strip compaction and maximum roll deformation, and this is on the plane joining the roll axes.

(ii) The rolls deform on the input side to a circular arc of contact.

(iii) The rolls deform on the exit side to produce an arc of contact which is very nearly flat.

Condition (i) is justified if the elastic recovery of the strip is negligible compared to its plastic deformation, and if the maximum pressure corresponds to the maximum radial deformation of the rolls.

Condition (ii) is an approximation. It has been shown [169] that a solid cylinder is deformed to a circular arc if the pressure distribution along the contact arc is elliptical. Fig.49 shows that if the arc of contact was circular, the pressure distribution would not be elliptical. The data for this graph were calculated for powder V for a roll radius of 152mm and a green strip thickness of 0.41mm. Nevertheless this assumption has been used with some success for cold rolling of steel strip by Hitchcock[88], Stone [170], and Ford and Alexander [171], among others. An analysis by Bland [172] shows that although the shape of the deformed roll surface is not circular, the values of roll force calculated with the aid of Hitchcock's formula fall within the range of possible error of the more accurate solution.

APPENDIX V11

A Proposed Relationship between Roll Load and Green Strip Density cont'd

It has been shown experimentally by Orowan [173] that the roll shape can deviate considerably from circular, and the stresses are usually further from elliptically distributed than in the present case. Thus the principal justification for condition (ii) will be its experimental validity.

Condition (iii) results from consideration of two rolls in direct contact. Here if the rolls are identical, the contact will necessarily be flat. Any curvature will result only from the elastic recovery of the strip. As the strip is thin, this is small compared to the elastic recovery of the rolls, and will be neglected here.

The analysis is made in three stages.

(1) The load on the input side of the rolls is calculated in terms of the deformed roll radius.

(2) This is transformed to an equation in terms of undeformed roll radius.

(3) The load on the exit side of the rolls is calculated from the maximum pressure at the centre line.

It is assumed that the powder compresses according to Kawakita's equation [66] $BP = \frac{1}{1-D} - \frac{1}{1-D_o}$ This has been verified for water atomised powder *

Then $$Pi = \frac{1}{B} \int_o^{Lo} \left[\frac{1}{1-D} - \frac{1}{1-D_o} \right] .dL \qquad \text{----------(1)}$$

$$= \frac{-Lo}{B(1-Do)} + \frac{1}{B} \int_{t_f}^{to} \frac{1}{1-M/Apt} .dt.\frac{dL}{dt} \qquad \text{--------(2)}$$

$$t = tf + 2L \sin \frac{\theta}{2} \text{ (Fig. 14)} \qquad \text{----------(3)}$$

---

* For list of symbols, see page 212

APPENDIX V11

As θ is a small angle,

$$t = tf + L^2/R^1 \qquad \text{----------} \quad (4)$$

$$\therefore \quad L = \sqrt{R^1(t-tf)} \qquad \text{----------} \quad (5)$$

from (4) and (5)

$$\frac{dt}{dl} = \frac{2L}{R^1} = \frac{2\sqrt{R^1(t-tf)}}{R^1} \qquad \text{----------} \quad (6)$$

from (6) and (2)

$$Pi = \frac{-Lo}{B(1-Do)} + \frac{1}{B} \int_{tf}^{to} \frac{1}{1-M/A\rho t} \cdot \frac{R^1}{2\sqrt{R^1(t-tf)}} \cdot dt \quad \text{----(7)}$$

$$= \frac{-Lo}{B(1-D_o)} + \frac{1}{B} \int_{tf}^{to} \frac{A\rho t/M}{A\rho t/M-1} \cdot \frac{\sqrt{R^1}.dt}{2\sqrt{t-tf}} \qquad \text{----------(8)}$$

$$= \frac{-Lo}{B(1-D_o)} + \frac{A\rho\sqrt{R^1}}{2MB} \int_{tf}^{to} \frac{t.dt}{\sqrt{t-tf}\ .(A\rho t/M-1)} \qquad \text{----------(9)}$$

This integral is of the type $I = \int \frac{xdx}{(mx+n)\sqrt{ax+b}}$ ----------(a)

where $a = 1$, $b = -tf$, $m = A\rho/M$, $n = -1$ (reference 22)

$$I = \frac{1}{m} \frac{dx}{\sqrt{ax+b}} - \frac{n}{m} \int \frac{dx}{(mx+n)\sqrt{ax+b}} \qquad \text{----------(b)}$$

$$= \frac{2}{am}\sqrt{ax+b} - \frac{2n}{m\sqrt{m(an-bm)}} \arctan \sqrt{\frac{m(ax+b)}{an-bm}} \qquad \text{------(c)}$$

APPENDIX V11

$$\therefore \quad Pi = \frac{Lo}{B(1-Do)} + \frac{A\rho\sqrt{R^1}}{2MB} \cdot \frac{2M}{A\rho}\left[\sqrt{t-tf} + \frac{1}{\sqrt{(tfA\rho/M-1)A\rho/M}} \arctan\sqrt{\frac{(t-tf)A\rho/M}{tfA\rho/M-1}}\right]_{tf}^{t} \quad \text{----------(10)}$$

$$Pi = \frac{-Lo}{B(1-Do)} + \frac{\sqrt{R^1}}{B}\left[\sqrt{to-tf} + \frac{1}{\sqrt{(1/Df-1)/Dftf}} \arctan\sqrt{\frac{(to-tf}{Dftf(1/Df-1)}}\right] \quad \text{-----(11)}$$

Putting $Lo = \sqrt{R^1(to-tf)}$ from (5) ----------(5a)

$$Pi = \frac{-\sqrt{R^1(to-tf)}}{B(1-Do)} + \frac{\sqrt{R^1(to-tf)}}{B} + \frac{\sqrt{R^1}}{B} \cdot \frac{1}{\sqrt{(1-Df)/Df^2tf)}} \arctan\sqrt{\frac{to-tf}{tf(1-Df)}}$$

---------(12)

$$= \frac{-Do\sqrt{R^1(to-tf)}}{B(1-Do)} + \frac{\sqrt{R^1tf}}{B} \cdot \frac{Df}{\sqrt{1-Df}} \arctan\sqrt{\frac{to-tf}{tf(1-Df)}} \quad \text{----------(13)}$$

$$= \sqrt{R^1} \cdot Z \quad \text{----------(14)}$$

where $Z = \frac{1}{B}\left[Df\sqrt{\frac{tf}{1-Df}} \arctan\sqrt{\frac{to-tf}{tf(1-Df)}} - \frac{Do\sqrt{to-tf}}{1-Do}\right]$ ----------(15)

.....

To find Pi in terms of R:

For elliptical stress distribution, [169, 175]

$$\frac{4(1-\nu^2)Pt}{E\pi lo^2} = \frac{1}{R} - \frac{1}{R^1} \quad \text{----------(16)}$$

where in this case complete symmetry is assumed for the purpose of calculation and $2Pi = Pt$

Considering the input side only,

$$\frac{8(1-\nu^2)Pi}{E\pi lo^2} = \frac{1}{R} - \frac{1}{R^1} \quad \text{----------(17)}$$

$$Pi = \frac{R^1 - R}{RR^1} \cdot \frac{E\pi}{8(1-\nu^2)} \cdot R^1(to-tf) \quad \text{----------(18)}$$

from (5a) and (17)

APPENDIX V11

from (14), $R^1 = Pi^2/Z^2$ ---------- (19)

$$\therefore \quad Pi = \frac{Pi^2/Z^2 - R}{R} \cdot \frac{E\pi(to-tf)}{8(1-\vartheta^2)} \qquad \text{----------} \quad (20)$$

$$Pi^2 - \frac{Pi\ R\ Z^2 \cdot 8(1-\vartheta^2)}{E\pi(to-tf)} - RZ^2 = 0 \qquad \text{----------} \quad (21)$$

$$\therefore \quad Pi = \frac{1}{2}\left[\frac{8RZ^2(1-\vartheta^2)}{E\pi(to-tf)} \pm \sqrt{\left[\frac{8RZ^2(1-\vartheta^2)}{E\pi(to-tf)}\right]^2 + 4RZ^2}\right] \qquad \text{----------} \quad (22)$$

$$= \frac{4RZ^2(1-\vartheta^2)}{E\pi(to-tf)} + \sqrt{\left[\frac{4RZ^2(1-\vartheta^2)}{E\pi(to-tf)}\right]^2 + RZ^2} \qquad \text{----------} \quad (23)$$

.....

To find the load on the output side of the rolls:

For two identical rolls in contact, maximum pressure is given by [176]

$$Pmax = \sqrt{\frac{Pt\ E}{R\pi(1-\vartheta^2)}} \qquad \text{----------} \quad (24)$$

Assuming symmetry, $Pt = 2Po$ ----------(25)

Since the maximum pressure also gives the greatest compression of the strip,

$$Pmax = \frac{1}{B}\left[\frac{1}{1-Df} - \frac{1}{1-Do}\right] \qquad \text{----------} \quad (26)$$

$$\therefore \quad \sqrt{\frac{2Po\ E}{R\pi(1-\vartheta^2)}} = \frac{1}{B}\left[\frac{1}{1-Df} - \frac{1}{1-Do}\right] \qquad \text{----------} \quad (27)$$

$$\therefore \quad Po = \frac{R\pi(1-\vartheta^2)}{2EB^2} \cdot \left[\frac{1}{1-Df} - \frac{1}{1-Do}\right]^2 \qquad \text{----------} \quad (28)$$

.....

APPENDIX V11

Total load = Po + Pi = Pt ---------- (29)

$$Pt = R\pi\frac{(1-\nu^2)}{2EB^2}\cdot\left[\frac{1}{1-Df} - \frac{1}{1-Do}\right]^2 + \frac{4RZ^2(1-\nu^2)}{E\pi(to-tf)} + \sqrt{\left[\frac{(4RZ^2(1-\nu^2)}{E\pi(to-tf)}\right]^2 + RZ^2}$$

----------(30)

List of symbols used in appendix

P	=	pressure.
Pt	=	total roll load per unit width.
Pi	=	roll load per unit width on input side of rolls.
Po	=	roll load per unit width on output side of rolls.
M/A	=	mass per unit area of strip.
ρ	=	true density of powder.
t	=	thickness of strip.
to	=	initial thickness of strip.
tf	=	final thickness of strip.
D	=	relative density of strip = M/Atρ.
Do	=	initial relative density of strip.
Df	=	final relative density of strip.
l	=	distance from centre line to the point on the arc of contact.where the strip has thickness t.
lo	=	distance from centre line to the input end of the arc of contact.
R	=	roll radius.
R^1	=	deformed roll radius.
B	=	constant in Kawakita's equation $BP = \frac{1}{1-D} - \frac{1}{1-D_o}$
θ	=	angle subtended at centre of curvature of deformed roll by the projected contact length l.
ν	=	Poisson's ratio for the roll material.
E	=	Young's modulus for the roll material.
Pmax	=	maximum pressure.